

Chromosomal instability in tumorigenesis:

**The importance of how much,
where and when**

Wilma H. M. Hoevenaar

ISBN: 978-94-6375-401-9

Copyright: © 2019 by Wilma Hoevenaar

Printed by: Ridderprint

Cover design by: W.H.M Hoevenaar & Ridderprint

The cover shows an edited picture of an intestinal crypt of a mouse stained with Ki-67 antibody

Chromosomal instability in tumorigenesis: The importance of how much, where and when

Chromosomale instabiliteit in
tumorontwikkeling: Het belang van hoeveel,
waar en wanneer

(met een samenvatting in het Nederlands)

Proefschrift

ter verkrijging van de graad van doctor aan de Universiteit Utrecht op
gezag van de rector magnificus, prof.dr. H.R.B.M. Kummeling, ingevolge het
besluit van het college voor promoties in het openbaar te verdedigen op
donderdag 20 juni 2019 des ochtends te 10.30 uur

door

Wilhelmina Hendrika Maria Hoevenaar

geboren op 12 januari 1989 te Hooge en Lage Zwaluwe

Promotor:

Prof. dr. G.J.P.L. Kops

Copromotor:

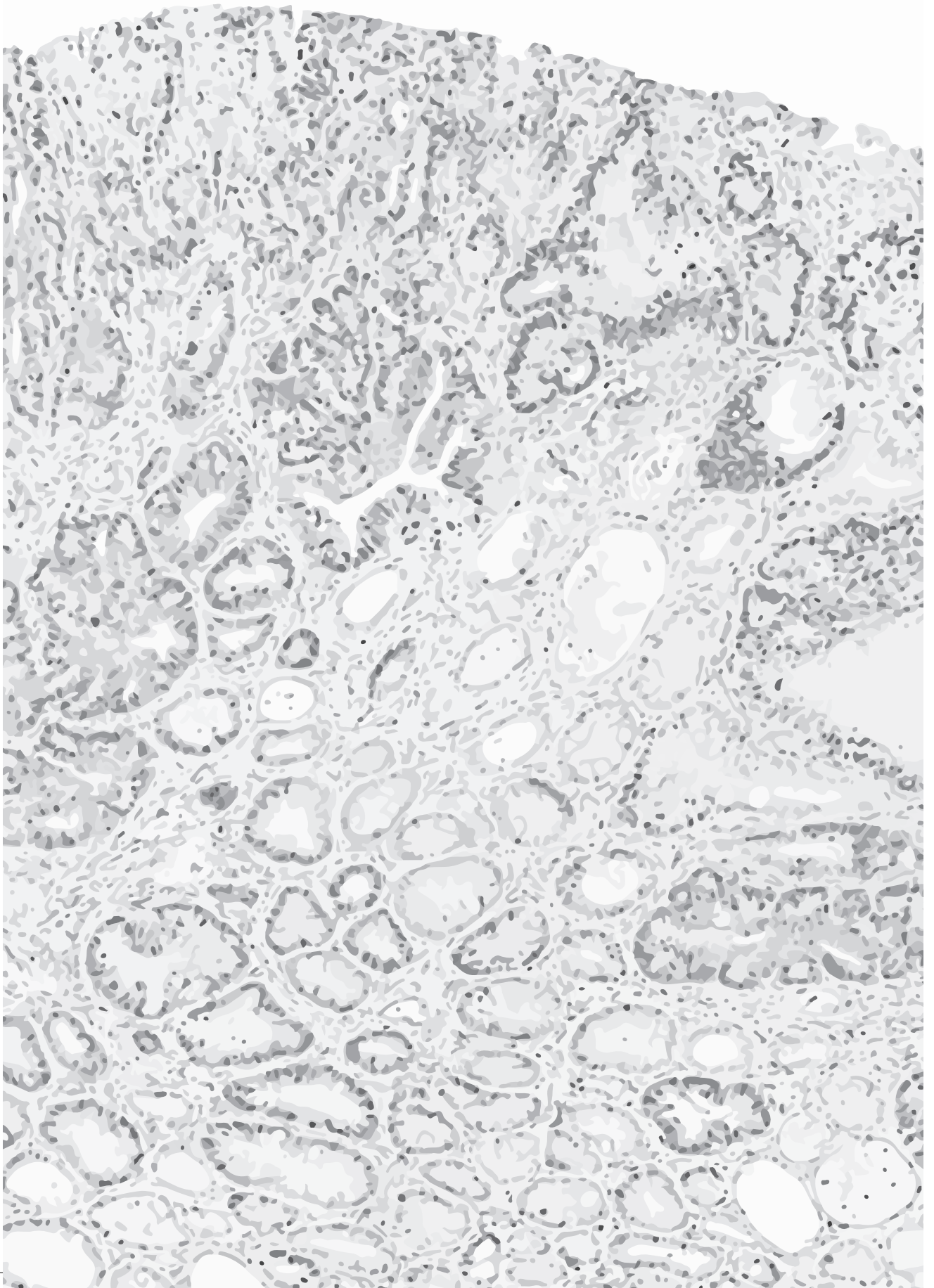
Dr. N. Jelluma

**"If you do not change direction, you
may end up where you are heading"**

Lao Tzu, Chinese philosopher

Table of Contents

<i>Chapter 1</i>	9
General Introduction	
<i>Chapter 2</i>	27
Degree and site of chromosomal instability define its oncogenic potential	
<i>Appendix chapter 2</i>	59
Oncogenic impact of chromosomal instability depends on time of induction	
<i>Chapter 3</i>	71
Distinct effects of various chromosomal instability levels on skin tumorigenesis	
<i>Chapter 4</i>	95
Drug screening to identify synergy between chromosomal instability and anti-cancer drugs in organoids	
<i>Chapter 5</i>	127
General Discussion	
<i>Addendum</i>	141
Nederlandse Samenvatting	
Nederlands Curriculum Vitae	
Dankwoord	



Chapter 1

General Introduction

Genomic instability in cancer

1

Transformation from normal cell to cancer: genomic instability

Cancer is a disease of cell division; tumours arise through uncontrolled propagation of cells. Cell division is needed to replace damaged tissues or cells, but this process is tightly regulated to assure that cells only divide when needed and when they are healthy. Cells can become malignant when undergoing a multistep process in which they gain the capability to keep on proliferating and to resist cell death and growth suppression^{1,2}.

A common way by which cells acquire these oncogenic properties is through acquiring genetic mutations. Mutations occur at a rate of 1 per cell division, but most of these are silent and do not affect gene function³. Deactivating or activating mutations in genes that regulate cell cycle, apoptosis or DNA repair however can underlie oncogenic transformation of cells. For complete transformation of cells to form a malignant tumour, around four of these so-called driver mutations are required, but numbers vary between tumour types⁴. Large-scale sequencing efforts have shown that the mutational spectra are highly specific for tumour types and mutational signatures have been established for various cancer types⁵⁻⁸. These signatures can be attributed to, for example, UV exposure or tobacco smoking, but also to aging or hereditary factors⁵. Furthermore, many genes are directly linked to (hereditary) tumour types, such as *BRCA* to breast and ovarian cancer^{9,10}, and *APC* to intestinal cancer¹¹. Mutations in *P53* and the *RAS* genes are common across many tumour types, but the exact mutations and the order in which they occur are again specific for certain tissue/tumour types^{6,8,12}. In the case of colorectal cancer (CRC) for example, an adenoma-to-carcinoma sequence has been described: early inactivating mutations in the *APC* gene lead to loss of function of *APC*, leading to constitutive activation of the *WNT* signalling pathway, and consequent activation of proliferation¹³⁻¹⁵. Mutation of *APC* is followed by mutations in *P53*, *KRAS* and *SMAD4*, *TGF β* , *PIK3C* and *PTEN*, which are involved in cell cycle arrest, apoptosis, and DNA damage repair¹⁶⁻²⁰.

The genomic changes in these genes are often on the base level; indels or substitutions change gene functions and this mutational phenotype is often the instigator of oncogenic transformation, but it is not the only form of genomic instability. Epigenetic changes can for example change gene expression²¹, as well as copy number alterations². The latter is a form of genetic instability that is of special interest for this thesis, as copy number changes can be oncogenic by causing overexpression of oncogenes, or decreased expression and possible loss of heterozygosity (LOH) of tumour suppressor genes²²⁻²⁶.

Aneuploidy and chromosomal instability

In diploid organisms, two copies of all autosomal chromosomes are present in most cells. If this is not the case and the chromosome number is not the exact multiple of the haploid set, this cell is aneuploid. Genomic content of cells is tightly regulated and the occurrence of aneuploidy in normal cells is rare²⁷. Aberrations in chromosome numbers are the prime cause for early abortions and only trisomies of chromosome 13, 18 or 21 are viable (but cause severe developmental disorders)²⁸. In cancer cells however, aneuploidy is common in the form of whole chromosome gains or losses and structural aberrations such as translocations, fusions, and duplications or deletions of parts of chromosomes. In fact, the majority of human solid tumours is aneuploid²⁹, and therefore aneuploidy can be considered as a hallmark of cancer².

Aneuploidy results from incorrect chromosome segregation during mitosis, and the process of ongoing missegregations is called chromosomal instability (CIN)^{23,24}. When cells need to divide, the DNA is duplicated in S-phase and each daughter cell receives a complete set of chromosomes after mitosis. To achieve equal division, chromosomes have to orient the sister chromatids to opposite sides of the spindle. Stable attachments are made between microtubules that emanate from the spindle poles and the protein complexes on the centromeric region of chromosomes called kinetochores. The chromosome pairs together thereby form a metaphase plate (Fig. 1). At anaphase onset, the sister chromatids are pulled apart by the spindle and the actual cell division can take place. If cells fail to correctly align, attach or separate their chromosomes, this will result in unequal division and/or damaged chromosomes.

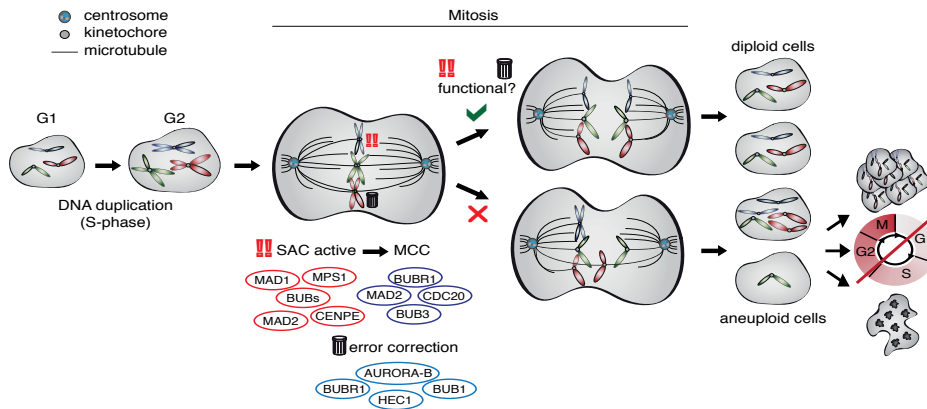


Figure 1: Chromosome segregation in cell division

Cells duplicate their genome during S-phase, so two copies of each chromosome are present to divide over the daughter cells. During mitosis, biorientation must be achieved and all chromosome pairs must be attached to microtubules. As long as this is not achieved (blue chromosomes) or attachments are not correct (red chromosomes) the spindle assembly checkpoint (SAC, core components in red) and error correction machinery (core components in blue) are active to ensure proper attachments and recruitment of the mitotic checkpoint complex (MCC, in purple) to inhibit anaphase onset. When correct attachments are made for all chromosomes, the SAC is satisfied and anaphase can commence, and diploid daughter cells will be produced (upper part). If error correction and SAC signaling fail, anaphase can start without correct attachments, leading to aneuploid daughter cells that will either keep proliferating, arrest, or die (lower part).

To prevent these errors from happening, multiple safeguard systems are in place. Firstly, the spindle assembly checkpoint (SAC) monitors kinetochore-microtubule (KT-MT) attachments and produces an anaphase inhibitory signal as long as unattached kinetochores are present. One of the key regulators of the SAC is MPS1 kinase (reviewed in ³⁰), which phosphorylates -among others- KNL1 and BUB1 to recruit other checkpoint proteins such as the BUBs (BUB1/BUB3/BUBR1), CENPE, MAD1 and MAD2. Recruitment and activation of these proteins eventually results in production of the mitotic checkpoint complex (MCC) consisting of MAD2, BUBR1, BUB3, and CDC20 to inhibit the anaphase promoting complex. This pauses progression into anaphase until all kinetochores are attached in the right way (reviewed in ³¹, Fig. 1). Deregulation of checkpoint proteins, especially of master regulators like MPS1 lead to weakening of the SAC and missegregations³². Secondly, the error correction pathway ensures that faulty KT-MT attachments are destabilised in order to be corrected. Important proteins in this pathway are

AURORA B, which phosphorylates HEC1 to reduce KT-MT binding affinity, BUB1 that regulates AURORA B localisation and BUBR1 that provides negative feedback on AURORA B (reviewed in^{31,33,34}). The SAC and error correction machineries are strongly intertwined and feedback on each other to regulate faithful cell division. The importance of tight regulation of mitosis is underscored by the severe consequences of unequal division, which include cell cycle arrest, and in case of severe missegregations, cell death^{22,32,35-39} (Fig.1).

On an organismal level, cell cycle arrest or apoptosis are probably the most favourable outcomes of CIN and aneuploidy because these cells then no longer contribute to the population. Tolerance of CIN and aneuploidy allows cells to propagate with their incorrect DNA content, increasing the risk of further genome destabilization by the induction of DNA damage, and translocations after chromosome breakage and fusion⁴⁰⁻⁴⁵. Tolerated CIN and aneuploidy can therefore have major detrimental effects: CIN is implicated in intra-tumour heterogeneity due to ongoing changes in genomic content⁴⁶. Furthermore, CIN and aneuploidy have been related to immune evasion and even metastasis: missegregated chromosomes can be captured in micronuclei that are prone to burst and thereby releasing DNA in the cytosol, which triggers inflammatory responses. This response involves cGAS-STING (cyclic GMP-AMP synthase-stimulator of interferon genes) activation and upregulation of NF-κB signalling activation. These pathways are implicated in increased dissemination and epithelial to mesenchymal transition (EMT), which are needed for migration to distant sites to metastasise⁴⁷.

CIN is related to unfavourable outcome in cancer

CIN is a feature of many tumours, and it has been described that CIN and aneuploidy correlate with tumour aggressiveness, therapy resistance and poor prognosis for the patient^{39,48-54}. For example, a meta-analysis of 63 studies with a total of 10.126 CRC patients (of which 60% CIN) showed that CIN tumours responded worse than diploid tumours to 5-Fluoruracil treatment, and (progression free) survival was decreased in CIN patients⁵¹. Looking further in the Consensus Molecular Subtype (CSM) classifications of CRC, the CIN phenotype is included in

two of the four subtypes and these two are correlated to worse survival and to the mutational phenotype that fits the adenoma-carcinoma sequence as described before^{15,55}. In another example, CIN and aneuploidy have been implicated in tumour progression in squamous cell carcinoma of the skin, where elevated aneuploidy levels were found in metastasis⁵⁶. In line with this, aneuploidy levels correlated to tumour stage in mouse studies using a two-stage chemical skin carcinogenesis protocol⁵⁷. Finally, CIN has also been implicated in therapy resistance: the ongoing genetic changes can give rise to resistant cells which can repopulate the tumour site and remain unresponsive to further therapies^{49,54,58}.

Exploiting CIN to kill tumour cells

In contrast to the tolerance for, and probably beneficial effects of CIN and aneuploidy in tumours, aneuploidy has been linked to decreased cell fitness (reviewed in^{38,59}). Cellular stresses that are linked to CIN and aneuploidy include metabolic stress, proteotoxicity, and high burden on DNA repair machinery and cell cycle checkpoints^{42,43,45,60-62}. Moreover, high levels of CIN are lethal to tumour cells^{32,37-39,63}. Targeting tumour cells specifically by elevating their CIN levels (in combination with anti-cancer drugs) has been proposed as treatment strategy^{60,64,65}. Induction of sufficiently high levels of CIN could be an effective way to kill tumour cells, and currently MPS1 inhibitors that cause massive missegregations are tested in clinical trials for cancer treatment⁶⁶⁻⁷².

Study of CIN in murine models

Mouse models or CIN

Many efforts have been made to gain more knowledge on the role of CIN in tumorigenesis. It has been debated whether CIN is a driver or merely a by-product of tumorigenesis^{24,26}, and the best way to settle this debate is to study the consequences of CIN in murine models, since these are the best representation available for tumour studies. To this end, many genetically modified mouse models for CIN have been generated and studied. Most of these models are based on mutation or knock-out of genes that function at the kinetochore or centrosomes,

in the SAC, MCC, and/or error-correction machinery (table 1). Homozygous knock-outs of the genes used in these mouse models are usually embryonically lethal (hence the heterozygous knock-outs, Table 1), probably due to the severity of CIN. This complicates the assessment of how severe CIN affects tumorigenesis. To allow for higher CIN levels, hypomorphs of *Bub1* and *BubR1*⁷³⁻⁷⁵, double mutants for *CenpE* and *Mad2*⁶³, or overexpression of *Mad2*, *Bub1*, *BubR1* and *Hec1* were generated (Table 1)⁷⁶⁻⁸⁰.

CIN and tumorigenesis in mice

Spontaneous tumorigenesis occurred in mice with impaired *Mad1*, *Mad2*, *Bub1*, *Cdc20*, *CENPE*, *Mps1*, or *Plk1* function, and mice with overexpression of *Hec1*, *Mad2*, *Bub1* or *CyclinB*, albeit with long latencies (table 1). In mice with heterozygous *Plk1* knock-out, or with overexpression of *Hec1* or *CyclinB*, mostly lymphomas and lung and liver tumours were present at 14 months of age, while in *Bub1* hypomorph, *Mad2* overexpression, heterozygous *Cdc20* mutant and heterozygous *AuroraB* knock-out mice, it took 20 months to develop tumours (Table 1). Furthermore, tumour incidence was lower than 30% in *Mad1*, *Mad2*, *CenpE* and *Plk1* mutant mice, but higher than 60% in *Bub1* and *CyclinB* overexpression mice (Table 1). No spontaneous tumours were found in *Bub1* or *Bub3* heterozygous knock out mice (Table 1). Tumours were most likely to develop in lung, liver or spleen and were classified mostly as lymphomas, sarcomas or adenomas (*Plk1*, *Hec1*, *Mad1*, *Mad2*, *CenpE*, *Bub1* and *Cdc20*, Table 1). These results indicate that CIN can drive tumorigenesis, but is not very potent and results strongly vary depending on the mouse model used.

In tumour-prone mice, the effect of CIN was more pronounced in some cases. CIN aggravated tumorigenesis in for example the colon of *Apc*^{Min/+} mice when *Bub1*, *BubR1* or *CyclinB* function was altered^{75,78,85}. In the small intestine however, heterozygosity for *BubR1* caused a decrease in tumour numbers, while *Bub1* mutation did not affect tumorigenesis in this tissue (Table 1). When CIN was combined with carcinogens like DMBA (7,12-dimethylbenz[a]-anthracene), the outcomes were variable as well: *BubR1* overexpression and *AuroraB* and *CenpE* heterozygosity acted tumour suppressive and decreased skin and lung



Table 1: Chromosome segregation in cell division overview of mouse models for CIN based on core components of the SAC, error correction machinery, MCC, and cell cycle regulation

Gene	Alteration	Back-ground	Role	Ploidy/ CIN assay	Spontaneous tumorigenesis	Tumor prone/ carcinogen	Refs
Mad1	HET KO	BALB/c x C57BL/6	SAC	MEF (FISH)	20% - lung - 18-20 months.	x	81
Mad2	HET KO	C57BL/6	SAC, MCC	MEF (spreads)	20% - lung - 18 months.	x	82,83
Mad2	OX	n.s.	SAC MCC	MEF (spreads)	50% - lymphomas lung/liver - 20 months.	<i>Eμ-MYC</i> mutant: increase in lymphomas	76
Bub1	HET KO	129Sv/E x C57BL/6	SAC, EC	MEF, splenocytes (spreads)	no	DMBA treatment on skin of pups: increase in lung tumours, <i>Apc^{Mn/+}</i> ; increase colon tumours	73,75
Bub1	Hypomorph	129Sv/E x C57BL/6	SAC, EC	MEF, splenocytes (spreads)	50% - lymphomas - 20 months.	P53 HET KO: increase in lymphomas PTEN HET KO: decrease in prostate tumours	73,75
Bub1	OX	129Sv/E x C57BL/6	SAC, EC	MEF, Live imaging lymphocytes (spreads)	65% - lymphomas, lipomas, liver - 17 months.	<i>Eμ-MYC</i> mutant, increase in lymphomas	79
BubR1	HET KO	C57BL/6	SAC, EC, MCC	MEF (spreads)	no	Azoxy methane, <i>Apc^{Mn/+}</i> colon tumours, decrease small intestine tumors	74,84,85
BubR1	Hypomorph	C57BL/6	SAC, MCC, EC	MEF (SKY, IF)	No, but aging phenotype	x	74
BubR1	OX	129Sv x C57BL/6	SAC MCC EC	MEF, splenocytes (FISH)	No, but delayed aging	DMBA, KRAS, decrease in skin and lung tumours	80
Cdc20	HET mutant	129Sv x C57BL/6	MCC	MEF (IF)	50% - lymphomas - 24 months	x	86
AuroraB	HET KO	129/Sv x CD1 x C57BL/6J	EC	x	60% - pituitary/liver adenocarcinoma - 24 months.	DMBA/TPA, slight, but not significant decrease in skin tumorigenesis	87
CenpE	HET KO	C57BL/6	KT-MT congress-ion, SAC	MEF (spreads, IF, SKY)	10% - splenic lymphomas - 19-21 months.	Combined with Mad2 HET KO, decrease in splenic lymphomas - DMBA treatment on skin of pups: decrease in lung tumours - p19 (HET) KO, decrease in lymphoma & sarcoma	63,88
Mps1 (specific in T cells)	KT binding domain mut. (HET)	C57BL/6 x 129/Sv D3	SAC EC	aCGH on tumours	50% - lymphomas - 17 months.	P53 HET KO - 100% lymphoma incidence	89
Plk1	HET KO	C57BL/6	SAC Cell cycle	Splenocytes (spreads)	27.5% - lung, lymphoma - 12-17 months.	<i>P53^{-/-}</i> background -100% lymphoma incidence	90
Hec1	OX	n.s.	EC	x	13% - lung - 16 months. 26% - liver - 14 months.	x	77
Bub3	HET KO	n.s.	MCC	MEF (spreads)	no	P53 HET KO: No added effect. RB1 HET KO: No added effect. RAE1 HET KO combined with DMBA treatment on skin of pups, increase in lung tumors	91,92
Cydin B1/2	OX	129Sv x C57BL/6	Cell cycle	MEF (spreads, live imaging)	75% - lung, liver lymphoma - 14 months.	<i>Apc^{Mn/+}</i> , increase in colon tumours - DMBA treatment on skin of pups, increase in skin and lung (B2) tumours	78

HET KO = heterozygous knock-out, OX = overexpression, SAC = spindle assembly checkpoint, MCC = mitotic checkpoint complex, EC = error correction, MEF = mouse embryonic fibroblast, SKY = spectral karyotyping, FISH = Fluorescence in situ hybridisation, n.s. = not specified

tumorigenesis^{80,88}, while DMBA-induced tumorigenesis was enhanced in *Bub1*, *Bub3/Rae1* (lung) and *CyclinB* (lung and skin) mutated mice (Table 1)^(74,75,93,94) Taken together, the above-mentioned studies suggest that CIN could have different impacts depending on tissues, tumour types and genetic backgrounds. But since they vary greatly in their set-up and outcomes it is impossible to draw uniform conclusions on the impact of CIN on tumorigenesis.

Limitations of current models for CIN

The reasons why no conclusive evidence has been found for the role of CIN in tumour development and progression are multiple. As mentioned, the genetic models used so far do not allow the induction of very high CIN levels and use various means (knock-outs, overexpression models) and pathways (error correction, SAC) to induce CIN. Also, CIN levels in the tissues are often unknown since aneuploidy was used as proxy for CIN. Ploidy levels were assessed on chromosome spreads of MEFs and splenocytes mostly, but not in the tumour-developing tissues (Table 1). It is therefore unclear what the level of CIN in the tissues or tumours is, and whether that varies between tissues or the various ways CIN was induced.

Another issue with most genetic models is that germline mutations do not allow for tissue specific expression, nor for control over the moment of CIN induction. This lack of specificity does not only impose problems during development, it also prevents studying how CIN plays a role during various stages of tumorigenesis. So far, it is unclear at which moment during tumorigenesis CIN plays a role and whether this role could change over time. Aberrant chromosome numbers have been found in human early colorectal adenomas, so it is possible that CIN is an early event and may therefore drive tumorigenesis^{95,96}. Still, the extent of aneuploidy increases with tumour progression in various types of cancer, so CIN could have a continuous contribution to tumour progression^{62,95,96}. Timed induction of CIN has been done chemically in mice with an MPS1 inhibitor⁶⁶. However, CIN is induced systemically and levels may vary between tissues depending on how well compounds are absorbed and metabolised. Another way in which timed induction has been accomplished, is by use of tetracycline induced overexpression of genes (for example *HEC1* and *Mad2*), which had the advantage



that the induction was timely and reversible, and in the case of *Mad2*, even cell type specific by use of a type II alveolar epithelial cell-specific doxycycline-inducible transactivator transgene^{77,97}.

Lastly, genetic background can have a major impact on the results of tumour studies in different mouse strains^{98,99}. In the above described published studies, experiments were done in varying genetic backgrounds, e.g. pure C57BL/6, or mixed with 129/SV and CD1, and some studies do not specify which strains were used (Table 1). This poses yet another caveat in reaching uniform conclusions on the impact of CIN in tumorigenesis, since it known that for example, *Apc*^{Min/+} induced tumorigenesis is most prominent in C57BL/6 compared to other strains, while these mice are more resistant to heterozygous p53 knock-out induced mammary tumorigenesis than for example BALB/c mice (reviewed in⁹⁹). Altogether, the current models proved to be insufficient to study the importance of level, onset and location of CIN for tumour development in one model.

Scope of this thesis

As described above, CIN and aneuploidy are key features of tumours. Still their exact role in tumour initiation, progression, and regression remain unclear. So far, major efforts toward clarification of the role of CIN in tumorigenesis have been made by using a variety of mouse models for CIN, but unfortunately, these did not lead to unequivocal answers. Therefore, we have developed an improved mouse model for CIN in which the issues described here can be overcome. We designed the CiMKi (Cre-inducible *Mps1* Knock-in) model, in which various levels of CIN can be induced in a timely and tissue specific manner in the same genetic background. This model is based on conditional knock-in of mutant alleles of *Mps1* that decrease or abolish *Mps1* kinase activity. The Cre-Lox system was used to ensure these mutations are only induced after Cre-mediated recombination. This way, CIN induction can be controlled time and tissue specifically, based on the choice of promoter that drives Cre(ER^{T2}). The studies described in this thesis focused on elucidating the role of various CIN levels in tumour development

and its possible potential for tumour treatment. For this, we performed tumour studies in mice, which were supported by *ex-vivo* experiments using organoids derived from these mice.

Organoids are a 3D culturing system that was recently developed where stem cells from tissues or tumours form tissue-like structures and therefore mimics tumours and tissues better than 2D cell lines^{100,101}. Importantly, the 3D context has been associated with improved mitotic fidelity over 2D systems, which is a great advantage when studying CIN¹⁰². The resemblance with their tissue of origin is reflected by the specific need of niche factors these organoids need for growing. Colon organoids depend on Wnt3a and its ligand R-spondin due to the absence of Wnt producing Paneth cells in colon (organoids). Since these cells are present in (organoid derived from) small intestine, Wnt3a is not needed to culture these organoids. Finally, Wnt3a and R-spondin are dispensable for growing intestinal tumour organoids, since the Apc LOH ensures continuous activation of the Wnt pathway¹⁰³⁻¹⁰⁵, similar to tumours. By using organoids, we were able to assess CIN levels in our tissues of interest in real time. With that, we could assess if CIN levels induced by the same mutations were the same in different tissues, and whether CIN levels were different between healthy or tumor tissue. The reproducible method by which various CIN levels could be induced in small intestine adenoma organoids made it possible to set up a CIN-based drug screen. Our accurate assessment of effects of various CIN levels shows that the level, tissue and moment of CIN induction are important for the effect on tumour development and regression, and on drug sensitivity.

Outline of this thesis

1

In **chapter 2** I describe the CiMKi model for controlled induction of CIN and the first novel findings using this model. We first validated that the induction of the Mps1 mutants indeed led to a range of CIN, which was reproducible in various MEFs, intestinal organoids and *in-situ*. We next found that certain levels of CIN caused very early onset, spontaneous tumorigenesis, and that moderate to high CIN levels had strong, but distinct effects on intestinal tumorigenesis in *Apc^{Min/+}* mice. In this chapter, VillinCre mice were used to express Cre recombinase, which induced CIN from 12.5 dpc. We followed up on our findings in *Apc^{Min/+}* mice, which is described in an **appendix of chapter 2**, by using VillinCreER^{T2} mice in which Cre recombinase is activated after tamoxifen addition. This thus allowed to choose the moment of CIN induction. We found that the most prominent effect of CIN on intestinal tumorigenesis was achieved when induced before tumour onset. A downside of studying CIN in internal organs is that it is very difficult to follow tumour development or regression over time. Therefore, we also examined the effects of various CIN levels in another cancer type that is highly aneuploid in humans, skin cancer. **Chapter 3** focusses on unravelling the impact of CIN in a classical chemical two-stage skin carcinogenesis model. CIN induction before tumour onset caused differential effects on tumour onset and growth rate, dependent on CIN level. We further showed that induction of moderate to very high CIN in tumours caused almost immediate tumour regression, followed by fast relapses. The results from chapter 3, combined with the proposition that CIN could serve as potential anti-tumour therapy^{60,64,65}, resulted in a drug screen as described in **chapter 4**, in which we sought for synergy between (specific levels of) CIN and chemotherapeutic drugs in mouse small intestinal adenoma organoids. We optimised small scale screening methods, and while taxanes synergised with CIN in mouse adenoma organoids, these findings did not extend to human CRC organoids, high-lighting the challenges in using CIN levels as a predictor of killing potential of anti-cancer drugs in human tumours. Finally, in **chapter 5**, the results described in this thesis are summarised and discussed in the light of current literature, and this thesis will be concluded with recommendations for future experiments to further assess the role of CIN in tumour development, progression and treatment.

References

1. Hanahan, D. & Weinberg, R. A. The Hallmarks of Cancer. 1-14 (1999).
2. Hanahan, D. & Weinberg, R. A. Hallmarks of Cancer: The Next Generation. *Cell* **144**, 646-674 (2011).
3. Salk, J. ., Fox, E. . & Loeb, L. A. Mutational Heterogeneity in Human Cancers: Origin and Consequences. *Annu. Rev. Pathol. Mech. Dis.* **5**, 51-75 (2010).
4. Martincorena, I. et al. Universal Patterns of Selection in Cancer and Somatic Tissues. *Cell* **171**, 1029-1041.e21 (2017).
5. Alexandrov, L. B. et al. Signatures of mutational processes in human cancer. *Nature* **500**, 415-421 (2013).
6. Pfeifer, G. P. & Besaratinia, A. Mutational spectra of human cancer. *Hum. Genet.* **125**, 493-506 (2009).
7. Phillips, D. H. Mutational spectra and mutational signatures: Insights into cancer aetiology and mechanisms of DNA damage and repair. *DNA Repair (Amst)* **71**, 6-11 (2018).
8. Li, S., Balmain, A. & Counter, C. M. A model for RAS mutation patterns in cancers: finding the sweet spot. *Nat. Rev. Cancer* **18**, 767-777 (2018).
9. Irminger-Finger, I., Siegel, B. D. & Leung, W. C. The functions of breast cancer susceptibility gene 1 (BRCA1) product and its associated proteins. *Biol. Chem.* **380**, 117-128 (1999).
10. Zhang, X. et al. Attenuation of RNA polymerase II pausing mitigates BRCA1-associated R-loop accumulation and tumorigenesis. *Nat. Commun.* **8**, 1-11 (2017).
11. Kinzler, K. W. & Vogelstein, B. Lessons from Hereditary Colorectal Cancer. **87**, 159-170 (1996).
12. Hussain, S. P. & Harris, C. C. Molecular epidemiology of human cancer: Contribution of mutation spectra studies of tumor suppressor genes. *Cancer Res.* **58**, 4023-4037 (1998).
13. Fearon, E. R. & Vogelstein, B. A genetic model for colorectal tumorigenesis. *Cell* **61**, 759-767 (1990).
14. Fodde, R., Smits, R. & Clevers, H. APC, signal transduction and genetic instability in colorectal cancer. *Nat. Rev. Cancer* **1**, 55-67 (2001).
15. Cho, K. R. & Vogelstein, B. Genetic Alterations in the Adenoma- Carcinoma Sequence. *Cancer* **70**, 1727-1731 (1992).
16. Pino, M. S. & Chung, D. C. The Chromosomal Instability Pathway in Colon Cancer. *Gastroenterology* **138**, 2059-2072 (2010).
17. Samuels, Y. et al. High Frequency of Mutations of the PIK3CA Gene in Human Cancers. *Science (80-)*. **304**, 554 (2004).
18. Leystra, A. A. et al. Mice expressing activated PI3K rapidly develop advanced colon cancer. *Cancer Res.* **72**, 2931-2936 (2012).
19. Muñoz, N. M. et al. Transforming growth factor receptor type II inactivation induces the malignant transformation of intestinal neoplasms initiated by Apc mutation. *Cancer Res.* **66**, 9837-9844 (2006).
20. Pehesse, T. J., Durban, V. M. & Sansom, O. J. Defining key concepts of intestinal and epithelial cancer biology through the use of mouse models. *Carcinogenesis* **38**, 953-965 (2017).
21. Ellis, L., Atadja, P. W. & Johnstone, R. W. Epigenetics in cancer: Targeting chromatin modifications. *Mol. Cancer Ther.* **8**, 1409-1420 (2009).
22. Santaguida, S. & Amon, A. Short - and long-term effects of chromosome mis-segregation and aneuploidy. **16**, 473-485 (2015).
23. Kops, G. J. P. L., Weaver, B. A. A. & Cleveland, D. W. On the road to cancer: aneuploidy and the mitotic checkpoint. *Nat. Rev. Cancer* **5**, 773-785 (2005).
24. Gordon, D. J., Resio, B. & Pellman, D. Causes and consequences of aneuploidy in cancer. *Nat. Rev. Genet.* **13**, 189-203 (2012).
25. Orr, B., Godek, K. M. & Compton, D. Aneuploidy. *Curr. Biol.* **25**, R538-R542 (2015).
26. Weaver, B. A. & Cleveland, D. W. Does aneuploidy cause cancer? *Curr. Opin. Cell Biol.* **18**, 658-667 (2006).
27. Knouse, K. A., Wu, J., Whittaker, C. A. & Amon, A. Single cell sequencing reveals low levels of aneuploidy across mammalian tissues. *Proc. Natl. Acad. Sci.* **111**, 13409-13414 (2014).
28. Cohen, J. Sorting out chromosome errors. *Science (80-)*. **296**, 2164-2166 (2002).
29. Duijf, P. H. G., Schultz, N. & Benezra, R. Cancer cells preferentially lose small chromosomes. *Int. J. Cancer* **132**, 2316-2326 (2012).
30. Pachis, S. T. & Kops, G. J. P. L. Leader of the SAC: Molecular mechanisms of Mps1/TTK regulation in mitosis. *Open Biol.* **8**, (2018).
31. Sacristan, C. & Kops, G. J. P. L. Joined at the hip: kinetochores, microtubules, and spindle assembly checkpoint signaling. *Trends Cell Biol.* **25**, 21-28 (2015).
32. Jelluma, N. et al. Chromosomal Instability by Inefficient Mps1 Auto-Activation Due to a Weakened Mitotic Checkpoint and Lagging Chromosomes. *PLoS One* **3**, e2415 (2008).
33. Etemad, B. & Kops, G. J. Attachment issues: kinetochore transformations and spindle checkpoint



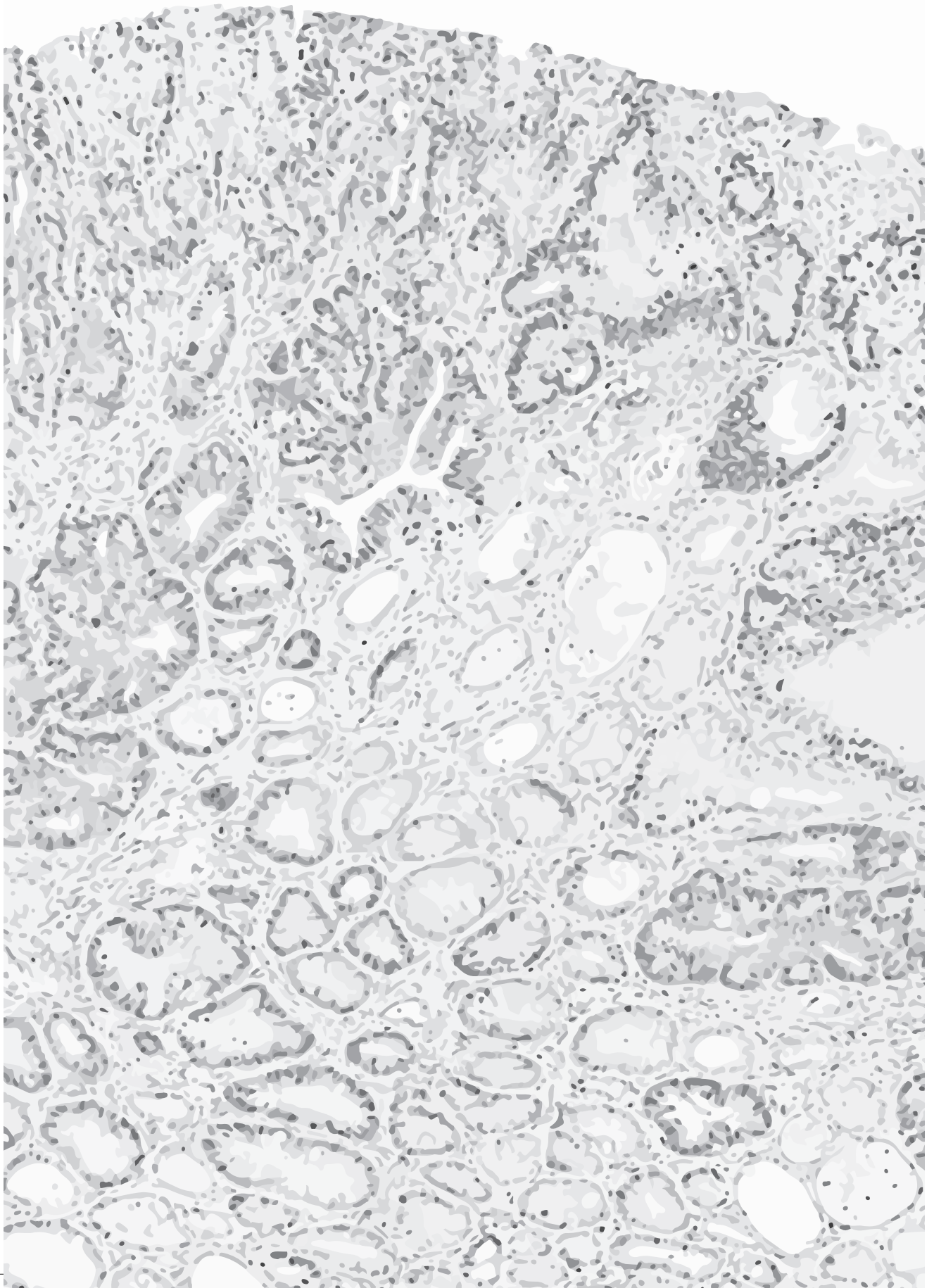
- silencing. *Curr. Opin. Cell Biol.* **39**, 101-108 (2016).
34. Carmena, M., Wheelock, M., Funabiki, H. & Earnshaw, W. C. The chromosomal passenger complex (CPC): From easy rider to the godfather of mitosis. *Nat. Rev. Mol. Cell Biol.* **13**, 789-803 (2012).
 35. Santaguida, S. et al. Chromosome Mis-segregation Generates Cell-Cycle-Arrested Cells with Complex Karyotypes that Are Eliminated by the Immune System. *Dev. Cell* **41**, 638-651.e5 (2017).
 36. Michel, L. et al. Complete loss of the tumor suppressor MAD2 causes premature cyclin B degradation and mitotic failure in human somatic cells. *Proc. Natl. Acad. Sci. U. S. A.* **101**, 4459-4464 (2004).
 37. Kops, G. J. P. L., Foltz, D. R. & Cleveland, D. W. Lethality to human cancer cells through massive chromosome loss by inhibition of the mitotic checkpoint. 1-6 (2004).
 38. Sheltzer, J. M. & Amon, A. The aneuploidy paradox: costs and benefits of an incorrect karyotype. *Trends Genet.* **27**, 446-453 (2011).
 39. Roylance, R. et al. Relationship of Extreme Chromosomal Instability with Long-term Survival in a Retrospective Analysis of Primary Breast Cancer. *Cancer Epidemiol. Biomarkers Prev.* **20**, 2183-2194 (2011).
 40. Torres, E. M. et al. Identification of Aneuploidy-Tolerating Mutations. *Cell* **143**, 71-83 (2010).
 41. Tomasini, R., Mak, T. W. & Melino, G. The impact of p53 and p73 on aneuploidy and cancer. *Trends Cell Biol.* **18**, 244-252 (2008).
 42. Crasta, K. et al. DNA breaks and chromosome pulverization from errors in mitosis. *Nature* **482**, 53-58 (2012).
 43. Stephens, P. J. et al. Massive genomic rearrangement acquired in a single catastrophic event during cancer development. *Cell* **144**, 27-40 (2011).
 44. Bunting, S. F. & Nussenzweig, A. End-joining, translocations and cancer. *Nat. Rev. Cancer* **13**, 443-454 (2013).
 45. Janssen, A., van der Burg, M., Suzhai, K., Kops, G. J. P. L. & Medema, R. H. Chromosome Segregation Errors as a Cause of DNA Damage and Structural Chromosome Aberrations. *Science (80-.)*. **333**, 1895-1898 (2011).
 46. Jamal-Hanjani, M. et al. Tracking the Evolution of Non-Small-Cell Lung Cancer. *N. Engl. J. Med.* **376**, 2109-2121 (2017).
 47. Bakhroum, S. F. et al. Chromosomal instability drives metastasis through a cytosolic DNA response. *Nature* **553**, 467-472 (2018).
 48. Lee, A. J. X. et al. Chromosomal Instability Confers Intrinsic Multi-Drug Resistance. *Cancer Res.* **71**, 1858-1870 (2011).
 49. McClelland, S. E., Burrell, R. A. & Swanton, C. Chromosomal instability: A composite phenotype that influences sensitivity to chemotherapy. *Cell Cycle* **8**, 3262-3266 (2009).
 50. Orsetti, B. et al. Impact of chromosomal instability on colorectal cancer progression and outcome. *BMC Cancer* **14**, 1-13 (2014).
 51. Walther, A., Houlston, R. & Tomlinson, I. Association between chromosomal instability and prognosis in colorectal cancer: A meta-analysis. *Gut* **57**, 941-950 (2008).
 52. Choi, C. M. et al. Chromosomal instability is a risk factor for poor prognosis of adenocarcinoma of the lung: Fluorescence in situ hybridization analysis of paraffin-embedded tissue from Korean patients. *Lung Cancer* **64**, 66-70 (2009).
 53. Carter, S. L., Eklund, A. C., Kohane, I. S., Harris, L. N. & Szallasi, Z. A signature of chromosomal instability inferred from gene expression profiles predicts clinical outcome in multiple human cancers. *Nat. Genet.* **38**, 1043-1048 (2006).
 54. Birkbak, N. J. et al. Paradoxical relationship between chromosomal instability and survival outcome in cancer. *Cancer Res.* **71**, 3447-3452 (2011).
 55. Guinney, J. et al. The consensus molecular subtypes of colorectal cancer. *Nat. Med.* **21**, 1350-1356 (2015).
 56. Robinson, J. K., Rademaker, A. W., Ph, D., Goolsby, C. & Zoladz, C. DNA Ploidy in Nonmelanoma Skin Cancer. 284-291 (1996).
 57. Aldaz, C. M., Conti, C. J., Klein-szanto, A. J. P. & Slaga, T. J. Progressive dysplasia and aneuploidy are hallmarks of mouse skin papillomas: Relevance to malignancy (cancer/tumor. **84**, 2029-2032 (1987).
 58. Bakhroum, S. F. & Cantley, L. C. The Multifaceted Role of Chromosomal Instability in Cancer and Its Microenvironment. *Cell* **174**, 1347-1360 (2018).
 59. Simonetti, G., Bruno, S., Padella, A., Tenti, E. & Martinelli, G. Aneuploidy: cancer strength or vulnerability. *Int. J. Cancer* (2018).
 60. Shaikat, Z. et al. Chromosomal instability causes sensitivity to metabolic stress. *Oncogene* **34**, 4044-4055 (2015).
 61. Ohashi, A. et al. Aneuploidy generates proteotoxic stress and DNA damage concurrently with p53-mediated post-mitotic apoptosis in SAC-impaired cells. *Nat. Commun.* **6**, 1-16 (2014).

62. Ried, T. et al. The consequences of chromosomal aneuploidy on the transcriptome of cancer cells. *Biochim. Biophys. Acta - Gene Regul. Mech.* **1819**, 784–793 (2012).
63. Silk, A. D. et al. Chromosome missegregation rate predicts whether aneuploidy will promote or suppress tumors. *Proc. Natl. Acad. Sci.* **110**, E4134–E4141 (2013).
64. Janssen, A., Kops, G. J. P. L. & Medema, R. H. Elevating the frequency of chromosome missegregation as a strategy to kill tumor cells. *PNAS* **106**, 1–6 (2009).
65. Burrell, R. A. et al. Targeting chromosomal instability and tumour heterogeneity in HER2-positive breast cancer. *J. Cell. Biochem.* **111**, 782–790 (2010).
66. Maia, A. R. R. et al. Inhibition of the spindle assembly checkpoint kinase TTK enhances the efficacy of docetaxel in a triple-negative breast cancer model. *Ann. Oncol.* **26**, 2180–2192 (2015).
67. Wengner, A. M. et al. Novel Mps1 Kinase Inhibitors with Potent Antitumor Activity. *Mol. Cancer Ther.* **15**, 583–592 (2016).
68. Colombo, R. et al. Targeting the Mitotic Checkpoint for Cancer Therapy with NMS-P715, an Inhibitor of MPS1 Kinase. *Cancer Res.* **70**, 10255–10264 (2010).
69. Maia, A. R. R. et al. Mps1 inhibitors synergise with low doses of taxanes in promoting tumour cell death by enhancement of errors in cell division. *Br. J. Cancer* **118**, 1586–1595 (2018).
70. Jemaã, M. et al. Characterization of novel MPS1 inhibitors with preclinical anticancer activity. *Cell Death Differ.* **20**, 1532–1545 (2013).
71. Tannous, B. A., Kerami, M., Van der Stroop, P. M. & al, et. effects of the Selective MPS1 inhibitor MPS1-IN-3on Glioblastoma Sensitivity to Antimitotic Drugs. 1–10 (2013).
72. Swanton, C. et al. Chromosomal instability determines taxane response. *Proc. Natl. Acad. Sci. U. S. A.* **106**, 8671–8676 (2009).
73. Jeganathan, K., Malureanu, L., Baker, D. J., Abraham, S. C. & van Deursen, J. M. Bub1 mediates cell death in response to chromosome missegregation and acts to suppress spontaneous tumorigenesis. *J. Cell Biol.* **179**, 255–267 (2007).
74. Baker, D. J. et al. BubR1 insufficiency causes early onset of aging-associated phenotypes and infertility in mice. **36**, 744–749 (2004).
75. Baker, D. J., Jin, F., Jeganathan, K. B. & van Deursen, J. M. Whole Chromosome Instability Caused by Bub1 Insufficiency Drives Tumorigenesis through Tumor Suppressor Gene Loss of Heterozygosity. *Cancer Cell* **16**, 475–486 (2009).
76. Sotillo, R. et al. Mad2 Overexpression Promotes Aneuploidy and Tumorigenesis in Mice. *Cancer Cell* **11**, 9–23 (2007).
77. Díaz-Rodríguez, E., Sotillo, R., Schwartzman, J.-M. & Benezra, R. Hec1 overexpression hyperactivates the mitotic checkpoint and induces tumor formation in vivo. *Proc. Natl. Acad. Sci. U. S. A.* **105**, 16719–24 (2008).
78. Nam, H. J. & Van Deursen, J. M. Cyclin B2 and p53 control proper timing of centrosome separation. *Nat. Cell Biol.* **16**, 535–546 (2014).
79. Ricke, R. M., Jeganathan, K. B. & Deursen, J. M. Van. Bub1 overexpression induces aneuploidy and tumor formation through Aurora B kinase hyperactivation. **193**, (2011).
80. Baker, D. J. et al. Increased expression of BubR1 protects against aneuploidy and cancer and extends healthy lifespan. *Nat. Cell Biol.* **15**, 96–102 (2013).
81. Iwanaga, Y. et al. Heterozygous deletion of mitotic arrest-deficient protein 1 (MAD1) increases the incidence of tumors in mice. *Cancer Res.* **67**, 160–166 (2007).
82. Dobles, M., Liberal, V., Scott, M. L., Benezra, R. & Sorger, P. K. Chromosome missegregation and apoptosis in mice lacking the mitotic checkpoint protein Mad2. *Cell* **101**, 635–645 (2000).
83. Michel, L. S. et al. MAD2 haplo-insufficiency causes premature anaphase and chromosome instability in mammalian cells. *Nature* **409**, 355–359 (2001).
84. Dai, W. et al. Slippage of Mitotic Arrest and Enhanced Tumor Development in Mice with BubR1 Haploinsufficiency. *Cancer Res.* **64**, 440 LP-445 (2004).
85. Rao, C. V et al. Colonic tumorigenesis in BubR1^{+/-} ApcMin^{+/+} compound mutant mice is linked to premature separation of sister chromatids and enhanced genomic instability. 1–6 (2005).
86. Li, M., Fang, X., Wei, Z., York, J. P. & Zhang, P. Loss of spindle assembly checkpoint-mediated inhibition of Cdc20 promotes tumorigenesis in mice. *J. Cell Biol.* **185**, 983–994 (2009).
87. Fernandez-Miranda, G. et al. Genetic disruption of aurora B uncovers an essential role for aurora C during early mammalian development. *J. Cell Sci.* **124**, e1–e1 (2011).
88. Weaver, B. A. A., Silk, A. D., Montagna, C., Verdier-Pinard, P. & Cleveland, D. W. Aneuploidy acts both oncogenically and as a tumor suppressor. *Cancer Cell* **11**, 25–36 (2007).
89. Foijer, F. et al. Chromosome instability induced by Mps1 and p53 mutation generates aggressive lymphomas exhibiting aneuploidy-induced stress. *Proc. Natl. Acad. Sci.* **111**, 13427–13432 (2014).
90. Lu, L.-Y. et al. Polo-Like Kinase 1 Is Essential for Early Embryonic Development and Tumor Suppression. *Mol. Cell. Biol.* **28**, 6870–6876 (2008).
91. Kalitsis, P. et al. Increased chromosome instability but not cancer predisposition in



- haploinsufficient Bub3 mice. *Genes Chromosom. Cancer* **44**, 29–36 (2005).
92. Baker, D. J. et al. Early aging-associated phenotypes in Bub3/Rae1 haploinsufficient mice. *J. Cell Biol.* **172**, 529–540 (2006).
93. Jeganathan, K., Malureanu, L., Baker, D. J., Abraham, S. C. & Van Deursen, J. M. Bub1 mediates cell death in response to chromosome missegregation and acts to suppress spontaneous tumorigenesis. *J. Cell Biol.* **179**, 255–267 (2007).
94. Babu, J. R. et al. Rae1 is an essential mitotic checkpoint regulator that cooperates with Bub3 to prevent chromosome missegregation. **2**, 341–353 (2003).
95. Borrás, E. et al. Genomic Landscape of Colorectal Mucosa and Adenomas. *cancer Prev. Res.* 417–428 (2016).
96. Shih, I. et al. Evidence That Genetic Instability Occurs at an Early Stage of Colorectal Tumorigenesis. *Cancer Res.* **61**, 818–822 (2001).
97. Sotillo, R., Schwartzman, J. M., Socci, N. D. & Benzra, R. Mad2-induced chromosome instability leads to lung tumour relapse after oncogene withdrawal. *Nature* **464**, 436–440 (2010).
98. Moser, A. R., Dove, W. F., Roth, K. A. & Gordon, J. I. The Min (multiple intestinal neoplasia) mutation: Its effect on gut epithelial cell differentiation and interaction with a modifier system. *J. Cell Biol.* **116**, 1517–1526 (1992).
99. Reilly, K. M. The effects of genetic background of mouse models of cancer: Friend or foe? *Cold Spring Harb. Protoc.* **2016**, 227–233 (2016).
100. Liu, Y. & Chen, Y.-G. 2D- and 3D-Based Intestinal Stem Cell Cultures for Personalized Medicine. *Cells* **7**, 225 (2018).
101. van de Wetering, M. et al. Prospective Derivation of a Living Organoid Biobank of Colorectal Cancer Patients. *Cell* **161**, 933–945 (2015).
102. Knouse, K. A., Lopez, K. E., Bachofner, M. & Amon, A. Chromosome Segregation Fidelity in Epithelia Requires Tissue Architecture. *Cell* **175**, 200–211.e13 (2018).
103. Sato, T. et al. Long-term Expansion of Epithelial Organoids From Human Colon, Adenoma, Adenocarcinoma, and Barrett's Epithelium. *YGAST* **141**, 1762–1772 (2011).
104. Drost, J. et al. Sequential cancer mutations in cultured human intestinal stem cells. *Nature* **521**, 43–47 (2015).
105. Leedham, S. J. et al. A basal gradient of Wnt and stem-cell number influences regional tumour distribution in human and mouse intestinal tracts. *Gut* **62**, 83–93 (2013).





Chapter 2

Degree and site of chromosomal instability define its oncogenic potential

W.H.M. Hoevenaar ¹, A. Janssen ^{2,#} A.I. Quirindongo ^{1,#}, H. Ma ^{3,#}, S. Klaasen ¹, A. Teixeira ¹, G.J.A. Offerhaus ³, R.H. Medema ⁴, N. Jelluma ^{1,\$,*}, G.J.P.L. Kops ^{1,\$}

¹Oncode Institute, Hubrecht Institute-KNAW and University Medical Center Utrecht, Utrecht, The Netherlands.

²University Medical Center Utrecht, Center for Molecular Medicine, Section Molecular Cancer Research, Utrecht, The Netherlands

³University Medical Center Utrecht, Department of Pathology, Utrecht, The Netherlands

⁴Oncode Institute, Division of Cell Biology, Netherlands Cancer Institute, Amsterdam, The Netherlands

These authors contributed equally to this work

\$ Joint senior authors

*Corresponding author: n.jelluma@hubrecht.eu

Abstract

Most human cancers are aneuploid, due to a chromosomal instability (CIN)¹⁻³ phenotype. CIN can lead to genome destabilization and is associated with genomic heterogeneity and immune evasion⁴⁻¹¹. Despite being hallmarks of cancer, however, the roles of CIN and aneuploidy in tumour formation have not unequivocally emerged from animal studies. CIN can both promote and suppress tumorigenesis¹²⁻²⁸ but variances in mechanisms and timings of CIN induction in different oncogenic backgrounds and associated tissues limit interpretation of the contributions of CIN. We here present a novel conditional mouse model for induction of diverse degrees of CIN, from very low to very high, allowing direct comparisons between different CIN levels and their impacts on distinct tissues. We find for the first time that CIN can drive early onset tumour formation, as a particular range of CIN induces intestinal adenomas within 12 weeks. In *Apc*^{Min/+} mice, moderate and high CIN cause remarkable tumour burden of the distal colon and loss of heterozygosity without whole chromosome 18 loss, resembling human disease. By contrast, high CIN does not promote tumour formation in the small intestine, and correspondingly, colonic crypts of high CIN mice at the time of tumour initiation more readily maintain aberrant proliferative cells than those of the small intestine. Our model enables interrogation in distinct tissues of the contributions of CIN to tumour formation and of the feasibility of inducing CIN as a therapeutic strategy.

Introduction and results

Aneuploidy is associated with poor patient outcome¹, and the underlying CIN phenotype promotes metastases^{8,29}. The role of CIN in the formation of tumours is however unclear. Mouse models of CIN have occasionally shown sporadic, spontaneous tumours with very long latency (>12-18 months)^{12,14,17,20,22-24,28,30}, suggesting CIN is not a potent cancer driver. In mice predisposed to cancer, CIN is either neutral^{13,21,27}, promotes tumour formation^{15,16,18,20,21,25,26,28,30}, or, in some conditions, suppresses it^{12,13,18,21}. This may be related to CIN levels reached in the

various conditions, but comparisons between studies is exceedingly difficult due to the use of different oncogenic backgrounds and tissues examined, as well as differences in the manner and time by which the tissues are exposed to CIN. Moreover, technical limitations often precluded direct measurements of CIN in the relevant tissues. We therefore sought to establish a genetic model that allows controlled induction of various degrees of CIN in a tissue-specific manner. To this end, we created mouse strains carrying a conditional T649A or D637A mutation in the spindle assembly checkpoint kinase *Mps1*, which in human cell lines caused mild or severe CIN, respectively³¹ (Fig. 1a, b, S1a-c). We reasoned that combining these Cre-inducible *Mps1* knock-in (*CiMKi*) alleles (together and with wild-type *Mps1*) would result in an allelic series of CIN, ranging from very low (few missegregations with mostly mild errors) to very high (many missegregations with mostly severe errors).

CiMKi mice were born healthy and at Mendelian ratios. Activation of Cre recombinase by addition of 4-hydroxytamoxifen (4-OHT) to mouse embryonic fibroblasts (MEFs) from *CiMKi;Rosa26-CreER^{T2}* mice resulted in efficient recombination and expression of mutant *Mps1* mRNA (Fig. S1d), from which mutant *Mps1* protein was translated to comparable levels as wild-type protein (Fig. S1e). As expected, the allelic series caused graded reductions in *Mps1* activity, as evidenced by acceleration of mitosis after mutant induction³² (Fig. 1c) and reduced Mad1 levels at kinetochores³³ (Fig. S1f). Time-lapse microscopy of 4-OHT-treated immortalized MEFs and small intestinal organoids showed a striking increase in mitotic errors with diminishing *Mps1* kinase activities (Fig. 1d, e, Movie S1, S2), verifying the predicted phenotypes of the allelic series. As expected, induced CIN resulted in increased aneuploidy in primary MEFs (Fig. S1g). Mutant induction also occurred efficiently *in vivo* in four-week old *CiMKi;Rosa26-CreRT2* mice (Fig. S1h), and analysis of anaphase figures in intestinal tissue sections showed that the expected range of CIN was induced (Fig. 1f). We thus conclude that the *CiMKi* mouse model enables spatio-temporal control of a range of CIN *in vivo*.

Whole-body mutant inductions in *CiMKi;Rosa26-CreER^{T2}* mice disrupted small intestinal tissue organization (Fig. 2a). The extent of disorganization

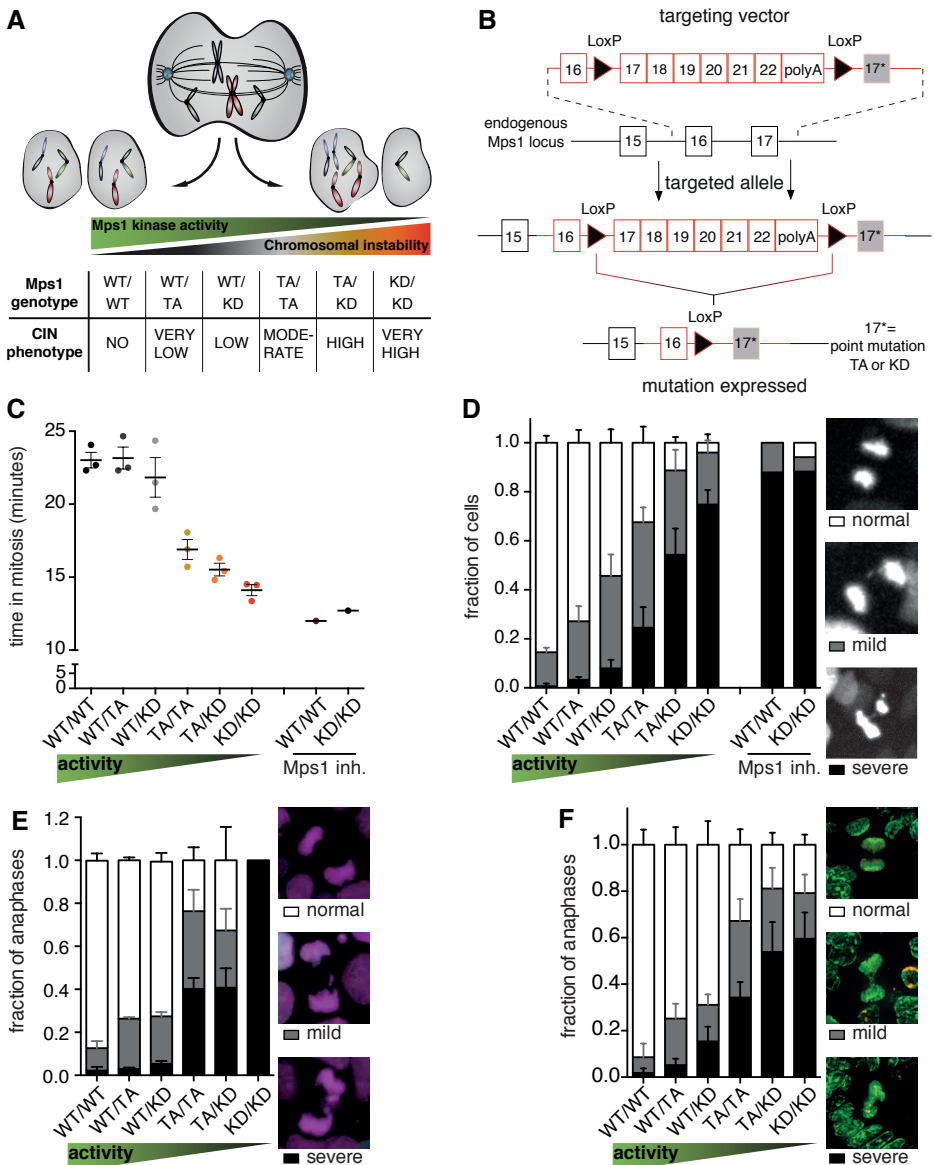


Figure 1. An allelic series for graded increases in CIN in vivo. **a**, Scheme showing the theoretical inverse correlation of decreased function of the spindle assembly checkpoint (by genetically reduced Mps1 activities) with increased severity of CIN. **b**, Schematic overview of generation and activation of the CiMKi alleles: the targeting vectors harbour a cDNA cassette of WT exons 17-22, that is flanked by lox-P sites, and the mutated exon 17 (TA or KD, indicated with an asterisk) in the right homologous recombination arm. In the targeted CiMKi alleles, wild-type Mps1 is replaced with mutant Mps1 upon Cre-mediated loxP recombination. **c**, Quantification of time in mitosis (prophase to anaphase) by time lapse imaging of immortalized MEFs of the CiMKi;Rosa26-CreERT2 genotypes 56 hours after 4-OHT addition. Mps1 inhibitor CPD5 was used as control. Error bars indicate \pm SEM of three independent MEF lines per genotype; 50 cell divisions per line). **d**, Quantification of chromosome segregation fidelity by time lapse imaging of

Legend continues on next page

Continued from previous page. *Mps1* inhibitor CPD5 was used as control. DNA was visualized by H2B-mNeon. Segregations were scored as indicated; images depict examples. Error bars as in c. See also supplemental movies 1. e, As d, but in small intestinal organoids of *CiMKi;Villin-CreERT2* mice, 56 hours after 4-OHT. Missegregations were quantified in three independent experiments. WT/WT group includes ethanol controls of other genotypes (425 divisions over 44 organoids). Error bars indicate \pm SEM of three independent experiments; ((113 - 202 cell divisions per line, except for TA/KD (39 divisions in 14 of the 52 organoids imaged) and KD/KD (4 divisions over 5 of the 43 organoids imaged) which did not divide or died after 4-OHT). See also supplemental movies 2. f, Quantification of chromosome segregation fidelity in situ in small intestine of *CiMKi;Rosa26-CreERT2* mice one week after tamoxifen injection. DAPI (green) and anti-H3S10ph (red) were used to identify mitotic nuclei. Graph shows quantification by category as in d and e, for at least 47 anaphases per small intestine. Error bars indicate \pm SEM (n=3-12 mice per genotype, WT/WT group includes oil controls of other genotypes).

correlated with the degree of CIN and likely explained the severe weight loss seen in mice with high and very high CIN (Fig. S2a). To study early CIN induction in the intestine without adverse effects on other organs, we generated *CiMKi;Villin-Cre* mice to enable mutant induction specifically in the intestinal tract from 12.5 days post coitum (dpc)³⁴. Although all *CiMKi;Villin-Cre* mice were overtly healthy (Fig. S2b), moderate CIN had caused one or more adenomas in the small intestine of two-thirds (4/6) of the mice by as early as 12 weeks of age (Fig 2b, c). These adenomas were positive for nuclear β -catenin, showing that CIN was sufficient to induce constitutive Wnt pathway activation (Fig. 2d). To our knowledge, this is the first report of early onset, spontaneous tumorigenesis as a result of CIN. By the age of eight months, a wider range of CIN had caused increases in spontaneous adenomas (Fig. 2e, f), further underscoring a role for CIN in tumour initiation. In line with what we observed at 12 weeks, the strongest effect was again found in mice with moderate CIN.

Human colorectal cancers (CRCs) are often aneuploid³⁵, and the vast majority is caused by loss-of-function mutations in genes of Wnt pathway components such as *APC*^{36,37}. Moreover, loss of heterozygosity (LOH) of *APC* causes extensive polyp growths in patients with familial adenomatous polyposis coli (FAP) syndrome^{38,39}. To examine the impact of CIN on a tissue predisposed to cancer, we next investigated mice carrying a mutant *Apc* allele (*Apc*^{Min/+}). These mice normally develop \pm 30 adenomas in the small intestine and no or very few in the colon⁴⁰. Note that the expected degrees of CIN in this tissue in *CiMKi* mice were directly verified by live imaging of small intestinal organoids and supported by

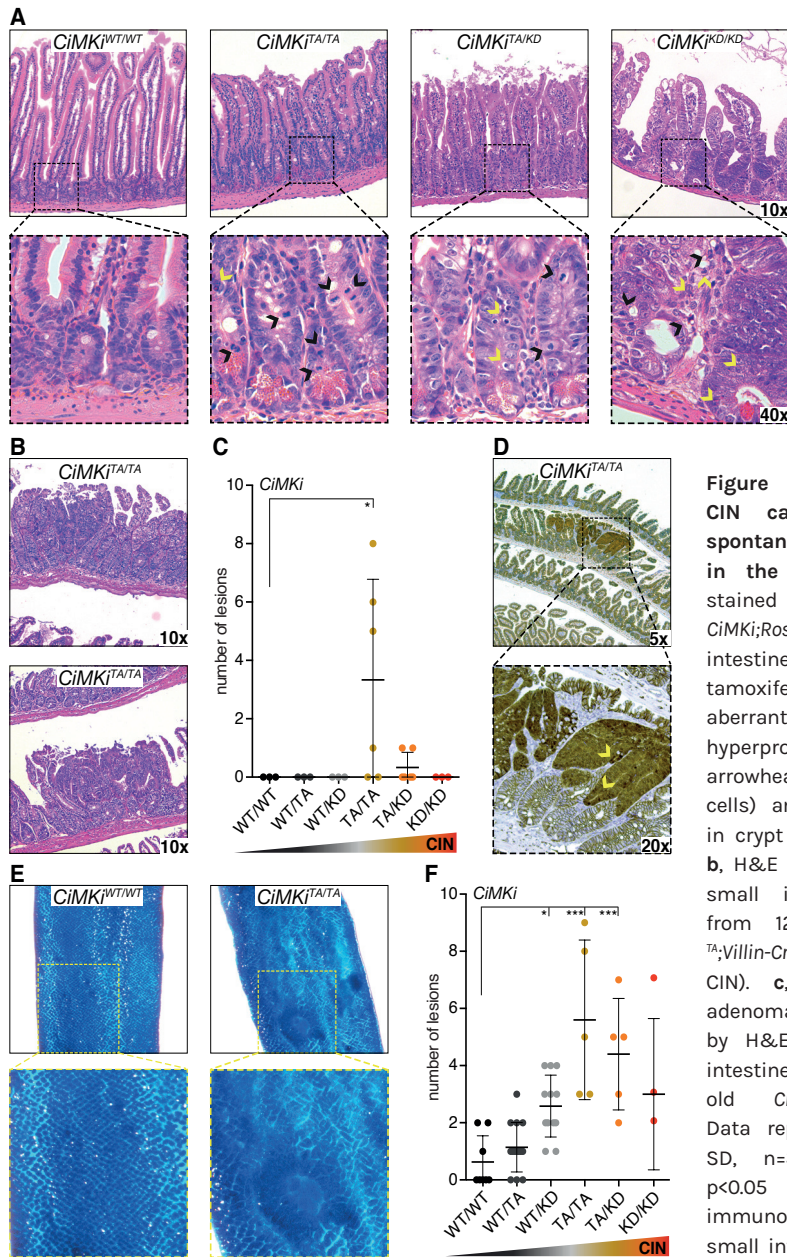


Figure 2: Moderate CIN causes early onset spontaneous tumorigenesis in the intestine. **a**, H&E stained sections of *CiMKi*;*Rosa26CreER*^{T2} small intestines one week after tamoxifen injection, showing aberrant crypt and cell size, hyperproliferation (black arrowheads indicate mitotic cells) and apoptotic bodies in crypt (yellow arrowheads). **b**, H&E stained examples of small intestine adenomas from 12-week old *CiMKi*^{TA/TA};*Villin-Cre* mice (moderate CIN). **c**, Quantification of adenomas as determined by H&E staining in small intestine tissue in of 12-week-old *CiMKi*;*Villin-Cre* mice. Data represents mean \pm SD, n=3-6 per genotype. p<0.05 (*). **d**, β -catenin immunohistochemistry on small intestine lesions in 12-

week old *CiMKi*^{TA/TA};*Villin-Cre* mice. Arrowheads indicate nuclear B-catenin in lesion. **e**, Examples of methylene blue stained, formalin-fixed whole mount small intestine at 8 months of *CiMKi*;*Villin-Cre* mice. Zoom boxes indicate normal (WT/WT) and aberrant (TA/TA) mucosa. **f**, Quantification of lesions as determined on whole mount methylene blue staining in small intestine of 8-month-old *CiMKi*;*Villin-Cre* mice. Data represents mean \pm SD (N=3-14 per genotype), asterisk indicate significance (one-tailed t-test, comparing each group to WT/WT, p<0.001 (***), p<0.005 (**), p<0.05 (*)).

in situ analyses (see Fig. 1e, f). In contrast to *CiMKi;Villin-Cre* mice, very high CIN in the *Apc^{Min/+}* background (*CiMKi;Apc^{Min/+};Villin-Cre*) was embryonic lethal, precluding further analysis of this level of CIN. While mice with low CIN were sacrificed by the expected 12 weeks of age^{21,26,41}, mice with moderate or high CIN had to be sacrificed at 6-8 weeks due to severe weight loss. *Apc^{Min/+}* mice with moderate CIN presented with a striking increase in the amount of small intestinal adenomas (Fig. 3a-c, S3a). Neither high nor low CIN, however, increased tumorigenesis, suggesting that tumour formation in the small intestine is sensitive to a narrow range of CIN.

Macroscopic examination of the colons of the same *CiMKi;Apc^{Min/+};Villin-Cre* mice revealed that in contrast to control and low CIN mice, colons from moderate and high CIN mice were widely covered with large adenomas (Fig. 3d-f, S3d). This was most striking in the distal region of the colon, where aneuploid APC-mutant tumours also most frequently occur in humans^{42,43}. Tumour incidence was 100% (Fig. S3g), and the number of tumours was substantially higher than reported for other CIN models in the *Apc^{Min/+}* background^{18,21,26}. Importantly, CIN in organoids established from these colon adenomas still corresponded to the expected levels (Fig. 3g), suggesting that high CIN levels were not selected against after tumour initiation and that there was no drift towards an 'optimal' CIN level. Of note: while individual tumour sizes were comparable between all induced CIN levels (Fig. S3b, c, e, f), tumours with moderate or high CIN level had reached this size substantially earlier (6-8 vs. 12 weeks). We thus hypothesize that CIN advanced tumour initiation, accelerated tumour growth, or both.

In humans, tumours in the distal part of the colon are often considered CIN as they are typically aneuploid and karyotypically heterogeneous^{44,45}. Since the *CiMKi;Apc^{Min/+};Villin-Cre* mice with moderate and high CIN mimicked such distal colon tumours, we next assessed aneuploidy and heterogeneity of copy number alterations (CNAs) of colon tumours. Single cell whole genome karyotype sequencing (scKaryo-seq) showed that both aneuploidy and karyotype heterogeneity were increased with moderate and high CIN (Fig. 3g, h, S3i). Chromosome 18, which harbours the *Apc* allele and is often subject to LOH in human FAP tumours^{38,48}, was diploid in the vast majority of cells. Since tumour

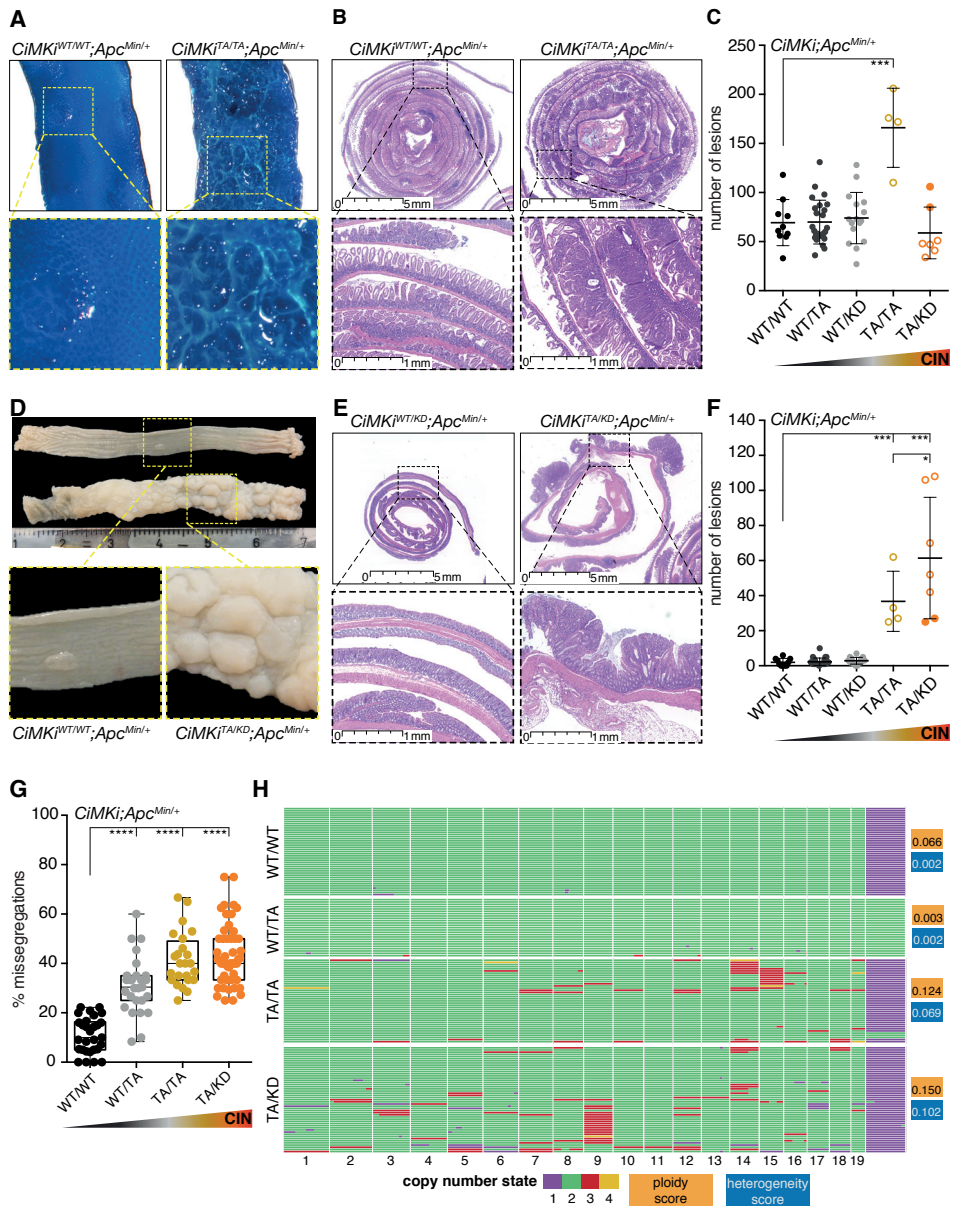


Figure 3: Degree and site define oncogenic potential of CIN in tumour-prone intestines. **a**, Examples of formalin-fixed, methylene blue stained whole mount intestines of 12-week-old (WT/WT) and 7-week-old (TA/TA) mice (*Apc*^{Min/+};*Villin-Cre* background), showing mucosal architecture and abnormalities. **b**, H&E sections of 12-week-old (WT/WT) and 7-week-old (TA/TA) mice (*Apc*^{Min/+};*Villin-Cre* background). **c**, Quantification of small intestine adenomas on methylene blue stained whole mount small intestine of *CiMKi*;*Apc*^{Min/+};*Villin-Cre* mice. Each mouse is represented by an individual dot (n=4-25 mice per group), data represents mean ± SD, asterisk indicate significance (one-tailed t-test, comparing each group to wt, p<0.001 (***)). Open dots represent mice euthanized 6-8 weeks of age, closed dots are 12-week-old mice. *Legend continues on next page*

Continued from previous page **d**, Formalin-fixed whole mount colons of 12-week-old (WT/WT) and 7-week-old (TA/KD) mice (*Apc^{Min/+};Villin-Cre* background) are predominantly located in the distal colon. Zooms indicate adenoma(s) in both genotypes. **e**, H&E examples of colons of 12-week-old (WT/WT) and 7-week-old (TA/KD) mice (*Apc^{Min/+};Villin-Cre* background). **f**, Quantification of adenomas on methylene blue stained whole mount colon tissue. Each mouse is represented by an individual dot (n=4-25 mice per group), data represents mean \pm SD, asterisk indicate significance (one-tailed t-test, comparing each group to WT/WT, p<0.001 (***) , p<0.05 (*). Open dots represent mice euthanized before 12 weeks of age, closed dots are 12-week-old mice. **g**, Quantification of chromosome segregation fidelity by time lapse imaging of colon tumour organoids (n=3-5 tumours from different mice per genotype). Missegregations were quantified for at least 20 organoids with at least 5 divisions per genotype. Data represents mean \pm SD, each dot is one organoid (one-tailed t-test, comparing each group to WT/WT, p<0.0001 (****)). **h**, Single cell whole genome karyosequencing (bin size 5 MB) showing ploidy in individual cells in three colon tumours per genotype. Green is 2n, purple 1n, red 3n and yellow is 4n for a given chromosome. Graph shows cells of one tumour per genotype (see also S3i). Aneuploidy and heterogeneity scores are given for each sample.

initiation in *Apc^{Min/+}* mice requires LOH of wild-type *Apc⁴⁶* and since *CiMKi* colon tumour organoids grew independent of Wnt ligands, this indicated that LOH of *Apc* by CIN occurred in a manner other than whole chromosome 18 loss, as previously suggested²¹. Targeted PCR detected only *Apc^{Min}* alleles (Fig. S3h), strongly suggesting that LOH was accomplished either by double non-disjunction events of both chromosomes 18 or by somatic recombination^{21,46,47}, the latter of which is likely the cause of *Apc* LOH in FAP patients^{38,48}. Both these processes could be accelerated by CIN.

Our data thus far show that the effect of CIN on karyotype heterogeneity and tumour formation depends on the degree of CIN and the tissue in which CIN occurs. As high CIN caused massive colonic tumours but did not increase adenoma formation in the small intestine, the effects of a similar range of CIN can be profoundly different in different tissues. To better understand the tissue-dependent sensitivities to CIN, we first assessed the possibility that the same *CiMKi* mutations had resulted in different CIN levels in small intestine versus colon. Although time-lapse imaging of colon and small intestinal organoids showed that CIN levels were not identical between the two tissues, genotypes with drastically different impacts on tumour formation (Fig. 3c, f) had comparable CIN levels (e.g. TA/TA in colon vs TA/KD in small intestine) (Fig. 4a, b). Strikingly, however, moderate and high CIN caused significant expansion of the proliferative compartments in the colons of *CiMKi;Apc^{Min/+};Villin-Cre* mice at four weeks of age (roughly the time of tumour initiation), but not in the small intestine (Fig. 4c, d). The percentage of proliferating cells within the compartment

(proliferative index) was similar across genotypes (Fig. 4c, d), hence cells were more readily retained in a proliferate state in the colons of moderate and high CIN mice, increasing the chance that transformed cells propagate in colonic crypts. The fact that this increased proliferative state was not observed in the small intestine again underscores the difference in CIN response between these tissues.

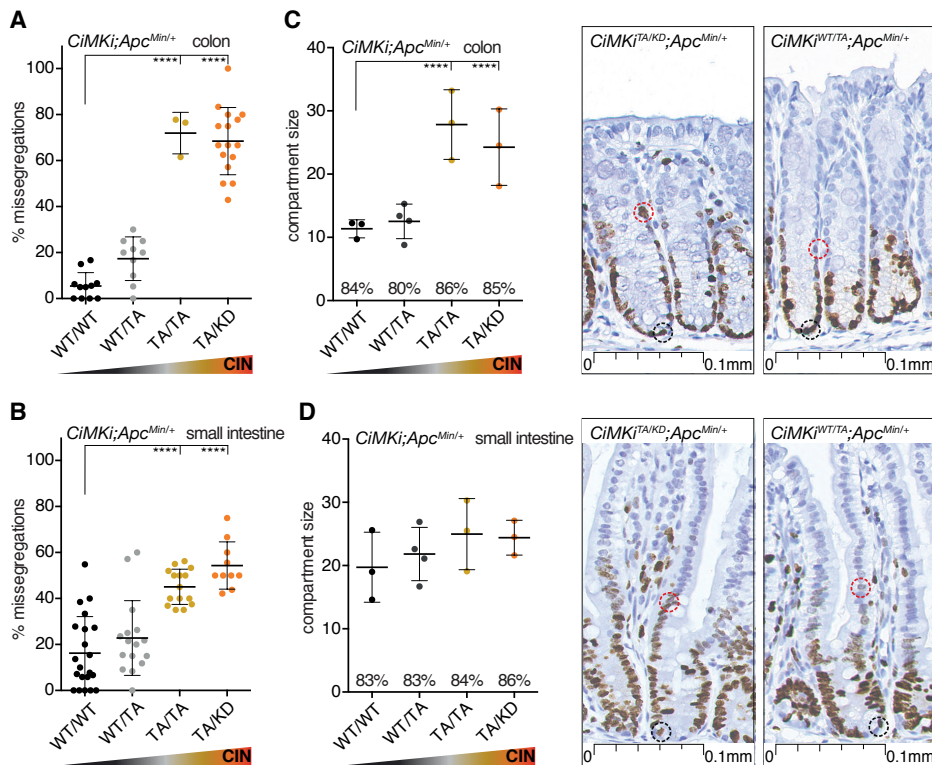


Figure 4: Colonic crypts retain proliferating CIN cells more readily than small intestinal crypts. a, b, Quantification of chromosome segregation fidelity by time lapse imaging of colon organoids (a) and small intestine organoids (b) from various *CiMKi*;*Apc*^{Min/+};*Villin-CreER*^{T2} genotypes. Missegregations were quantified for at least 10 organoids with at least 5 divisions per line. Data represents mean \pm SD, each dot is one organoid (one-tailed t-test, comparing each group to WT/WT, $p < 0.0001$ (****)). c, d, Proliferative compartment in colon (c) and small intestine (d) of 4-week old *CiMKi*;*Apc*^{Min/+};*Villin-Cre* mice as determined on Ki-67 stained FFPE slides by scoring the number of cells between the first positive cell at the bottom of the crypt (black dotted circle) and the last positive cell in the transit amplifying zone (red dotted circle). Images show crypts of colon and small intestine of *CiMKi*^{TA/KD} and *CiMKi*^{WT/TA}. Dot plot shows the average size of the compartment for each mouse (n=3-4 per genotype, 10 crypts per mouse) and error bars represent SD. Asterisk indicate significance (one-tailed t-test, $p < 0.01$ (**), $p < 0.05$ (*)). Proliferative index (percentage of Ki-67 positive cells within compartment) is indicated for each genotype.

Conclusion

Our new mammalian model for inducible, graded CIN levels, combined with direct visualization of chromosome segregation error frequencies in the relevant tissues allowed us to show that 1) moderate to high CIN levels are sufficient to drive tumour formation at early age, 2) the maximum effect on tumorigenesis is achieved by distinct CIN levels, and 3) this differs between tissues with an identical cancer predisposition mutation. With the CiMKi model, it is now possible to accurately study the interaction between CIN and tumour development in a host of tissues and genetic backgrounds. Because of tight spatio-temporal control of CIN, CiMKi also enables investigations into the effect of various levels of CIN on cancer cell dissemination, as well as on possible tumour regression. The latter may greatly aid ongoing efforts that examine if exacerbating CIN, for example by Mps1 small molecule inhibitors, has potential as cancer therapy.

Acknowledgements

We thank H. Snippert for helping designing the CiMKi targeting vectors, and H. Clevers for sharing reagents and help with ES cell targeting. We thank S. van Mil and J. van Rheenen for donating mouse strains. We thank the Hubrecht FACS facility, the Hubrecht Imaging facility, Single Cell Discoveries, and the Utrecht Sequencing Facility (USF) for assistance with the experiments. This work is part of the Cancer Genomics Centre and the Oncode Institute, and was further supported by the Dutch Cancer Society (grant numbers HUBR-2012-5321, HUBR-2012-5513, and 10126).

Author Contributions

W.H.M.H., A.J., R.H.M., N.J. and G.J.P.L.K. designed the research. W.H., A.J., and N.J. analysed and assembled the data. A.I.Q. assisted with animal maintenance and experiments. H.M. and G.J.A.O. performed pathology analyses. S.K. performed and analysed single cell karyosequencing. A.T. assisted with organoid culture and experiments. W.H.M.H., N.J. and G.J.P.L.K. wrote the paper.

References

1. Duijf, P. H. G. & Benezra, R. The cancer biology of whole-chromosome instability. *Oncogene* 32, 4727–4736 (2013).
2. Burrell, R. A., McGranahan, N., Bartek, J. & Swanton, C. The causes and consequences of genetic heterogeneity in cancer evolution. *Nature* 501, 338–345 (2013).
3. Thompson, S. L. & Compton, D. a. Chromosomes and cancer cells. *Chromosome Res.* 19, 433–444 (2011).
4. Crasta, K. et al. DNA breaks and chromosome pulverization from errors in mitosis. *Nature* 482, 53–58 (2012).
5. Stephens, P. J. et al. Massive genomic rearrangement acquired in a single catastrophic event during cancer development. *Cell* 144, 27–40 (2011).
6. Bunting, S. F. & Nussenzweig, A. End-joining, translocations and cancer. *Nat. Rev. Cancer* 13, 443–454 (2013).
7. Janssen, A., van der Burg, M., Szuhai, K., Kops, G. J. P. L. & Medema, R. H. Chromosome Segregation Errors as a Cause of DNA Damage and Structural Chromosome Aberrations. *Science (80-.)*. 333, 1895–1898 (2011).
8. Bakhoum, S. F. et al. Chromosomal instability drives metastasis through a cytosolic DNA response. *Nature* 553, 467–472 (2018).
9. Davoli, T., Uno, H., Wooten, E. C. & Elledge, S. J. Tumor aneuploidy correlates with markers of immune evasion and with reduced response to immunotherapy. *Science (80-.)*. 355, (2017).
10. Jamal-Hanjani, M. et al. Tracking the Evolution of Non-Small-Cell Lung Cancer. *N. Engl. J. Med.* 376, 2109–2121 (2017).
11. Turajilic, S. & Swanton, C. Metastasis as an evolutionary process. *Science (80-.)*. 352, 169–175 (2016).
12. Weaver, B. A. A., Silk, A. D., Montagna, C., Verdier-Pinard, P. & Cleveland, D. W. Aneuploidy acts both oncogenically and as a tumor suppressor. *Cancer Cell* 11, 25–36 (2007).
13. Silk, A. D. et al. Chromosome missegregation rate predicts whether aneuploidy will promote or suppress tumors. *Proc. Natl. Acad. Sci.* 110, E4134–E4141 (2013).
14. Diaz-Rodríguez, E., Sotillo, R., Schwartzman, J.-M. & Benezra, R. Hec1 overexpression hyperactivates the mitotic checkpoint and induces tumor formation in vivo. *Proc. Natl. Acad. Sci. U. S. A.* 105, 16719–24 (2008).
15. Dai, W. et al. Slippage of Mitotic Arrest and Enhanced Tumor Development in Mice with BubR1 Haploinsufficiency. *Cancer Res.* 64, 440 LP–445 (2004).
16. Chi, Y. H., Ward, J. M., Lily, I. C., Junichiro, Y. & Jeang, K. T. Spindle assembly checkpoint and p53 deficiencies cooperate for tumorigenesis in mice. *Int. J. Cancer* 124, 1483–1489 (2009).
17. Li, M., Fang, X., Wei, Z., York, J. P. & Zhang, P. Loss of spindle assembly checkpoint-mediated inhibition of Cdc20 promotes tumorigenesis in mice. *J. Cell Biol.* 185, 983–994 (2009).
18. Zasadil, L. M. et al. High rates of chromosome missegregation suppress tumor progression but do not inhibit tumor initiation. *Mol. Biol. Cell* 27, 1981–1989 (2016).
19. Ricke, R. M., Jeganathan, K. B., Malureanu, L., Harrison, A. M. & Van Deursen, J. M. Bub1 kinase activity drives error correction and mitotic checkpoint control but not tumor suppression. *J. Cell Biol.* 199, 931–949 (2012).
20. Jeganathan, K., Malureanu, L., Baker, D. J., Abraham, S. C. & Van Deursen, J. M. Bub1 mediates cell death in response to chromosome missegregation and acts to suppress spontaneous tumorigenesis. *J. Cell Biol.* 179, 255–267 (2007).
21. Baker, D. J., Jin, F., Jeganathan, K. B. & van Deursen, J. M. Whole Chromosome Instability Caused by Bub1 Insufficiency Drives Tumorigenesis through Tumor Suppressor Gene Loss of Heterozygosity. *Cancer Cell* 16, 475–486 (2009).
22. Sotillo, R. et al. Mad2 Overexpression Promotes Aneuploidy and Tumorigenesis in Mice. *Cancer Cell* 11, 9–23 (2007).
23. Iwanaga, Y. et al. Heterozygous deletion of mitotic arrest-deficient protein 1 (MAD1) increases the incidence of tumors in mice. *Cancer Res.* 67, 160–166 (2007).
24. Michel, L. S. et al. MAD2 haplo-insufficiency causes premature anaphase and chromosome instability in mammalian cells. *Nature* 409, 355–359 (2001).
25. Babu, J. R. et al. Rael is an essential mitotic checkpoint regulator that cooperates with Bub3 to prevent chromosome missegregation. *2*, 341–353 (2003).
26. Rao, C. V et al. Colonic tumorigenesis in BubR1^{-/-} ApcMin^{+/+} compound mutant mice is linked to premature separation of sister chromatids and enhanced genomic instability. 1–6 (2005).
27. Kalitsis, P. et al. Increased chromosome instability but not cancer predisposition in haploinsufficient Bub3 mice. *Genes Chromosom. Cancer* 44, 29–36 (2005).
28. Ree, J. H. Van, Jeganathan, K. B., Malureanu, L. & Deursen, J. M. Van. Overexpression of the E2

- ubiquitin-conjugating enzyme UbcH10 causes chromosome missegregation and tumor formation. *188*, 83–100 (2010).
29. Benhra, N., Barrio, L., Muzzopappa, M. & Milán, M. Chromosomal Instability Induces Cellular Invasion in Epithelial Tissues. *Dev. Cell* **47**, 161–174.e4 (2018).
 30. Ricke, R. M., Jeganathan, K. B. & Deursen, J. M. Van. Bub1 overexpression induces aneuploidy and tumor formation through Aurora B kinase hyperactivation. *193*, (2011).
 31. Jelluma, N. et al. Chromosomal Instability by Inefficient Mps1 Auto-Activation Due to a Weakened Mitotic Checkpoint and Lagging Chromosomes. *PLoS One* **3**, e2415 (2008).
 32. Sliedrecht, T., Zhang, C., Shokat, K. M. & Kops, G. J. P. L. Chemical Genetic Inhibition of Mps1 in Stable Human Cell Lines Reveals Novel Aspects of Mps1 Function in Mitosis. *PLoS One* **5**, e10251 (2010).
 33. Lan, W. & Cleveland, D. W. A chemical tool box defines mitotic and interphase roles for Mps1 kinase. *J. Cell Biol.* **190**, 25–34 (2010).
 34. El Marjou, F. et al. Tissue-specific and inducible Cre-mediated recombination in the gut epithelium. *genesis* **39**, 186–193 (2004).
 35. The Cancer Genome Atlas Network. Comprehensive molecular characterization of human colon and rectal cancer. *Nature* **487**, 330–337 (2012).
 36. Fearon, E. R. & Vogelstein, B. A genetic model for colorectal tumorigenesis. *Cell* **61**, 759–767 (1990).
 37. Fodde, R., Smits, R. & Clevers, H. APC, signal transduction and genetic instability in colorectal cancer. *Nat. Rev. Cancer* **1**, 55–67 (2001).
 38. Miyaki, M. et al. Genetic changes and histopathological types in colorectal tumors from patients with familial adenomatous polyposis. *Cancer Res.* **50**, 7166–7173 (1990).
 39. Ichii, S. et al. Detailed analysis of genetic alterations in colorectal tumors from patients with and without familial adenomatous polyposis (FAP). *Oncogene* **8**, 2399–2405 (1993).
 40. Jackstadt, R. & Sansom, O. J. Mouse models of intestinal cancer. *J. Pathol.* n/a-n/a (2015). doi:10.1002/path.4645
 41. Moser, A. R., C, P. H. & Dove, W. F. A Dominant Mutation That Predisposes to Multiple Intestinal Neoplasia in the Mouse. *Science* (80-). **247**, 322–324 (2008).
 42. Kinzler, K. W. & Vogelstein, B. Lessons from Hereditary Colorectal Cancer. *87*, 159–170 (1996).
 43. Liu, Y. et al. Comparative Molecular Analysis of Gastrointestinal Adenocarcinomas. *Cancer Cell* **33**, 721–735.e8 (2018).
 44. De Sousa E Melo, F. et al. Poor-prognosis colon cancer is defined by a molecularly distinct subtype and develops from serrated precursor lesions. *Nat. Med.* **19**, 614–8 (2013).
 45. Dunican, D. S., McWilliam, P., Tighe, O., Parle-McDermott, A. & Croke, D. T. Gene expression differences between the microsatellite instability (MIN) and chromosomal instability (CIN) phenotypes in colorectal cancer revealed by high-density cDNA array hybridization. *Oncogene* **21**, 3253–3257 (2002).
 46. Luongo, C., Moser, A. R., Gledhill, S. & Dove, W. F. Loss of Apc⁺ in intestinal adenomas from Min mice. *Cancer Res.* **54**, 5947–5952 (1994).
 47. Haigis, K. M. & Dove, W. F. A Robertsonian translocation suppresses a somatic recombination pathway to loss of heterozygosity. *Nat. Genet.* **33**, 33–39 (2003).
 48. Sieber, O. M. et al. Analysis of chromosomal instability in human colorectal adenomas with two mutational hits at APC. *Proc Natl Acad Sci USA* **99**, 16910–16915 (2002).
 49. Dankort, D. et al. A new mouse model to explore the initiation, progression, and therapy tumors. *Genes Dev.* **21**, 379–384 (2007).
 50. Saurin, A. T., van der Waal, M. S., Medema, R. H., Lens, S. M. A. & Kops, G. J. P. L. Aurora B potentiates Mps1 activation to ensure rapid checkpoint establishment at the onset of mitosis. *Nat. Commun.* **2**, 316–319 (2011).
 51. Shaner, N. C. et al. A bright monomeric green fluorescent protein derived from *Branchiostoma lanceolatum*. *Nat. Methods* **10**, 407–409 (2013).
 52. Drost, J. et al. Sequential cancer mutations in cultured human intestinal stem cells. *Nature* **521**, 43–47 (2015).
 53. Sato, T. et al. Single Lgr5 stem cells build crypt-villus structures in vitro without a mesenchymal niche. *Nature* **459**, 262–5 (2009).
 54. Verissimo, C. S. et al. Targeting mutant RAS in patient-derived colorectal cancer organoids by combinatorial drug screening. *Elife* **5**, 1–26 (2016).
 55. Muraro, M. J. et al. A Single-Cell Transcriptome Atlas of the Human Pancreas. *Cell Syst.* **3**, 385–394 (2016).
 56. Bakker, B. et al. Single-cell sequencing reveals karyotype heterogeneity in murine and human malignancies. *Genome Biol.* **17**, 1–15 (2016).
 57. Van Der Weyden, L. et al. Null and conditional Semaphorin 3B alleles using a flexible puro tk LoxP/FRT vector. *Genesis* **41**, 171–178 (2005).

Methods

Mice: strains, experiments and analysis

All animal experiments were approved by Animal Experimental Committee and the Dutch Central Authority for Scientific Procedures on Animals (CCD). All animals were bred and housed under standard conditions at the animal facility of the Gemeenschappelijk Dieren Laboratorium (GDL), Utrecht, the Netherlands, and the Hubrecht animal facility.

2

Genetically modified mice strains used in this study include: *ACTB:FLPe* (B6.Cg-Tg(ACTFLPe)9205Dym/J, stock number 005703), *Rosa26-CreER^{T2}* (B6.129Gt(ROSA)26Sor^{tm1(cre/ERT2)Tyj}/J, stock number 008463), and *Apc^{Min/+}* (C57BL/6J-*Apc^{Min}*/J, stock number 002020) and were purchased from JAX mice. *Villin-Cre* mice were a gift from S. van Mil (originated from JAX mice (B6.Cg-Tg(Vil1-cre)997Gum/J, stock number 004586). *Villin-CreER^{T2}* mice were a gift from J. van Rheenen. All mice were maintained in C57BL/6 background. Mice were genotyped using standard PCR and targeted sequencing procedures. For primers see Table 1.

CiMKi mice were generated under license of UMCU (DEC 2010.I.02.026). The *CiMKi* alleles were designed following the example of the BRAF-V600E inducible model by Dankort et al.⁴⁹: a cDNA cassette of wild-type exons 17-22 is followed by a stop codon and polyA sequence. The cassette is flanked by loxP sites, and the 3' recombination arm harbours one of the point mutations in exon 17 (D637A: GAT>GCT; T649A: GCA>ACA). The cassette was cloned into the pAC16 targeting vector (kind gift from J. Jonkers). For a detailed outline of construction of *CiMKi* vectors see Supplementary Information. 129/Ola-derived IB10 ES cells (kind gift from H. Clevers) were electroporated (Biorad gene pulser) with the linearized targeting construct pAC16-D637A or -T649A. Targeted cells were selected with puromycin (1mg/ml, Sigma) and single colonies were subsequently picked and cultured in 96-wells plates. Individual clones were analysed for presence of the *CiMKi* alleles using standard PCR (Primers used: Forward TCTATGGCTTCTGAGGCGG and Reverse AAGGGACATCAGGGAAGCAA). DNA from targeted ES cells yielded a band of ~2.8 kb.

Southern blot was performed according to standard protocols to confirm correct integration of the *CiMKi* alleles. 5' probe (500bp) was obtained from

genomic DNA from 129/Ola-derived IB10 ES cells, and labelled using a standard Rediprime II Random Prime labelling system (GE healthcare) and radioactive [α - 32 P] dCTP. Digestion of genomic DNA from ES cells with EcoRV and hybridization with the 5' probe resulted in a 9,5 kb band (when wildtype) or 4,7 kb band (when targeted with CiMKi allele).

Confirmed targeted ES cell clones for both CiMKi mutations were injected into C57BL/6 blastocyst, which were then transplanted into pseudo-pregnant females (standard techniques, performed under the license of the GDL Utrecht). Chimeric mice were bred with C57BL/6 mice to obtain germline transmission. Agouti mice were then backcrossed six times into a C57BL/6 background. Genotypic analysis of offspring was performed using standard PCR and targeted sequencing (Table 1, supplementary information). To remove the puro cassette from the original pAC16 construct, CiMKi mice were bred with ACT-Flp mice (C57BL/6 background). Only lines that had loss of the puro cassette (as confirmed by standard PCR) were used to maintain CiMKi lines.

To induce loxP recombination, MEFs were treated with 4-hydroxy-tamoxifen (4-OHT; 1 μ M, Sigma H6278). Mice were injected intraperitoneally with Tamoxifen (1 mg dissolved in corn oil; Sigma, C8267). In CiMKi;Apc^{Min};Villin-Cre mice, CiMKi alleles were induced at 12.5 dpc. when the Villin promotor is activated. To confirm recombination, RNA was isolated with a quick RNA kit (Zymo Research). cDNA was prepared using standard procedures, subjected to PCR and subsequently sequenced to determine the presence of T649A or D637A. For primers see Table 1, supplementary information.

Mice were sacrificed at four weeks, twelve weeks or eight months, and immediately dissected. small intestine was separated from colon, both were flushed with PBS and pieces of tissue were snap-frozen for later RNA/protein analysis. The organs were stored in formalin until further processing.

Histology and Immunohistochemistry

Formalin fixed intestines were cut open longitudinally and stained with 0,25% methylene blue in dH2O, and rinsed with PBS. Pictures were taken with 6.3x magnification using an Olympus SZX stereo microscope to count the number of

lesions in the small intestine and colon. After washing with PBS to remove the methylene blue, intestines were rolled into "Swiss rolls" for paraffin embedding.

For identification and assessment of tumours 4- μ m sections of paraffin-embedded tissue were cut and stained with haematoxylin/eosin (H&E). These slides were scanned (Nanozoomer XR, Hamamatsu) for digital image analysis. Grading of dysplasias was done following the existing guidelines for human intestinal adenomas.

Apoptotic bodies were recognized on H&E stained sections, according to strict morphological criteria such as cell shrinkage with retracted pink to orange cytoplasm, chromatin condensation and nuclear fragmentation and separation of cells by a halo from adjacent enterocytes.

For proliferation measurements slides were incubated with Ki-67 antibody (ThermoFisher, RM-9106, ARS pH9, 1:50 and 3 hr incubation). Sections were counterstained with haematoxylin, dehydrated and coverslipped using Pertex. Ki-67 positive cells were counted from the bottom to the top of the crypt till the upper most positive cell. The proliferative compartment was defined as the part of the crypt between the bottom and the upper most labelled cell. The proliferative activity (Ki-67 index) was calculated as the percentage of positively labelled cells divided by the total number of counted cells within the proliferative compartment. β -catenin localization was assessed on paraffin sections stained with anti- β -catenin (BD Transduction Laboratories, Clone 14/Beta-Catenin 610154, 1:1000, overnight incubation), anti-Mouse Envision-HRP (DAKO, one hour) as secondary antibody, and counterstained with hematoxylin.

MEFs (isolation, immunofluorescence, mitotic spreads, Western blot, and live microscopy)

CiMKi mice were bred with R26-CreER^{T2} mice and maintained in a stable homozygous CreER^{T2} background. Pregnant females were sacrificed at day 13-17 p.c. by cervical dislocation. Uterine horns were dissected out and placed in tubes containing PBS. Embryos were separated from their placenta and surrounding membranes. Red organs, brains and tail (for genotyping) were removed. Embryos were finely minced using razor blades and the remaining cells/tissues were

suspended in a tube containing 2 ml Trypsin and kept at 37°C for 15 minutes. Two volumes of media (DMEM supplemented with 10% FBS, non-essential amino acids, glutamin and Pen/Strep) were added and remaining tissues were removed by allowing them to settle down at the bottom of the tube. Supernatant was subjected to centrifugation for 5 minutes at 1000 rpm, cell pellet was resuspended in medium and plated in 10 cm dishes.

For immunofluorescence cells were plated on 12mm coverslips and harvested after one hour nocodazole (250 ng/ml, Sigma, M1404) and MG132 (2 μ M, Sigma C2211) treatment. Cells were pre-extracted with 0.1% Triton X-100 in PEM (100 mM PIPES (pH 6.8), 1 mM $MgCl_2$ and 5 mM EGTA) for one minute at 37°C before fixation with 4% paraformaldehyde in PBS. Coverslips were subjected to antibody staining following standard procedures (primary antibodies anti-Mad1 (Santa Cruz sc67337, 1:1000), anti-Centromere Protein (ACA) (Antibodies Incorporated 15-234-0001, 1:2000). Images were acquired on a DeltaVision RT system (Applied Precision) with a 100/1.40NA UPlanSApo objective (Olympus) using SoftWorx software. Images are maximum intensity projections of deconvolved stacks. Quantifications were done using ImageJ software and a macro to threshold and specifically select kinetochores as described previously⁵⁰.

For mitotic spreads, MEFs were treated with STLC (1 μ M, Sigma 164739) for 4 hours. Mitotic cells (isolated by shake-off) were treated for 10 minutes in hypotonic buffer (75 mM KCl), fixed with acetic acid/methanol, dropped onto glass cover slides and stained with DAPI (1mg/ml, Sigma 32670). Images were acquired on a DeltaVision RT system (Applied Precision) with a 100/1.40NA UPlanSApo objective (Olympus) using SoftWorx software. Chromosomes were counted manually using Image J software.

For Western blot, MEFs were treated with 4-OHT or EtOH for 72 hours, and then lysed with Laemmli buffer. Protein levels were assessed by standard Western blot procedures (anti-ESK (Santa Cruz sc-541, 1:1000), and anti- α -Tubulin (Sigma T5168; 1:10000)).

For live cell imaging, immortalized MEFs (transduced with large T and small T expressing lentivirus (Plasmid #22298, Addgene) were transduced with an H2B-Neon expressing lentivirus (pLV-H2B-Neon-ires-Puromycin)^{51,52}, and selected with puromycin (1mg/ml, Sigma P7255). These stably H2B-mNeon expressing MEFs were plated in 24-well plates and imaged 56 hours after 4-OHT treatment for sixteen hours in a heated chamber (37°C and 5% CO₂) using a 20/0.5NA UPLFLN objective on an Olympus IX-81 microscope, controlled by Cell-M software (Olympus). Images were acquired using a Hamamatsu ORCA-ER camera and processed using Cell-M and ImageJ software.

Organoids (isolation, culture and live microscopy)

Organoids were isolated from *CiMKi;Apc^{Min/+};Villin-Cre(ERT2)* mice as described previously⁵³. In brief, intestines of six-to-twelve weeks-old mice were dissected and cleaned with PBS. They were incubated in 0.5mM EDTA on ice for 30 minutes (normal tissue), or EDTA treatment followed by 45 minutes in DMEM 2% FBS 1% PenStrep supplemented with 75u/ml collagenase and 125 µg/ml Dispase (tumour tissue). Intestines were put in tubes with PSB, and crypts were removed from their niche by harsh shaking. After filtering the suspension using a 70 µm strainer, crypts or tumour cells were seeded in Matrigel (Corning, 356231). Organoids were cultured in medium containing advanced DMEM/F12 medium (Invitrogen,126334-010), Hepes Buffer (Sigma, H0887,1 mM), Pencilin/Strep (Sigma, P0781, 1%), Ala-Glu (Sigma, G8541, 0.2 mM), R-Spondin conditioned medium (20%, kind gift from Hans Clevers) (wild-type only), Noggin conditioned medium (10%) (Thermo/Life Technologies, PHC1506, 1x), B27 (Thermo/Life Technologies, 17504001, 1x), nicotinamide (Sigma-Aldrich, 72340, 10 mM) (colon only), N-acetylcysteine (Sigma-Aldrich, A7250, 1.25 mM), EGF 0,1% (Invitrogen/Life Technologies, 53003-018) and Primocin 0.5% (Invivogen, ant-pm1). For passaging, organoids were sheared by repetitive pipetting and re-plated in Matrigel in a pre-warmed 24-well plate.

To establish stable organoid lines expressing H2B-mNeon, organoids were transduced with an H2B-Neon expressing lentivirus (pLV-H2B-Neon-ires-Blasticidin)^{51,52}, and selected with blasticidin (InvivoGen; 20µg/ml). For induction

of CiMKi alleles organoids were treated with 1 μM 4-OHT for 56 hours. Organoids were seeded and imaged in 8-chamber IBIDI slides using a confocal spinning disk (Nikon/Andor CSU-W1 with Borealis illumination), equipped with atmospheric and temperature control. Organoids were imaged in XYZT-mode (12 to 20 z-sections at 2,5 μm intervals, for 8 to 12 hours) at 37°C at 3-minute intervals, using a 30X silicon objective and an additional 1.5X lens in front of the CCD-camera. 3% 448nm laser and 50nm disk pinhole were used. Raw data were converted to videos using an ImageJ macro as described^{52,54}. Fidelity of all observed chromosome segregations was scored manually, guided by custom-made ImageJ/Fiji macro for ordered data output.

Single cell karyotype sequencing (scKaryo-seq)

Snap-frozen tumour tissue was stained with 10 $\mu\text{g}/\text{ml}$ Hoechst 34580 (Sigma-Aldrich) and minced in a petri dish, on ice, using a cross-hatching motion with two scalpels. The minced tissue was kept on ice for 1h after which it was filtered through 70 μm and 35 μm strainer. Nuclei were sorted in a 384-well plate containing 5 μl of mineral oil (Sigma) in each well and stored at -20C until further processing. Cell lysis was performed overnight at 50°C using 0.05 units of Qiagen Protease in 1x NEBuffer 4 (NEB) followed by heat inactivation at 75°C for 20 min and 80°C for 5 min. The genomic DNA was subsequently fragmented with 100 nL 1 U NlaIII (NEB) in 1x Cutsmart (NEB) for 60 min at 37°C followed by heat inactivation at 80°C for 20 min. 100 nL of 1 μM barcoded double-stranded NlaIII adapters and 100 nL of 40 U T4 DNA ligase (NEB) in 1x T4 DNA Ligase buffer (NEB) supplemented with 3mM ATP (Invitrogen) was added to each well and ligated overnight at 16°C. After ligation samples were pooled and library preparation was performed as described previously⁵⁵. Libraries were sequenced on an Illumina Nextseq 500 with 1 x 75 bp single-end sequencing. The fastq files were mapped to GRCH38 using the Burrows-Wheeler Aligner. The mapped data was further analysed using custom scripts in Python, which parsed for library barcodes, removed reads without a NlaIII sequence and removed PCR-duplicated reads. Copy number analysis was performed as described previously⁵⁶.

Statistical analysis

Power analysis predicted the number of animals that had to be used in each group to detect differences with 80% power and 95% confidence. Animals were not randomized, but assigned to the experimental groups based on their genotype. Statistical analyses were done in GraphPad Prism. Comparisons between CiMKi wildtype and CiMKi mutants were analysed with one-tailed student's t-tests. Data is presented as mean \pm SD unless otherwise stated in legends.

2

Data Availability

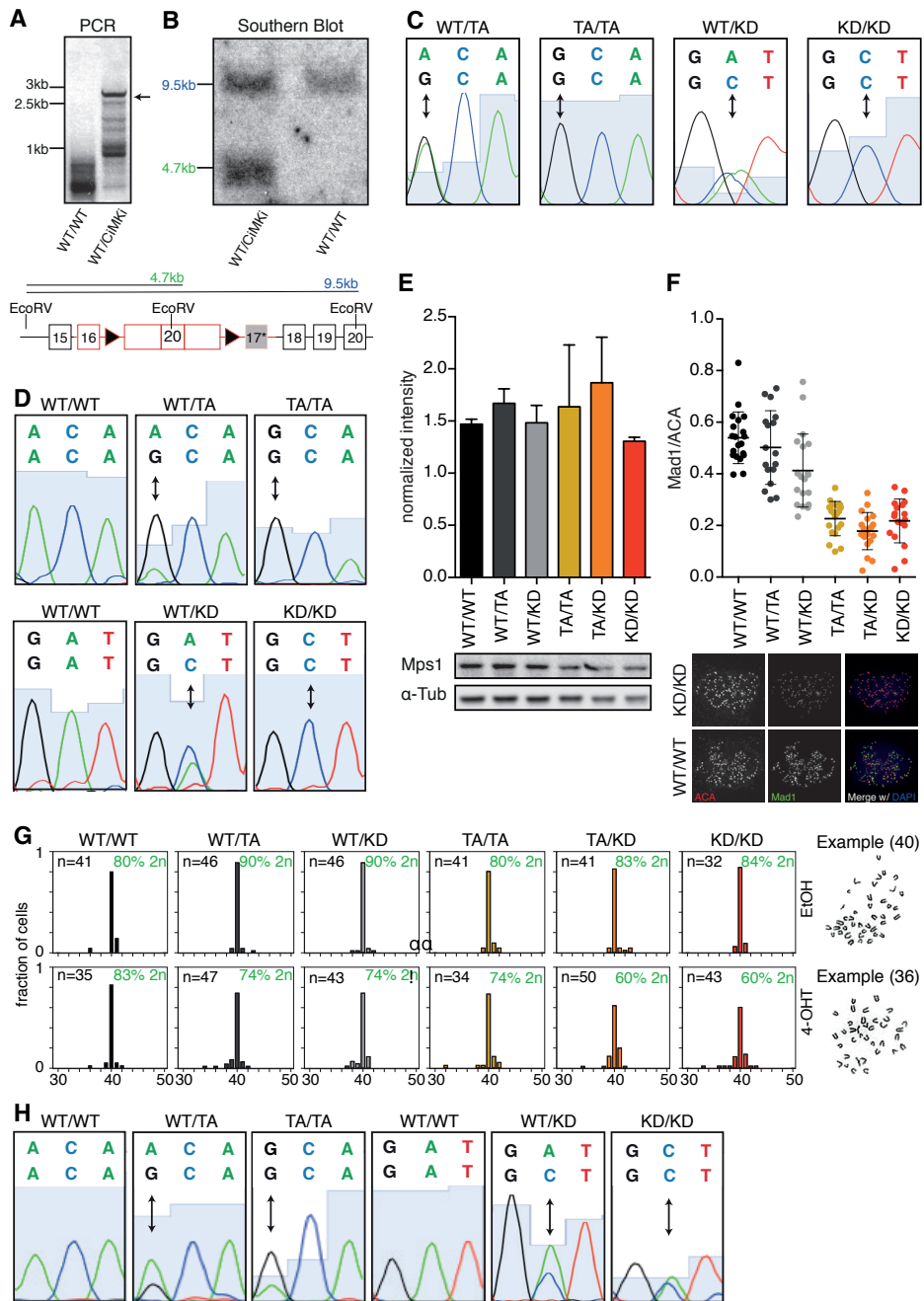
The data that support the findings of this study are available from the corresponding author upon reasonable request. scKaryo-seq data are available via the ENA repository.

Supplemental figures

Figure on next page

Figure S1: A novel mouse model for CIN: Cre-inducible Mps1 Knock-in (CiMKi). **a**, Genomic PCR of targeted ES cells confirming presence of the CiMKi allele. Shown here specifically is the CiMKi-T649A ES clone that was used for blastocyst injection. **b**, Confirmation of correct integration of the CiMKi alleles by Southern blot. Shown here specifically is the CiMKi-T649A ES clone that was used for blastocyst injection. Lower schematic shows EcoRV restriction sites used for Southern blot, indicated 5' of exon 15 and in exon 20. **c**, Targeted sequencing confirming presence of Mps1 mutations in mouse ear genomic DNA. **d**, RT-PCR followed by targeted sequencing of cDNA from CiMKi MEF lines 56 hours after 4-OHT treatment shows hetero- or homozygous expression of both D637A (A \rightarrow C) or T649A (A \rightarrow G) alleles. **e**, Western blot of Mps1 protein expression in CiMKi;Rosa26-CreER^{T2} MEFs 56 hours after 4-OHT treatment. Intensity is normalized over α -tubulin. **f**, Examples and quantification of Mad1 localization on kinetochores as a proxy for Mps1 activity in CiMKi;Rosa26-CreER^{T2} MEFs 72 hours after 4-OHT treatment. Cells were blocked in mitosis by nocodazole and MG132 for 30 minutes. Graph shows quantifications of kinetochore signals as ratios over ACA signals. Data represents mean \pm SD of at least 20 cells per condition. **g**, Examples and quantification of diploid and aneuploid cells on metaphase spreads (dapi) of CiMKi;R26CreER^{T2} primary MEFS 56 hours after 4-OHT treatment. MEFS were blocked in mitosis by 4 hours treatment with nocodazole. Ploidy was assessed by counting the number of chromosomes per cell, percentage of diploid cells is given. **h**, RT-PCR followed by targeted sequencing on cDNA from CiMKi; R26CreER^{T2} small intestine tissue one week after tamoxifen injection confirms effective recombination and expression of the mutant alleles. Hetero- or homozygous expressions of both D637A (A \rightarrow C) or T649A (A \rightarrow G) alleles are shown.

Legend on previous page



2

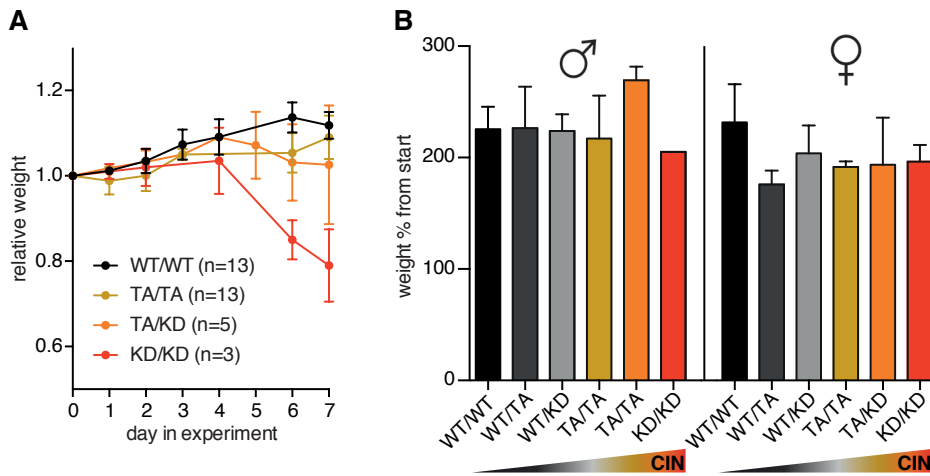
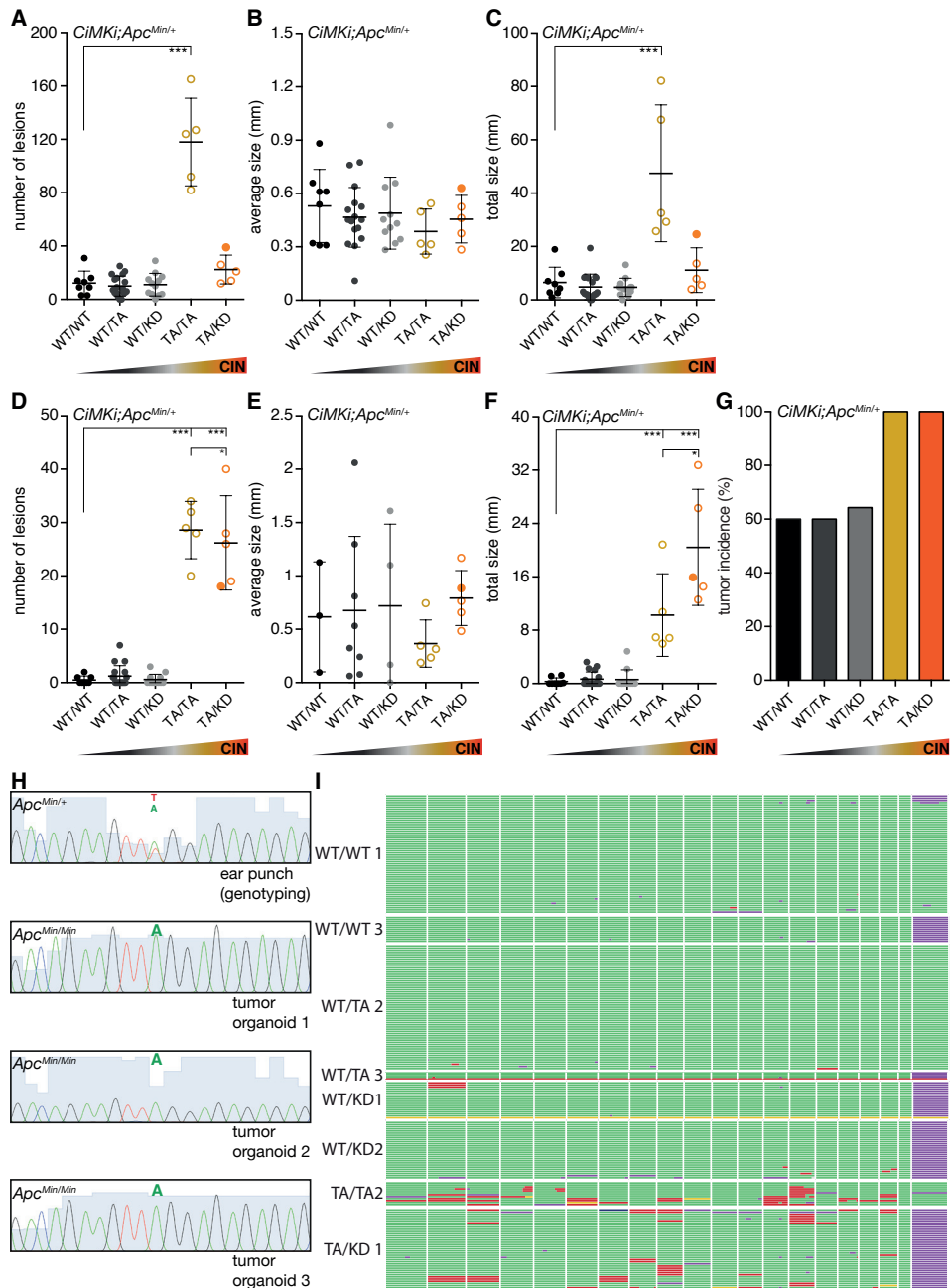


Figure S2: CIN leads to spontaneous tumorigenesis in the intestine. **a**, Relative bodyweight of *CiMKi;R26CreER^{T2}* mice after three consecutive days of i.p. tamoxifen injection. Lines represent change in bodyweight per group as fraction of their weight at the start of the experiment (mean \pm SD). **b**, Relative body weight in male (left) and female (right) *CiMKi;Villin-Cre* mice of all genotypes. Increase in weight is shown as percentage from start of the experiment (4 weeks) to end (8 months). Data is shown as mean percentage increase \pm SD.

Figure on next page

Figure S3. CIN differently affects small intestine and colon tumour formation in *Apc^{Min/+}* mice. **a**, Quantification of small intestine adenomas on H&E sections of *CiMKi;Apc^{Min/+};Villin-Cre* mice. Each mouse is represented by an individual dot (n=4-15 mice per group), data represents mean \pm SD, asterisk indicate significance (one-tailed t-test, comparing each group to WT/WT, $p < 0.001$ (***)). Open dots represent mice euthanatized before 12 weeks of age, closed dots are 12-week-old mice. **b**, Average size of small intestine adenoma for each mouse was measured by taking the diameter of the lesion on H&E slides of *CiMKi;Apc^{Min/+};Villin-Cre* mice. Data represents mean \pm SD. **c**, Total tumour burden in small intestine as the sum of all tumour diameters per mouse. Data represents mean \pm SD, asterisk indicate significance (one-tailed t-test, $p < 0.001$ (***)). **d**, Quantification of colon adenomas on H&E sections of *CiMKi;Apc^{Min/+};Villin-Cre* mice. Each mouse is represented by an individual dot (n=4-15 mice per group), data represents mean \pm SD, asterisk indicate significance (one-tailed t-test, comparing each group to wt, $p < 0.001$ (***)). **e**, Average size of colon adenoma for each mouse was measured by taking the diameter of the lesion on H&E slides of *CiMKi;Apc^{Min/+};Villin-Cre* mice. Data represents mean \pm SD. **f**, Total tumour burden in colon as the sum of all tumour diameters per mouse. Data represents mean \pm SD, asterisk indicate significance (one-tailed t-test, $p < 0.001$ (***)). **g**, Colon tumour incidence in *CiMKi;Apc^{Min/+};Villin-Cre* mice of the indicated genotypes. **h**, Targeted sequencing confirming absence of wild-type *Apc* gDNA in tumour organoids. *Apc^{Min/+}* mouse ear gDNA is given as reference. **i**, Single cell whole genome karyosequencing (bin size 5 MB) showing ploidy in individual cells in three colon tumours per genotype. Green is 2n, purple 1n, red 3n and yellow is 4n for a given chromosome. One example was given in 3f, show here are the other samples that had at least five cells with good sequencing results.

Legend on previous page



2

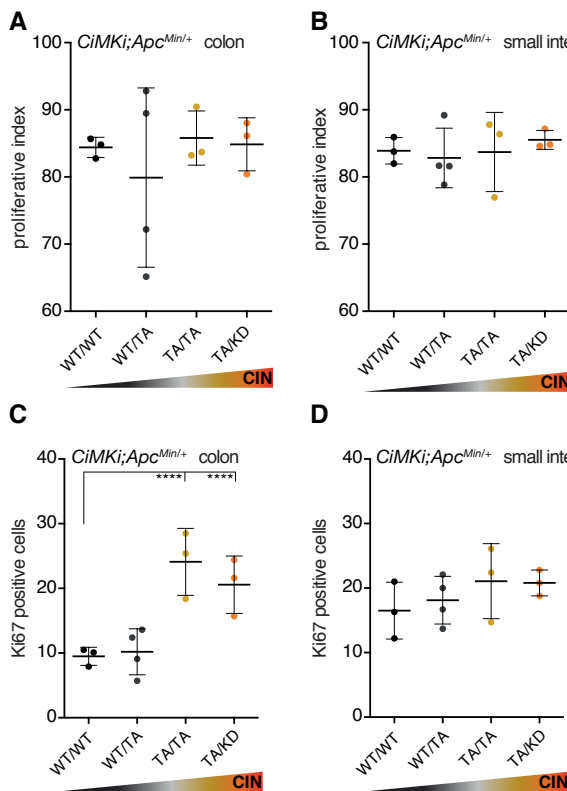


Figure S4: Colonic crypts retain proliferating CIN cells more readily than small intestinal crypts. **a, b,** Proliferative index in colon (**a**) and small intestine (**b**) of 4-week old *CiMKi;Apc^{Min/+};Villin-Cre* mice as determined on Ki-67 stained FFPE slides by calculating the percentage of Ki-67 positive cells within the proliferative compartment. Data represents mean ± SD, n=3-4 mice per genotype. **c, d,** Number of Ki-67 positive cells in proliferative compartment of 4-week old *CiMKi;Apc^{Min/+};Villin-Cre* mice. Data represents mean ± SD, n=3-4 mice per genotype. Asterisk indicate significance (one-tailed t-test, p<0.01 (**), p<0.05 (*)).

Supplemental movies

Supplemental movies 1: Increased missegregation rates in *CiMKi;R26CreER^{T2}* MEFs **a,** Time lapse imaging of *CiMKi^{WT/WT};R26CreER^{T2}* immortalised MEFs 56 hours after 4-OHT. **b,** As **a**, but for *CiMKi^{KD/KD}*.

Supplemental movies 2: Increased missegregation and death rates in *CiMKi;Villin-CreER^{T2}* organoids. **a,** Time lapse imaging of *CiMKi^{TA/KD};VillinCreER^{T2}* small intestine organoids 56 hours after EtOH. Colour depth-coding (purple is bottom of organoid, red is top) was used to identify the position of the cells, left panel) and maximum projections are depicted in the right panel. **b,** As **a**, but for *CiMKi^{WT/KD};VillinCreER^{T2}* 56 hours after 4-OHT. **c,d,** As **a**, but for *CiMKi^{KD/KD};VillinCreER^{T2}* 56 hours after 4-OHT. Note the presence of micronuclei in **c**, the severe missegregation in **d** (frame 8-20), the aberrant shape of the nuclei and the lack of further divisions.



Supplemental information

Table S1: Primers for genotyping and cDNA analysis

Gene	Forward primer	Reverse primer	Expected band size	Sequence primer	Mutation sequence
<i>CiMKi</i>	CCAAATGGCTAGG GGAGCCACTGATG	GGTGAGGTTGTTT CCAACTGGTAG	Mutant 250 bp	NA	NA
<i>CiMKi</i> (mutation)	GTGTCTCACCTG AAAATG	CAAAGCACAGCTG GGCTGTAGAG	~1000 bp	CGGATTTTATTTG AAGGTATTG	T649A: ACA <u>A</u> /G CA D637A: TTGG <u>A</u> /CT
<i>CiMKi</i> cDNA (mutation)	CCTAGAAGACGCC GATAGCC	GTCTCTGATTGCTT CTGGGGC	~400 bp	GATAAGATCATCC GCCTCTATG	T649A: ACA <u>A</u> /G CA D637A: TTGG <u>A</u> /CT
<i>Apc</i> ^{Min/+}	CCGGAGTAAGCAG AGACACAAG	CTGTCGTCTGCCAC ACAATG	~400 bp	CATGACTGTTCTTT CACC	GACAGAAGTT <u>T/A</u>
<i>Rosa26-CreER</i> ^{T2} (mut)	GGCAGGAAGCACT TGCTCTCCC	CCTGATCCTGGCAA TTTCG	~825 bp	NA	NA
<i>Rosa26-CreER</i> ^{T2} (wt)	GGCAGGAAGCACT TGCTCTCCC	GGAGCGGGAGAA ATGGATATG	~650 bp	NA	NA
Villin-Cre(ER ^{T2})	CAAGCCTGGCTCG ACGGCC	CCTGATCCTGGCA ATTCG	~220 bp	NA	NA

2

Cloning of CiMKi targeting vectors

CiMKi alleles were cloned into the pAC targeting vector (based on pFlexible⁵⁷) (kind gift from Jos Jonkers). Three fragments were ligated separately into the vector as follows:

- 1) Conditional fragment into HindIII-Pacl (between loxP sites)
- 2) 5' Recombination arm into PmeI-Ascl (upstream of 5' loxP site)
- 3) 3' Recombination arm, including either point mutation, into SbfI-NotI (downstream of 3' loxP site).

Details for the three fragments:

- 1) *Conditional fragment*

The conditional fragment was obtained by assembling three separate PCR products by ligation into pCDNA3 (see details below):

#1=*HindIII*-(last part of)intron16-*XhoI* (~600 bp)

#2=*XhoI*-**exon17-exon18-exon19-exon20-exon21-exon22**-*BamHI* (~1000 bp)

#3=*BamHI*-intron22(polyA signal)-*Pacl* (~600 bp)

This resulted in the following complete sequence of the conditional fragment (exon17-22 part (PCR product #2) in bold):

```
AAG CTT ATG GCC AGT TTT TCA GTC TCC AAA GGA TTT TCT CTT TGG AGC CCG GTG TGA GAG TTG GTC TGT TCT TGC
TGT TTT CTG TTT CAT TAT TTG TTT GTT CTT GTT CTC TCC AGT TTC CTC TGC CTT TCC CTT G TCT TTT AAA CAG ATG
TGT TCA ATC TCA TGC GCT TCC TCT GCT TCT CCT TTT AGA AGC AGT AAC TAA GCA GAG GAT AGG ACT CTT TGG
GGG TGA GGG AGG CCT TGC GAT CTT ATT GTC TGA CAG TTC TTG GTG GTG CTT TCC TGG CCT GTG CAT GGC AGT
GTG CAG CAC ACA CTG ACA GGC TAG GCC TGG AAT CCT GAA CAG TTC ACT TCA ACT CAA ATC ACA TTG AGT GTC
CTC ACC CTG AAA ATG ATG ATG ATA ATG GGA CTT ATT TGC TAT GCA TTG CTA TAG AAT GGT ACC TGG CCC ACA ACA
TTT GCT AAG AAA GTG TAG AAT GTA TAA TAA CTA AAT ATT AAT GTG TTG CCT AAT TGA AAG GAT AAG CCT GAC CTA
AAG ATT ATG AAA TGC TTT TTT GTC CCC TGG CCA TAG AAT GTT TTT CTT CAT CTA ACA GAA CGG ATT TTA TTT TGA
AGG TAT TGT TCA TAG TGA TCT GAA GCC TGC TAA CTT TGT GAT AGT GGA TGG AAT GCT AAA GCT AAT TGA
TTT TGG GAT TGC AAA CCA AAT GCA GCC AGA CAC AAC AAG CAT TGT TAA AGA TTC TCA GGT TGG CAC AGT
TAA CTA TAT GGC CCC AGA AGC AAT CAG AGA CAT GTC TTC TTC AAG AGA AAA TTC GAA AAT CAG AAC CAA
GGT AAG TCC CAG AAG TGA TGT CTG GTC CTT GGG GTG CAT TTT GTA CTA CAT GAC TTA TGG GAG GAC GCC
ATT TCA GCA CAT CAT CAA TCA GGT CTC TAA ACT GCA CGC CAT AAT CAA CCC TGC TCA TGA GAT TGA ATT
TCC CGA GAT TTC GGA AAA AGA TCT TCG AGA CGT GCT AAA GTG CTG TTT AGT GAG GAA CCC TAA AGA GAG
GAT ATC TAT CCC TGA GCT CCT CAC ACA TCC GTA TGT TCA AAT TCA GCC CCA TCC AGG CAG CCA AAT GGC
TAG GGG AGC CAC TGA TGA AAT GAA ATA TGT GTT GGG TCA ACT TGT TGG TCT GAA TTCT CCT AAC TCC ATC
TTG AAA ACT GCA AAA ACT TTG TAT GAA CGT TAT AAT TGT GGT GAA GGT CAA GAT TCT TCG TCA TCC AAG
ACT TTT GAC AAA AAG AGA GAA AGA AAG TGA TGC ACA GCT ACG TAC AAA CCA AGA ACA CTA GAT TGT TTC
CTC TGC CAT ACT CTT GAA TCT CTG AGG AAA TCT ACC AGT TGG AAA CAA CCT CAC CTG GAT TTT ATC AGT
TAA AAA AAC AAA CAA ACA AAA CTT CAG TAG ATT ATC CTC AAA AGA AAG CTG TAA AGT TAA CCA CTC ATA
GCA CTG TGT ATA TTA AAT TAT AGA GTT GTG CTT TTC TTT TAT GCT TTT CTG TAA ATC TGC TAA TGT TTT ACG
TTT GGA ACA GTG AAT GAT AGC TGG AAT GTT GAA GAG CTC TGT AAA TAA AGC GTC ACC ACA GTT CCA GAA
CTG TAC AGT GGT CAG TTT CTT CAA TCA AAT GTG TTC TTG GCA TGA TAG CAA AAT TTT TAG AAA AAC GGG ATT AAG
```

AAT AGA CCG TAG TAA ATA AAG TTT AAC AAT TAA ATT TCC AAA GGA TTT AGG ACT GTA AAC AGG CTC ACA CCT TTA
 GTC CCA GCA CTT GGG AGG CAG AGG CAG GCA GAT TTC TGA GTT CGA GGC CAG CCT GGT CTA CAG AGT GAG TTC
 CAG GAC AGC CAG GGC TAC ACA GAG AAA CCC TGT CTT GGC GGG GAG GGG CCG GGG AGG GGG GGA GAT CCA
 AAG GAT GTA GGA GGC AGA GAC AGG TGG ATCT CTG TGA TTCT GAA GCC AGC CTG GTC TACA GAA CTA GTTC TAG
 GAT AGC CAA GGC TAT ACA GAC ACT TTC TCC CCA CCA CCA TCC TGC CCT CAA AAA AAT TGT AAA TAA ATT TCC
 TAA TTG TGT ACA GCC ATG ATA CCA TCT ATA GTA TTT GGT CTG CAA GTG GCT TTT TCA GTT CTC CCT TTG ACT CTT
 CAA AGT ACA TAT GGG GTT TGG TGT TCT AAA TAT TGT GCT GGA GTT TGT GAT TTA ATG TCT ATA GTT AAT ACA TGC
 CAT TAT TGA GTT AA TTAA

Product #1 was obtained by standard PCR using genomic DNA from 129/Ola-derived IB10 ES cells (kind gift from Hans Clevers). Primers used (*Italic* is overhang, in *Capitals/Italic* the restriction sites):

#1 Forward: *cggcg*AAGCTTATGGCCAGTTTTTCAG

#1 Reverse: *cgccg*CTCGAGCTTCAAATAAAATCCGTC

Product #2 was obtained by standard PCR using mouse cDNA (Imagenes, Germany, BC 058851, ID: 30023533). Primers used (*Italic* is overhang, in *Capitals/Italic* the restriction sites):

#2 Forward: *ccggc*CTCGAGgcctactctggtgTATTGTTTCATAGTG

#2 Reverse: *ccgcg*GGATCCgcctactctggtgCTGGAAGTGTGGTGAC

Product #3 was obtained by standard PCR using genomic DNA from 129/Ola-derived IB10 ES cells (kind gift from Hans Clevers). Primers used (*Italic* is overhang, in *Capitals/Italic* the restriction sites):

#3 Forward: *ccgcc*GGATCCAACTGTACAGTGGTC

#3 Reverse: *ccgccg*TTAATTAAGTCAATAATGGCATG

First, products #1 and #2 were ligated by standard methods into pCDNA3 simultaneously. XhoI site was removed using site-directed mutagenesis. Primers used:

(XhoI)loop Forward: GACGGATTTTATTTGAAGGTATTGTTTCATAGTGATC

(XhoI)loop Reverse: GATCACTATGAACAATACCTTCAAATAAAATCCGTC

Second, product #3 was ligated into the pCDNA containing #1 and #2. BamHI site was removed using site-directed mutagenesis. Primers used:

(BamHI)loop Forward: GCGTCACCACAGTTCAGAACTGTACAGTGGTCAG

(BamHI)loop Reverse: CTGACCACTGTACAGTTCTGGAAGTGTGGTGACGC

This resulted in completion of the conditional fragment. Third, the conditional fragment was digested from pCDNA and ligated into pAC16 (using *HindIII* and *PacI* restriction sites).

2) 5' Recombination arm

The 5' recombination arm fragment was obtained by standard PCR using genomic DNA (from 129/Ola-derived IB10 ES cells (kind gift from Hans Clevers).

Primers used (*Italic* is overhang, in *Capitals/Italic* the restriction sites):

5'arm Forward: *ctagcgGTTTAAACTCGAAGGCCTCAACCTCACAGAGATCTTTC*

5'arm Reverse: *atcttaGGCGCGCCGGGCCCTCTCCTCCTATCTGTAGGATG*

This resulted in the following complete sequence of the 5' recombination arm:

(*PmeI*-(lastpartof)intron14-**exon15**-intron15-**exon16**-(firstpartof)intron16-

Apal-Ascl (~2kb):

```
GTT TAA ACT CGA AGG CCT CAA CCT CAC AGA GAT CTTT CTG CTTC TGC CTC TCTC CTG AGT GCT GAG ATT AAA GGT
GTG TGC AGC CAT GCC TAG CTG TGT GTG GCT TTC CTG TTA CCA CAT TCT GTG GAT AGC TTA TCT GTT GTT TGT GCC
CCA CCT TGT ACT TAA TAT CAA GAT GAG ATG TTT GGC TGT TCG GTG ATA CTA GCT CTG GTG ACT AAA ACT GAA TAG
GAC CTTT ATT CCT TTG CTG AGT GTT CCT CCT TGG CTA CAG GCT GTT TTA TGT TAT GGT GAT ACA TGA ACA GAG
ATA AAG GGC TTA TTTT AAG TTTT ACT GTA ATT CTC TAA GCC AGC TAG CTG TAA TTA GAC TTG CTT CTG GCT ATT TTA
TTA ACT TAT AGC AAG TAA TTG GAA AGC ATC CCA TCA GAC CCA TTT GTA TAA TTC CTG CAC ACA GTA CGC TGA GG
CGG GAT GAT TGC CTG GGC TAC ATA CAT GCA CTG TAT AGG CTG CTG CTA TGG CTT TGG TGC AGG GCC CTG GCT
TTA ATC TCT TAA CAT AAA AAC CAT AAG CAA AAG ACA AAA TAG GTA GGA GTG TAT ATT TCC ACA TGG AGC ATG TCT
TCC CAT AAA TAT TTT CCT TTT CAC GCT CCC CTT ATT AGA TTT TCA GTT ATG AGC ATA AGG AAG AAG GTG GGG TAA
GAG TGA TTG AAC AAG AGT GAC AGG GAA GAG GAT TCG TGC AGG GGA GGG AAG TGC ATG CAT GTT CTA GGC ACT
GAG TGA TGG GTG TGC TGG AAG CTG TAA ACT GCG TGG GGG CCT CTT CCT CAG TGC TTT AAG AAA TTG ATT CAT
AG GAA CAT CAT TGC TCC TGC CAA CCT AAC TCA ACT GTG ACT TGC GCT GCT TTC CAC AAA TGA ATG TAG TGA TGG
CTT ACA ATT ACT GTG ATT TTT AAA AAT ATT CCC TAT CAG AGA AAT GAA TTG GTT GAT AGT AGG CAC AAT GAA AAG
GTG GGA GTT GGT GGG GAG AGG GGT CTA GGA AGT GAA CTG TCA AAT CAC AGC CTT AGT CAT CCT TAT CGT CTT
CGA ATG TCT TTT CCT TGA TGT TTT CTC CCT GGA TAA GAA AGG CAT CCC TAG AAT TTT GTG GAT ATA GCA ACA TCA
TAT TTA AGT TGG TTT TCT TAG ACA CTG ATG TAG AAA ACC TTT GAA TTA TTT GAA TGT CCA TTG TTA TAG GGG CTG
GAA ATG GAT ACT TAG CTT CTC ATG TTG GTA TTT CTT TAG GAA TAT CCT CAG CCT GAG ACT GTT AGT GTT AAA TGG
AAA GGT ACT GCT CCA GTT TTCA GAG GGA GAC ATG TCCT AAG CTC TTT CTC CAC TTT TTA TGT AGG TGT TTC AGG
TAT TGA ATG AGA AAA AAC AGA TAA ACG CTA TCA AAT ATG TGA ACC TAG AAG ACG CCG ATA GCC AAA CTA
TTG AGA GCT ACC GCA ACG AGA TAG CGT TTT TGA ACA AAC TAC AGC AAC ACA GTG ATA AGA TCA TCC GCC
TCTA TGA TTA GTA TGA ATT CAT TTT TAT TTT AAA AAT AAA AGT TTG TTC TTG CCA TAA TTC TTA GGC AAA GAG TAA
ATC CTT AAT GAC ATA ATG TGG GCA TTTA TTG TTT TGT TGT GTC TGT TTA TCT TTA ATT GCA GTG AAA TCA CCG AGC
AGT ACA TCT ACA TGG TAA TGG AAT GTG GAA ACA TTG ACC TAA ATA GTT GGC TTA AAA AGA AAA AAT CCA
TCA ATC CAT GGG AAC GCA AGA GCT ACT GGA AAA ACA TGT TGG AGG CAG TAC ACA TAA TCC ATC AGC ATG
GTA TTT TCA TAT CTC TTC ATA CAC GTA AAG TTA AAA TAG TTG TTA ATT GTG CCA TTT TA GAA ACA TAC CCT TAA CTG
GAA GTT CAT TAG AGG TGA AGG CAC TCT TAA GAG TGG TTA TAC ACA GGC TAC AGA ACA CAA ACA AGC ACA GGA
TGT AGA ACA GAA ATG GCC ACA TGT ACA ATG TAA ACT TAC CCT CCT CTG GTA CCT GGG GAT TCC TAT CTT CAA GTC
CTG AGG ATT TGG ACA TCC TAC AGA TAG GAG GAG AGG GCC CGG CGC GCC
```

This fragment was ligated into pAC16 containing the conditional fragment (using *PmeI* and *Ascl* restriction sites, upstream of 5' loxP site).

3) 3' Recombination arm

The 3' recombination arm fragment was obtained by standard PCR using

genomic DNA (from 129/Ola-derived IB10 ES cells, (kind gift from Hans Clevers)).

Primers used (*Italic* is overhang, in *Capitals/Italic* the restriction sites):

3'arm Forward: *ccgccCCTGCAGGATGGCCAGTTTTTCAG*

3'arm Reverse: *ctagcgGCGGCCGCTATTTGCAAATCACAAAG*

This fragment was ligated into pAC16 (using *SbfI* and *NotI* restriction sites, downstream of 3' loxP site). CiMKi point mutations were introduced using site-directed mutagenesis.

Primers used for T649A mutation:

mMps1-T649A-F: CAAATGCAGCCAGACACA***GCA***AGCATTGTAAAGATTC

mMps1-T649A-R: GAATCTTTAAACAATGCTTGCTGTGTCTGGCTGCATTTG

Primers used for D637A mutation:

mMps1-D637A(KD)-F: GAATGCTAAAGCTAATT***GCT***TTTGGGATTGCAAAC

mMps1-D637A(KD)-R: GTTTGCAATCCCAAAGCAATTAGCTTTAGCATTC

This resulted in the following complete sequence of the 3' recombination arm (*SbfI*-(lastpartof)intron16-**exon17***-intron17-*NotI* (~2.2kb), containing either T649A or D637A point mutation in exon 17):

CCT GCA GGA TGG CCA GTT TTT CAG TCT CCA AAG GAT TTT CTC TTT GGA GCC CGG TGT GAG AGT TGG TCT GTT CTT
GCT GTT TTC TGT TTC ATT ATT TGT TTG TTC TTG TTC TCT CCA GTT TCC TCT GCC TTT CCC TTG TCT TTT AAA CAG ATG
TGT TCA ATC TCA TGC GCT TCC TCT GCT TCT CCT TTT AGA AGC AGT AAC TAA GCA GAG GAT AGG ACT CTT TGG GGG
TGA GGG AGG CCT TGC GAT CTT ATT GTC TGA CAG TTC TTG GTG GTG CTT TCC TGG CCT GTG CAT GGC AGT GTG
CAG CAC ACA CTG ACA GGC TAG GCC TGG AAT CCT GAA CAG TTC ACT TCA ACT CAA ATC ACA TTG AGT GTC CTC
ACC CTG AAA ATG ATG ATA ATG GGA CTT ATT TGC TAT GCA TTG CTA TAG AAT GGT ACC TGG CCC ACA ACA TTT
GCT AAG AAA GTG TAG AAT GTA TAA TAA CTA AAT ATT AAT GTG TTG CCT AAT TGA AAG GAT AAG CCT GAC CTA AAG
ATT ATG AAA TGC TTT TTT GTC CCC TGG CCA TAG AAT GTT TTT CTT CAT CTA ACA GAA CGG ATT TTA TTT TGA AGG
TAT TGT TCA TAG TGA TCT GAA GCC TGC TAA CTT TGT GAT AGT GGA TGG AAT GCT AAA GCT AAT T*GCT*TT
TGG GAT TGC AAA CCA AAT GCA GCC AGA CAC A*GCA*AG CAT TGT TAA AGA TTC TCA GGT AGG AGT TTT GCT
GTC TTG GTT GTA TTT TAG TGT TTT GAA CCA GGG TTT TGC ATC AGG GTT TTG CAT AAC CTA GAA TGC TCT TGA CTT
TGA TCA GTG GCC TTC AGC TCC TGA TCC TGC TGC CTG TGC ATC CCA GGT GTG GGC TTA TAG GTG TCA GCC CCG
ACA CCC GAC TTC AGG TAG GAT TTT AAT GAT GGC TGG TTA CTA CAA GGC TTA GTT CAT TTT TAT CTG TTA AAT ATG
TTG CCA ATA TTA TAT TTT TAC CAA CCA TGT TAT TCC AAA AAT TTG AAG TCT TTT TAA AGA ATA GAA ACT ATG TTT ATA
AAA GAC CAT GGT CAA AGC CAT GGT CAA TTT GAT TTA TAA AAG CAG TTC AAG ATC AGA CAA GTA TAT TTA TGA ATT
TTG GAT GAT TTT CTC ATA GCT GAG GCA GGG CAG AGA GTA ATT GCA CCT TCA TGT TCT CCA CTG TCC TGT TTC TTT
TTC TTA CTG CTT AAA TTT GGG AGA AAG TTT TAA GAG AGC CTT ATT GGG AAT ACT GAA GCG TTC CAC TCA GCT ACG
CGT TAA AAA GGA AAT ATT TTA CTT ACT GTT TGG GGG GCG GTG TGC GGA TTC CAG ATG TAA GTG TGC CAT TGT GGA
GGT GTG GGG ATG GCT TCG GTA AAC CAC TTCT CTC CTA CTG TGG GCC CTG GGA GCC AAA GTC AGA TTG TGT GTG
CAG CAA GCT CTA CAG CCC AGC TGT GCT TTG TAG TAA CAT TTG CTG TGG TAA ATC TCA TGA AGC TGA AGT AGT
GAG GGG AAA ACA GAG CTG AAA GGT GAT GTC GAC TGC ACC TCG CAG GCT GTG TCC AGG GAT GGA GAT AAA TCA
GAA GAT AAA TTA CCA TGC ACG TAG AAA GTC ATT CTT CTT GAC AGC CAT TCA TTG TTT TTT GTT TCA GAA GTA CAG
ATG ATG AAC AGT GAG TGT AGA TGA GAC TGA AGT TTT CTA TGG CAA GGT CTT AGC AGG CCG ACA TTT TGT TAC CTT
AGA ACT AAA GGA TTT TGC GTA TTA TCT CCA TGC CCA GCT AGA GAA GCT CTT CTC TGA TAT AGG TTT CCA ACC CAT
CTT GAT CTG CAC ATG GAG CCG AAG AAT ATT GGG AGA TAA AGC TAG CTG GTT CCT TTT ATT CAT GTA TTA ATT TGT

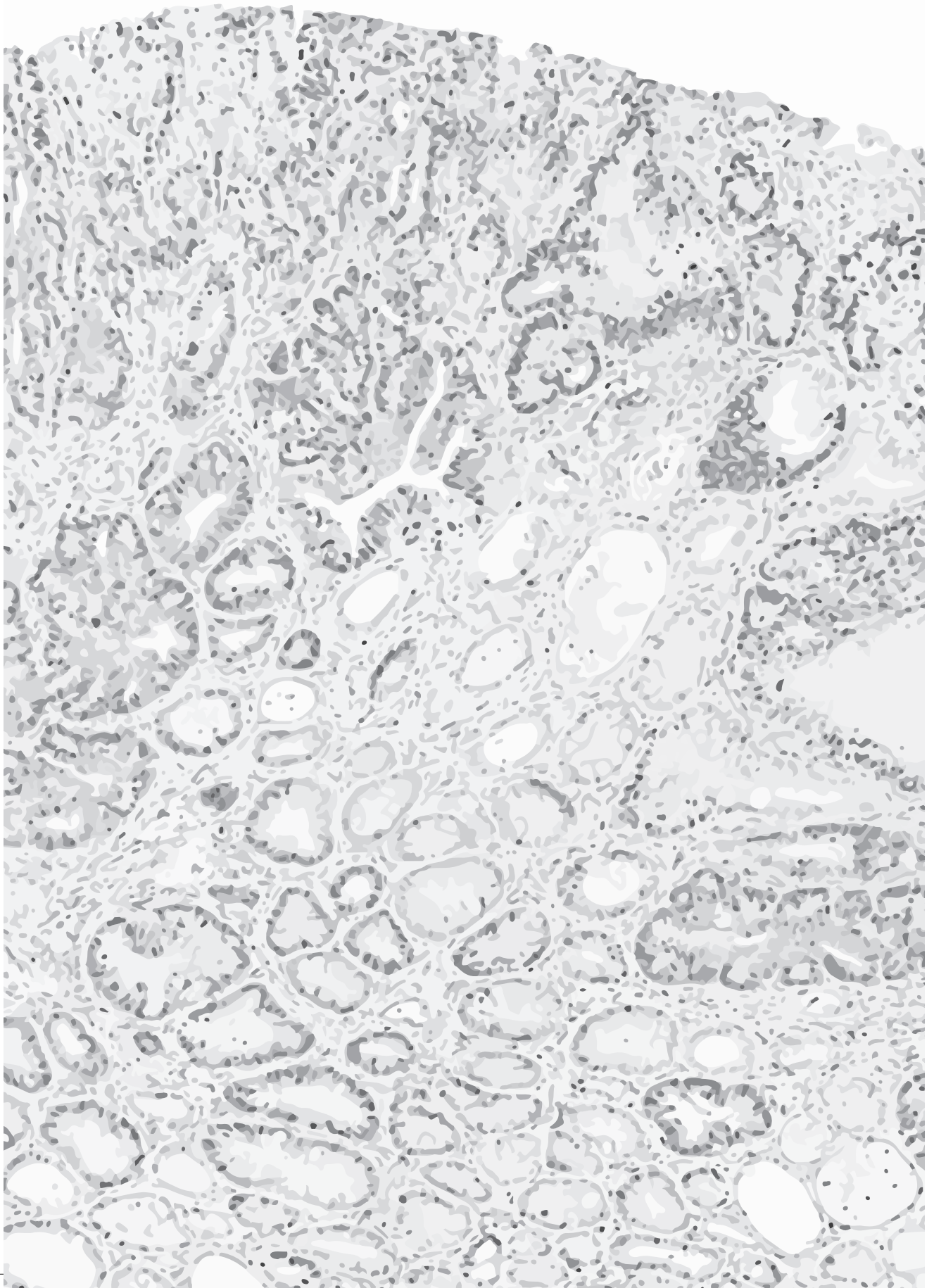
TGC TTG GTT TAT TGA GGG AAG AAT ATG TTG AAT TTA TTG GAA CAT GAA AGT GAA TGA AAG GCC AAG TTC AGA ATC
CGC CTA CGC AGT TGT AAA GAC TTA GTA CTT AGT ACT TAG TAC TTA GCA CTA GCT CTC CAG CAC AGC TGC AGA
CAG CAC AGT GCT CCC TGT GCT CCA GAC GGA GCC CGT TCA TTC TCA GCC CAG CTC ATC TGA TTG TAC CTG GGA
TGG GAT AGT ACA TAC ATT CTT ATA TTG TTA GCA GTT ATT TGA ATT TTT CAA GTC TGT CAT TTA AAT CAT TAG TTA TTC
AAA TTT CCA AGA ATC TGA CAT TTA CAT ATT TAC AAA TCT AGA AAG ATA TTC TCA TTG ATT TCT TTG TGA TTT GCA
AAT AGG CGG CCGC(*GCT* =D637A, *GCA* =T649A)

These fragments were ligated separately into pAC16 containing the conditional fragment and the 5' recombination arm (using *SbfI* and *NotI* restriction sites, downstream of 3' loxP site), to obtain the two separate complete targeting vectors containing CiMKi-T649A or CiMKi-D637A.

Fidelity of all PCR products, site-directed mutagenesis steps, and ligation steps were verified by sequencing.

2





Appendix Chapter 2

Oncogenic impact of chromosomal instability depends on time of induction

**W.H.M. Hoevenaar¹, A. Janssen^{2,#}, A.I. Quirindongo^{1,#}, H. Ma^{3,#},
B. van Gerwen¹, G.J.A. Offerhaus³, R.H. Medema⁴, N. Jelluma^{1,\$},
G.J.P.L. Kops^{1,\$}**

¹Oncode Institute, Hubrecht Institute-KNAW and University Medical Center Utrecht, Utrecht, The Netherlands.

²University Medical Center Utrecht, Center for Molecular Medicine, Section Molecular Cancer Research, Utrecht, The Netherlands

³University Medical Center Utrecht, Department of Pathology, Utrecht, The Netherlands

⁴Oncode Institute, Division of Cell Biology, Netherlands Cancer Institute, Amsterdam, The Netherlands

#, \$ equal contributions

Introduction

In chapter 2 we described the impact of various CIN levels on intestinal tumorigenesis in wild-type and $Apc^{Min/+}$ backgrounds. Moderate and high CIN had strong, but distinct effects on tumorigenesis in the intestine when induced at 12.5 days post coitum (dpc) by Cre expressed from the Villin promotor. The next step would be to more precisely control the moment of induction, since it is still a matter of debate when during tumorigenesis CIN arises and how it contributes to tumour development. Allelic imbalances found in early colorectal adenomas from familial adenomatous polyposis (FAP) and sporadic colorectal cancer (CRC) patients argue for early of CIN events^{1,2}. Still, the extent of aneuploidy increases further in stage I non-hypermuted CRC, which implies CIN is a continuous factor during tumour progression^{1,2}. Also, CIN and aneuploidy levels have been shown to correlate with tumour stage and aggressiveness³⁻⁵, and intra-tumour heterogeneity^{6,7}.



It has been difficult to assess the influence of various CIN levels at different timepoints during tumorigenesis. CIN in most murine models is not inducible and levels are not controlled (for reviews see^{8,9}). We have overcome these shortcomings in our *CiMKi* model in the background of CreER^{T2} expression: various levels of CIN can be induced in a time- (by tamoxifen injection) and tissue-specific manner, depending on the promotor used to drive CreER^{T2} expression. Here, we used *CiMKi;Apc^{Min/+};VillinCreER^{T2}* mice to induce CIN at two different timepoints during tumour development. *Apc^{Min/+}* mice start developing adenomas at approximately four weeks of age, which is generally the moment that spontaneous loss of heterozygosity (LOH) of *Apc* occurs. Tumours continue to develop until 12 weeks of age, when numbers stabilise and size increases¹⁰, though no progression beyond the adenoma phase occurs^{11,12}. We assessed the effects of various CIN levels on tumour development by CIN induction at the time of tumour onset (four weeks), and on tumours when these were already established (12 weeks).

Results

CIN induction at various time points in *CiMKi*; *Apc*^{Min/+}; *VillinCreER*^{T2} mice

To study the tumorigenic effect of CIN when induced at various timepoints during tumorigenesis, we generated *CiMKi*;*Apc*^{Min/+};*VillinCreER*^{T2} mice, in which various levels of CIN can be induced at defined timepoints by injecting the mice intraperitoneally (i.p.) with tamoxifen (Fig. A1a). All mice were born healthy and at Mendelian rates, contrary to the non-inducible *CiMKi*;*Apc*^{Min/+};*VillinCre* mice, where KD/KD mutations appeared to be embryonically lethal (Chapter 2). CIN was induced at the moment of tumour onset, or when tumours were established. Efficient induction of the *CiMKi* alleles was confirmed by targeted sequencing of intestinal tissue or tumor cDNA (Fig. A1b).

A2

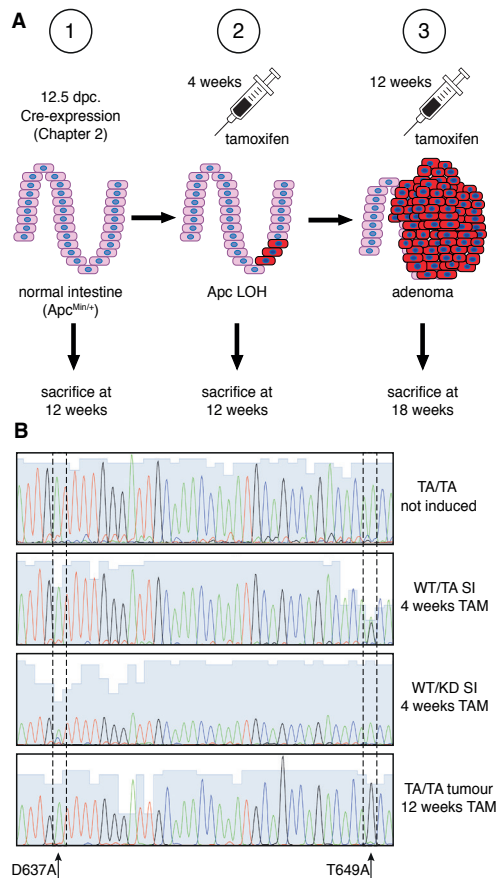


Figure A1: CIN induction at various time points in *CiMKi*;*Apc*^{Min/+};*VillinCreER*^{T2} mice. a, In *CiMKi*;*Apc*^{Min/+};*VillinCre* mice *Cre* is expressed from the *Villin* promoter from 12.5 dpc, *CiMKi* mutations were expressed already before tumour onset (1). *CiMKi*;*Apc*^{Min/+} mice were bred in a *VillinCreERT2* background, so CIN could be induced by 4-OHT injection at the moment of *Apc* LOH and onset of tumorigenesis (2) or when tumours were already established (3). b, cDNA sequences of *CiMKi* mutation sites in *Mps1* from intestinal or tumour tissue of *CiMKi*;*Apc*^{Min/+};*VillinCreER*^{T2} mice. Analysis was done four weeks (small intestinal tissue of 12-week-old mice) or one week (colon tumour, 13-week-old mouse) after tamoxifen injection. A non-induced tumour sample is given as reference.

CIN induction at tumour onset increases proliferation but does not affect tumorigenesis in the small intestine

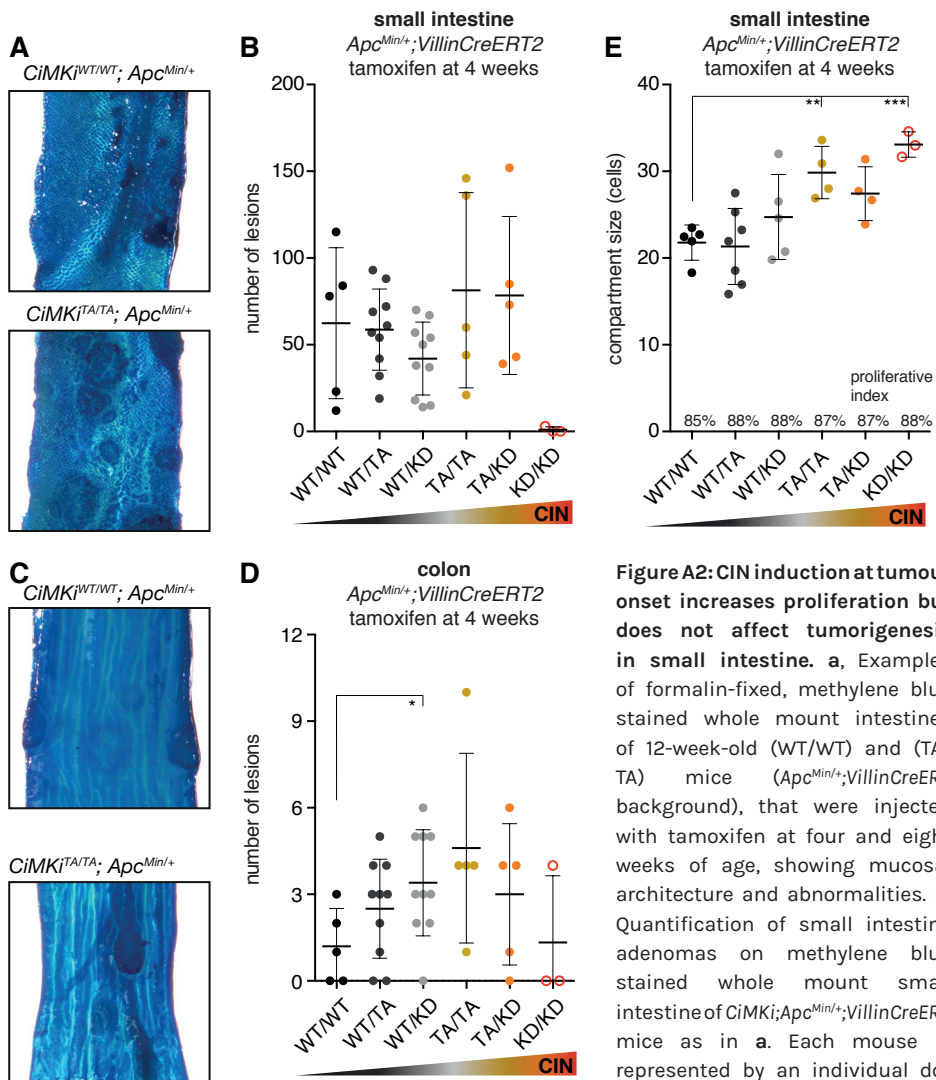
We first assessed whether certain levels of CIN could contribute to tumorigenesis when induced around the moment of tumour onset. *CiMKi;Apc^{Min/+};VillinCreER^{T2}* mice were injected with tamoxifen at four weeks of age, and injections were repeated after four weeks to ensure long-term recombination. Mice were euthanized at 12 weeks of age. Intestines were removed, cleaned, fixed in formalin, and stained with methylene blue to count the number of lesions in small intestine and colon.

CiMKi^{KD/KD};Apc^{Min/+};VillinCreER^{T2} mice had to be sacrificed after one week due to severe weight loss, similar to what we observed in *CiMKi^{KD/KD};Rosa26CreER^{T2}* mice. In the other *CiMKi* genotypes no significant differences in the number of lesions in the small intestine were observed at 12 weeks (Fig. A2a, b), though it has to be noted that tumour numbers were highly variable in this experiment (Fig. A2b). In colon, there was a small but significant increase in tumour numbers in *CiMKi^{WT/KD}* mice compared to *CiMKi^{WT/WT}* (Fig. A2c, d). Although no further obvious effects were observed on tumorigenesis, the acute induction of CIN at four weeks did cause increased proliferation rates in the small intestine. At 12 weeks, moderate and very high CIN mice showed an increase in size of the proliferative compartment of the intestinal crypts (Fig. A2e).

High CIN increases tumorigenesis when induced during tumour development

To determine whether the various CIN levels would affect tumour progression in already established tumours in *Apc^{Min/+}* mice, CIN was induced in 12-week old *CiMKi;Apc^{Min/+};VillinCreER^{T2}* mice by tamoxifen injection. Injections were repeated four weeks later, and mice were sacrificed at 18 weeks of age. This allowed sufficient time for expression of the *CiMKi* alleles to exert their effect, but is still in a range that *Apc^{Min/+}* mice can survive without excessive health problems. After autopsy, intestines were cleaned, fixed in formalin and stained with methylene blue. Lesions were counted in small intestine and colon of all genotypes. In the small intestine, the variance between mice of the same genotype was substantial,

A2



A2

Figure A2: CIN induction at tumour onset increases proliferation but does not affect tumorigenesis in small intestine. a, Examples of formalin-fixed, methylene blue stained whole mount intestines of 12-week-old (WT/WT) and (TA/TA) mice (*Apc^{Min/+}; VillinCreERT2* background), that were injected with tamoxifen at four and eight weeks of age, showing mucosal architecture and abnormalities. b, Quantification of small intestine adenomas on methylene blue stained whole mount small intestine of *CiMKi; Apc^{Min/+}; VillinCreERT2* mice as in a. Each mouse is represented by an individual dot

(n=3-10 mice per group), data represents mean \pm SD. Open dots represent mice euthanized five weeks of age, closed dots are 12-week-old mice. c, Examples of formalin-fixed, methylene blue stained whole mount intestines of 12-week-old (WT/WT) and (TA/TA) mice (*Apc^{Min/+}; VillinCreERT2* background), that were injected with tamoxifen at 4 weeks of age, showing mucosal architecture and abnormalities. d, Quantification of adenomas on methylene blue stained whole mount colon tissue as in c. Each mouse is represented by an individual dot (n=3-10 mice per group), data represents mean \pm SD, asterisk indicate significance (two-tailed t-test, comparing each group to WT/WT, $p < 0.05$ (*)). Open dots represent mice euthanized at five weeks of age, closed dots are 12-week-old mice. e, Proliferative compartment in small intestine of 12-week old *CiMKi; Apc^{Min/+}; VillinCreERT2* mice that were injected with tamoxifen at four weeks of age, as determined on Ki-67 stained FFPE slides by scoring the number of cells between the first positive cell at the bottom of the crypt and the last positive cell in the transit amplifying zone. Dot plot shows the size of the compartment for each mouse (n=3-7 per genotype, 10 crypts per mouse) and error bars represent SD asterisk indicate significance (two-tailed t-test, $p < 0.001$ (***), $p < 0.01$ (*)). Proliferative index (percentage of Ki-67 positive cells within compartment) is indicated for each genotype.

however, high CIN mice developed significantly more lesions than wild-type (Fig. A3a, b). For colon, the number of lesions was similar in all genotypes (Fig. A3c, d), indicating that late induction of CIN in *CiMKi*;*Apc*^{Min/+};*VillinCreERT2* had not affected tumour numbers. Induction of the *CiMKi* mutations was confirmed by targeted sequencing of tumour cDNA (Fig. A1b), excluding loss of Cre-expression in the tumours leading to uninduced tumours¹³. The late induction of CIN had also not affected proliferation rates in normal-looking crypts of the intestine at 18 weeks of age (Fig. A3e).

A2

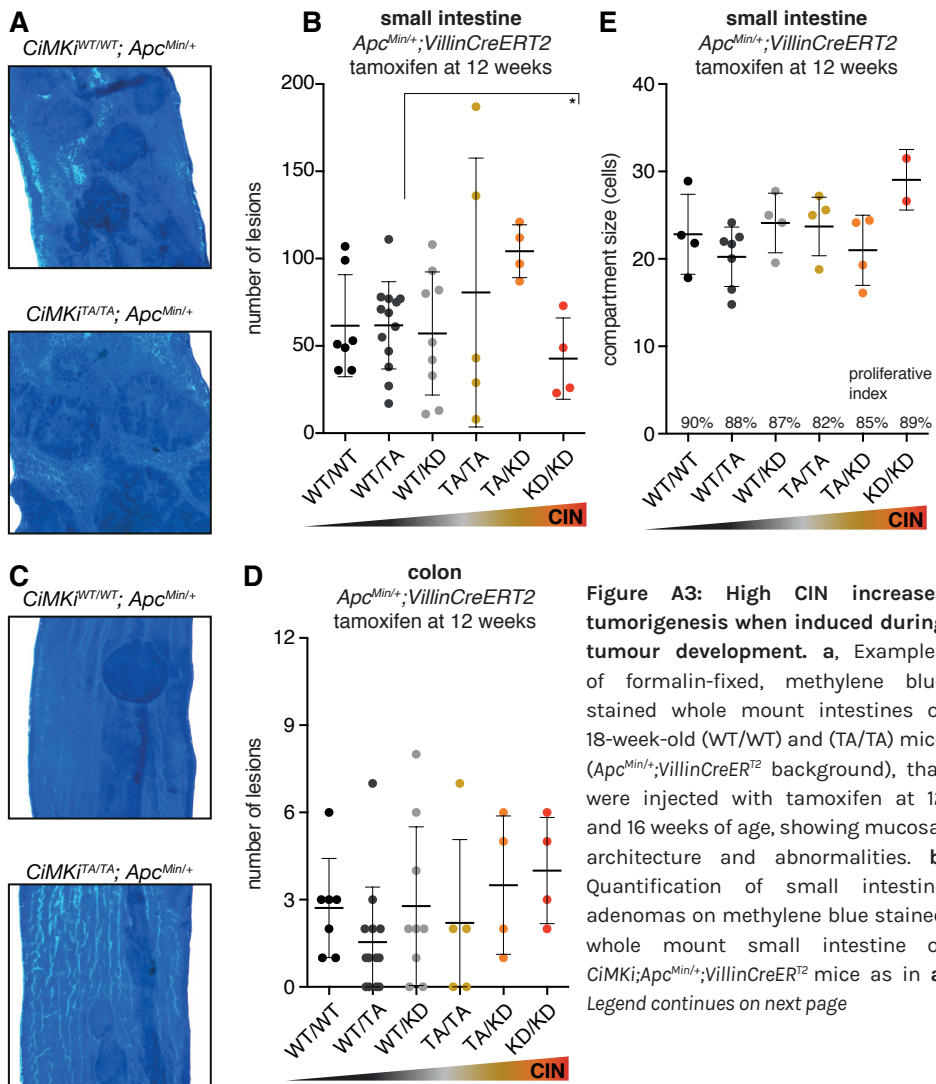


Figure A3: High CIN increases tumorigenesis when induced during tumour development. a, Examples of formalin-fixed, methylene blue stained whole mount intestines of 18-week-old (WT/WT) and (TA/TA) mice (*Apc*^{Min/+};*VillinCreERT2* background), that were injected with tamoxifen at 12 and 16 weeks of age, showing mucosal architecture and abnormalities. b, Quantification of small intestine adenomas on methylene blue stained whole mount small intestine of *CiMKi*;*Apc*^{Min/+};*VillinCreERT2* mice as in a. Legend continues on next page

Continued from previous page. Each mouse is represented by an individual dot (n=4-13 mice per group). data represents mean \pm SD, asterisk indicate significance (two-tailed t-test, comparing each group to WT/WT, $p < 0.05$ (*)). **c.** Examples of formalin-fixed, methylene blue stained whole mount intestines of 18-week-old (WT/WT) and (TA/TA) mice (*Apc^{Min/+}; VillinCreER^{T2}* background), showing mucosal architecture and abnormalities. **d.** Quantification of adenomas on methylene blue stained whole mount colon tissue as in **c.** Each mouse is represented by an individual dot (n=4-13 mice per group). **e.** Proliferative compartment in small intestine of 18-week old *CiMKi;Apc^{Min/+};VillinCreER^{T2}* mice as determined on Ki-67 stained FFPE slides by scoring the number of cells between the first positive cell at the bottom of the crypt and the last positive cell in the transit amplifying zone. Dot plot shows the size of the compartment for each mouse (n=2-6 per genotype, 10 crypts per mouse) and error bars represent SD. Proliferative index (percentage of Ki-67 positive cells within compartment) is indicated for each genotype.

Moment of CIN induction dictates its effect on tumorigenesis and proliferation

When comparing our data from the three moments of CIN induction, it became apparent that the impact of CIN on tumorigenesis is clearly dependent on the moment when CIN was induced during the process. Moderate CIN drastically increased tumour numbers in the small intestine when induced at 12.5 dpc, but had no effect when induced at four or 12 weeks of age (Fig. A4a). Moreover, high CIN did not affect small intestinal tumour numbers when induced very early, but it did lead to increased numbers when induced at 12 weeks of age (Fig A4a). In the colon, very early induction of moderate to high CIN highly increased tumour numbers, and this effect was absent when CIN was induced at later timepoints (Fig. A4b), although low CIN increased tumour numbers when induced at four weeks of age (Fig. A4b).

The various CIN levels also had distinct effects on proliferation in the small intestine between the different timepoints of induction. At 12 weeks of age, proliferative compartments were similar in size for all *CiMKi* genotypes when CIN was induced at 12.5 dpc, while induction at 4 weeks increased proliferation in higher CIN genotypes (Fig. A4c). CIN induction at 12 weeks did not affect proliferation in the small intestine at 18 weeks of age (Fig. A4c). In colon, there was no significant change in proliferation between the groups at 12 weeks of age, either when CIN was induced at four weeks, or at 12.5 dpc. (Fig A4d). The different phenotypes of the same *CiMKi* mutants induced at various moments in small intestine and colon underscores the different effects CIN has depending on where and when it is induced.

A2

A2

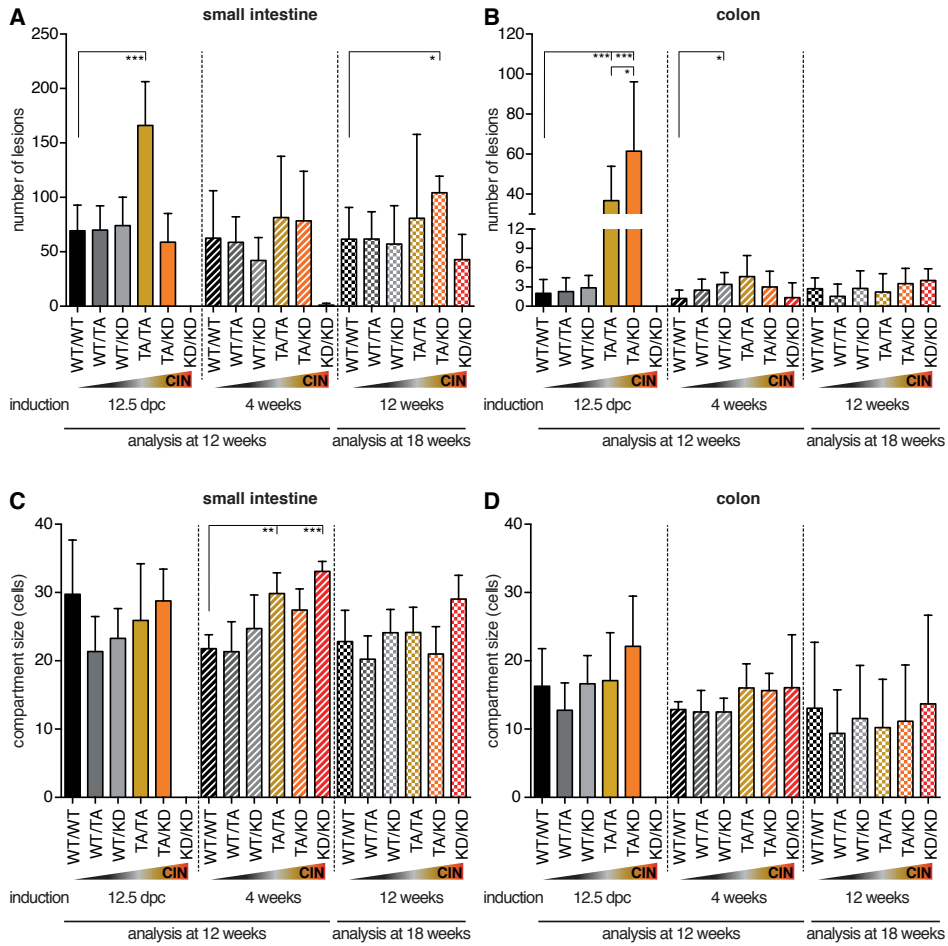


Figure A4: Moment of CIN induction dictates its effect on tumorigenesis and proliferation. **a**, Comparison of tumour numbers in the small intestine of the various *CimKi;Apc^{Min/+}* genotypes when CIN was induced very early (*VillinCre*, solid bars) or at the moment of tumour onset (*VillinCreER²*, striped bars), or when tumours were established (*VillinCreER²*, chequered bars), error bars represent SD. **b**, As in **a**, but for colon. **c**, Proliferative compartment in small intestine of the various *CimKi;Apc^{Min/+}* genotypes when CIN was induced very early (*VillinCre*, solid bars) or at the moment of tumour onset (*VillinCreER²*, striped bars), or when tumours were established (*VillinCreER²*, chequered bars), error bars represent SD. **d**, As in **c**, but for colon.

Discussion

This study aimed at identifying the possible roles of CIN at various stages of tumour development. While we showed in chapter 2 that CIN induction before the onset of tumorigenesis strongly affects tumour numbers in small intestine (moderate CIN) and colon (moderate and high CIN), this effect is not present when CIN is induced at the moment of tumour onset or when tumours are already established. Tumour numbers were slightly increased in colon of low CIN mice (induced at four weeks) and small intestine of high CIN mice (induced at 12 weeks), while this was not observed when CIN was induced at 12.5 dpc. These diverse effects on tumorigenesis indicate that the effect of CIN is dependent on the level, time, and location of induction. The same conclusion can be extended to the effects of CIN on proliferation. Various CIN levels impacted proliferation rates differently depending on the time and location of induction.

It has to be considered that tamoxifen-induced Cre activation can be more mosaic than when Cre is constitutively expressed, diminishing the effect of CIN. This holds both for CIN induction at the moment of tumour initiation and when the tumours are already established. Even though we confirmed mutant induction in normal-looking- and tumour tissue, the various CIN levels had minimal to no effect on tumour numbers or proliferation in both small intestine and colon, especially at 18 weeks of age.

The lack of effect when CIN was induced at or after tumour onset could imply that a main contribution of CIN to intestinal tumorigenesis is to accelerate LOH of *Apc*. In *Apc*^{Min/+} mice, tumour onset coincides with LOH of *Apc* which occurs at approximately four weeks of age^{14,15}. If CIN is induced after this event, the contribution to tumour initiation could therefore be lost or minimised in the timeframe we studied. Since we were not able to assess tumour sizes in the groups where CIN was induced at four or 12 weeks, we cannot exclude that CIN might have had an effect on tumour growth, even though there was no clear effect on tumour initiation. Furthermore, due to the short lifespan of *Apc*^{Min/+} mice, we were not able to assess possible effects of CIN that are manifested later during tumour progression, CIN driven stimulation of metastasis through for example

A2

the cGAS-STING pathway⁵.

Even though it was not possible to study the effects of various CIN levels during all stages of tumorigenesis, we can already conclude that the tumour promoting effects of CIN as described in Chapter 2 not only rely on its level, the tissue in which it is induced, but also strongly on the time of induction.

References

1. Borras, E. et al. Genomic Landscape of Colorectal Mucosa and Adenomas. *cancer Prev. Res.* 417-428 (2016).
2. Shih, I. et al. Evidence That Genetic Instability Occurs at an Early Stage of Colorectal Tumorigenesis. *Cancer Res.* **61**, 818-822 (2001).
3. Laubert, T. et al. Stage-specific frequency and prognostic significance of aneuploidy in patients with sporadic colorectal cancer—a meta-analysis and current overview. *Int. J. Colorectal Dis.* **30**, 1015-1028 (2015).
4. Benhra, N., Barrio, L., Muzzopappa, M. & Milán, M. Chromosomal Instability Induces Cellular Invasion in Epithelial Tissues. *Dev. Cell* **47**, 161-174.e4 (2018).
5. Bakhoun, S. F. et al. Chromosomal instability drives metastasis through a cytosolic DNA response. *Nature* **553**, 467-472 (2018).
6. Grady, W. M. & Carethers, J. M. Genomic and Epigenetic Instability in Colorectal Cancer Pathogenesis. *Gastroenterology* **135**, 1079-1099 (2008).
7. Amaro, A., Chiara, S. & Pfeffer, U. Molecular evolution of colorectal cancer: from multistep carcinogenesis to the big bang. *Cancer Metastasis Rev.* **35**, 63-74 (2016).
8. Ricke, R. M., van Ree, J. H. & van Deursen, J. M. Whole chromosome instability and cancer: a complex relationship. *Trends Genet.* **24**, 457-466 (2008).
9. Foijer, F., Draviam, V. M. & Sorger, P. K. Studying chromosome instability in the mouse. *Biochim. Biophys. Acta* **1786**, 73-82 (2008).
10. Puppa, M. J. et al. Gut barrier dysfunction in the ApcMin/+ mouse model of colon cancer cachexia. *BBA - Mol. Basis Dis.* **1812**, 1601-1606 (2011).
11. Shoemaker, A. R., Gould, K. A., Luongo, C., Moser, A. R. & Dove, W. F. Studies of neoplasia in the Min mouse. *Biochim. Biophys. Acta - Rev. Cancer* **1332**, F25-F48 (1997).
12. Fodde, R., Smits, R. & Clevers, H. APC, signal transduction and genetic instability in colorectal cancer. *Nat. Rev. Cancer* **1**, 55-67 (2001).
13. Arango, D. et al. Villin Expression Is Frequently Lost in Poorly Differentiated Colon Cancer. *Am. J. Pathol.* **180**, 1509-1521 (2012).
14. Moser, A., Pitot, H. & Dove, W. A dominant mutation that predisposes to multiple intestinal neoplasia in the mouse. *Science (80-)*. **247**, 322-324 (1990).
15. Jackstadt, R. & Sansom, O. J. Mouse models of intestinal cancer. *J. Pathol.* **238**, 141-151 (2016).



Methods

Animals

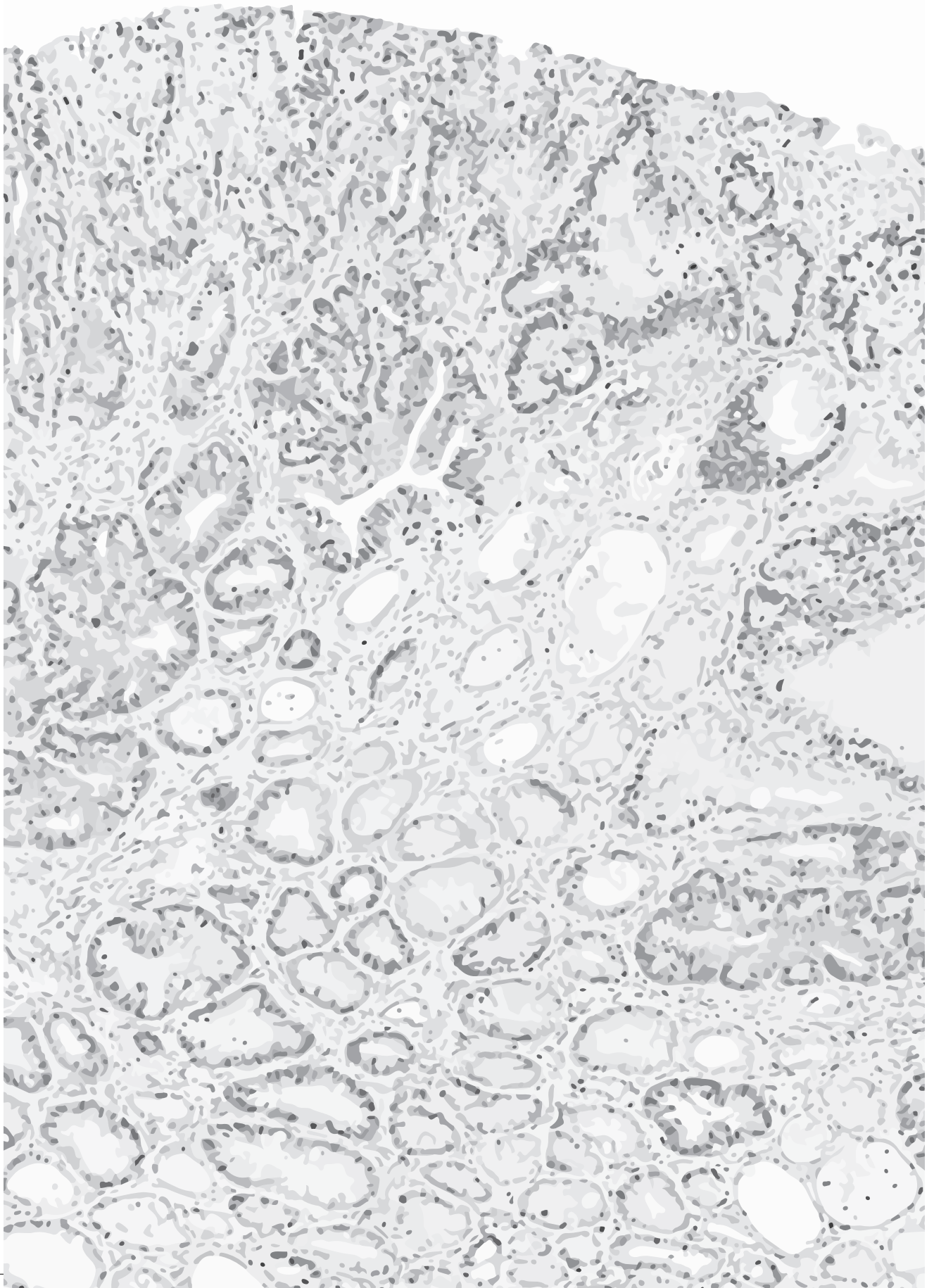
All animal experiments were approved by Animal Experimental Committee Utrecht under license number 2014.III.08.071. All animals were bred and housed under standard conditions at the animal facility of the Gemeenschappelijk Dieren Laboratorium (GDL), Utrecht, the Netherlands. *CiMKi* mice were generated as described in Hoevenaar et al. (Chapter 2 of this thesis). *VillinCreER^{T2}* were a gift from J. van Rheenen. All mice were maintained in C57BL/6 background. Mice were genotyped using standard PCR and targeted sequencing procedures. For primers see Table 1 (Chapter 2).

Treatment and analysis

Mice were assigned to groups based on their genotype and tamoxifen treatment started either at four weeks of age or at 12 weeks of age. Mice of all groups were intraperitoneally (i.p.) injected with 0.1 ml of 10mg/ml tamoxifen (Sigma) in corn oil (Sigma). These injections were repeated after four weeks to maintain proper induction levels. Mice that were injected at four weeks, were sacrificed at 12 weeks of age and mice that were injected at 12 weeks, were injected at 18 weeks of age.

All further procedures and analyses were done as described in chapter 2.

A2



Chapter 3

Distinct effects of various chromosomal instability levels on skin tumorigenesis

Ajit Quirindongo^{1*}, Aniek Janssen^{2*}, Wilma Hoevenaar¹, Pim Toonen¹, Banafsheh Etemad¹, Alain De Bruin³, Geert Kops^{1\$}, and Nannette Jelluma^{1\$}

¹Oncode Institute, Hubrecht Institute-KNAW and University Medical Center Utrecht, Utrecht, The Netherlands.

²University Medical Center Utrecht, Center for Molecular Medicine, Section Molecular Cancer Research, Utrecht, The Netherlands

³Department of Pathobiology, Dutch Molecular Pathology Center, Utrecht University, the Netherlands

#, \$ equal contributions

Abstract

Chromosomal instability (CIN) is a hallmark of cancer, and a primary cause of genetic heterogeneity in tumours. It is thought to enable survival and growth in changing environments during tumour progression and cancer therapy, but high CIN levels are lethal to cells, providing potential for tumour therapy. Here we use the novel CiMKi mouse model for graded CIN to study in real-time the potential of high CIN levels to cause regression of DMBA/TPA induced skin tumours, and the effects of various CIN levels on initiation and development of these tumours. We find increasing tumour killing potential by increasing CIN levels, which is generally followed by fast tumour relapse. When induced before tumour initiation, the distinct CIN levels all have specific tumour-promoting effects: low CIN levels increase tumour numbers, but not growth rate, whereas higher CIN levels accelerate tumour onset and aggravate growth rate. Remarkably, tumours induced by high CIN as well as relapsed tumours did not have fully induced CiMKi mutations, suggesting both were most likely initiated by low CIN cells present in the population. Our data suggests that tumorigenesis benefits from various CIN levels being present in the population, with high CIN leading to cell death and thereby opportunity for lower CIN populations to expand. This study therefore shows that various CIN levels have specific effects on skin tumorigenesis, and importantly, that induction of CIN as tumour therapy is not so straight-forward and potentially even harmful.

3

Keywords

Chromosomal Instability, aneuploidy, Skin Cancer, DMBA/TPA, cSCC

Introduction

Ongoing losses and gains of whole chromosomes by chromosomal instability (CIN) lead to aneuploidy and can result in copy number alterations of oncogenes and loss of heterozygosity (LOH) of tumour suppressor genes¹⁻³. CIN can also promote DNA damage and thereby induce various kinds of structural chromosome aberrations including translocations and chromothripsis⁴⁻⁸. CIN is thus at the heart of genome destabilization and intra-tumour heterogeneity⁹, which are thought to enable cancer cells to adjust to their changing environment during growth, progression, and treatment^{10,11}.

Even though aneuploidy has been widely observed in human tumours, cell culture and mouse studies have not led to an unequivocal answer to what the role of CIN in tumorigenesis is. Several studies modelling CIN in mice have shown that CIN can have a wide array of effects: CIN has been suggested to contribute to tumour progression, or to even induce spontaneous tumour formation, though with long latencies^{1,2,12-21}. In contrast, tumour suppressing effects of aneuploidy¹³, or premature ageing of the mice²² have also been reported. The different ways in which CIN was created, the CIN levels obtained and the timing thereof, the tissue types investigated, and the strains and oncogenic backgrounds used may all contribute to the different outcomes in the various mouse models²³. With our *CiMKi* mouse model, in which various levels of CIN can be genetically induced, we found clear distinct effects between the various CIN levels: high CIN levels were tumour promoting in the colon, but not in small intestine (Chapter 2 of this thesis), confirming that the effects of CIN on tumorigenesis are not uniform between various tissues.

Every one in three cancers diagnosed in humans is in the skin, and cutaneous squamous-cell carcinoma (cSCC) is the second most common and most aggressive form of non-melanoma skin cancer (NMSK)^{24,25}. In recent years global occurrence has grown, with two to three million new diagnoses each year, and repeated UV exposure probably being a major causal factor^{24,25}. The influence of CIN on cSCC is not known, despite high aneuploidy rates in this cancer type that concur with a malignant spectrum²⁶. cSCC goes through multi-stage development

ranging from a precursor actinic keratosis (AK) to squamous cell carcinoma (SCC), in situ (SCCIS), invasive cSCC, and finally metastatic SCC²⁷. Mutation of the proto-oncogene *RAS* (specifically *HRAS*) is described as an initiating event and loss of p53 function as a requirement for promotion to carcinoma. In the promotion phase, the epidermal growth factor receptor (EGFR), STAT3 and AKT-mediated signalling pathways are activated, while PKC, E-cadherin, NOTCH, and CDKN2A mediated signalling are negatively affected²⁷⁻³⁰. Progression from the AK to cSCC stage is accompanied by various forms of genomic instability, including chromosome rearrangements, amplifications and copy number alterations^{26,31}. Therefore, CIN could play a significant role during this multi-stage development of cSCC.

3 Much of what we know about the development and progression of cSCC comes from mouse experiments using a two-stage skin carcinogenesis approach consisting of topical application of 7,12-dimethylbenz[a]-anthracene (DMBA) for tumour initiation and consequent treatment with 12-O-tetradecanoylphorbol-13-acetate (TPA) for tumour promotion. In this model, human disease is recapitulated by *hras* and *p53* mutations and the tumours progress from papilloma to cSCC and even the metastatic phase can be reached^{28,32}. Interestingly, the level of aneuploidy correlates with the progressive stage of these skin tumours and with tumour aggressiveness^{33,34}, similar to what was described for human tumours^{26,35,36}.

Despite the potential relevance of CIN and aneuploidy, these studies have not investigated the effects of CIN on the initiation, development and possible regression of these tumours. Currently, clinical trials are executed with MPS1 inhibitors to assess their potential as therapeutic target and mouse studies show promising results on tumour regression, but the combined effects on tumour development and regression are not well investigated³⁷⁻⁴². Here, we used the *CiMKi* model mouse for CIN (see Chapter 2 of this thesis) to explore the effects of induction of various CIN levels on DMBA/TPA induced skin tumorigenesis. We studied how tumours respond to acute induction of various CIN levels, and how initiation and development of these tumours is affected by various degrees of CIN. We found that low CIN levels increase tumour numbers, but not growth rate, whereas high

levels of CIN can both support and suppress tumorigenesis depending on the timing of CIN induction. Thus, the effects of CIN on tumorigenesis heavily depend on the level of CIN and at what stage it arises. Therefore, tumour treatment by CIN induction might be a promising strategy, but the distinct effects of these levels on tumours and healthy tissue demand great caution when implementing this treatment strategy.

Results

Range of CIN to study skin tumorigenesis in mice

A range of CIN levels in the *CiMKi* model was previously verified in mouse embryonic fibroblasts (MEFs), in organoid cultures derived from colon and small intestine, and in situ in the intestinal tissues (see Chapter 2 of this thesis). In summary, two different point mutations in the kinase domain of *Mps1* lead to decreased or abolished activity of the kinase. Combining the mutated and wild-type alleles renders five distinct levels of CIN, ranging from very low to very high (Fig. 1A, B). We used the *CiMKi* model to study the effects of various levels of CIN on regression and tumorigenesis in a DMBA/TPA induced skin tumour model by inducing CIN at various stages of tumorigenesis specifically in skin tumours or skin (Fig. 1C, D). Skin tumours have high levels of aneuploidy, which has to be preceded by CIN events. Furthermore, by studying tumorigenesis in an external setting such as in skin, the effect of CIN can be followed in time.

High CIN causes tumour regression in DMBA/TPA induced tumours

High levels of CIN have been reported to be lethal to cells⁴³⁻⁴⁶, and could be potentially interesting as anti-cancer strategy. Therefore, we investigated the effect of moderate to very high CIN on DMBA/TPA induced skin tumours in *CiMKi;Rosa26-CreER^{T2}* mice. CIN was induced in DMBA/TPA promoted tumours by recombination of the *CiMKi* alleles specifically in tumours by topical treatment with 4-OHT (Fig. 2A). All three CIN levels led to initial regression of the tumours, the extent of which positively correlated with the level of CIN (Fig. 2B, S2A). Tumours

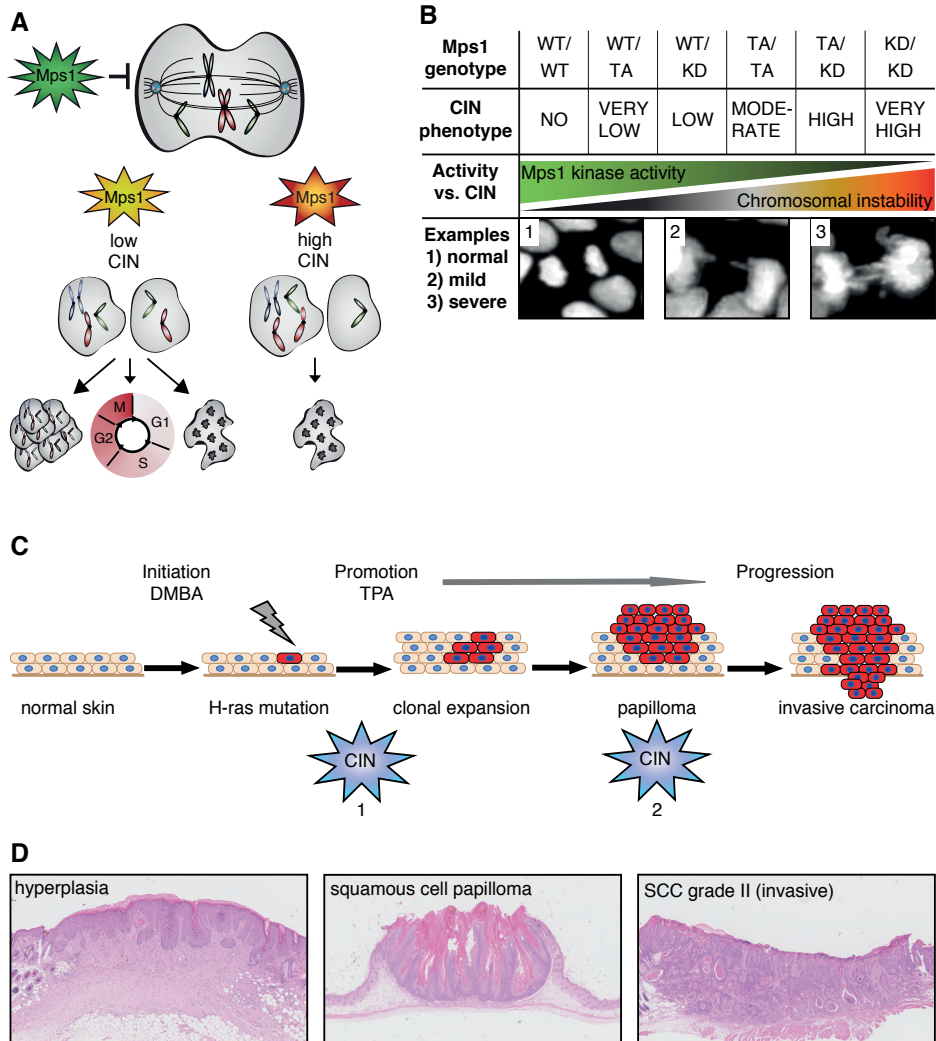


Figure 1: Range of CIN to study skin tumorigenesis in mice. **a.** Model of relation between Mps1 activity and CIN. Wild-type Mps1 (green) prevents cell cycle progression if not all chromosomes are correctly attached to the mitotic spindle. Various levels of Mps1 inhibition cause low (yellow) to high (orange) CIN, leading to proliferation of aneuploid cells, cell cycle arrest or cell death in low CIN cells, and invariable cell death in high CIN cells. **b.** Overview of CiMKi alleles and the expected levels of CIN matching Mps1 activity (WT=wild-type, TA=T649A point mutant, KD=D637A point mutant). Examples of normal mitosis, mild and severe missegregations (from CiMKi small intestine organoids) are indicated at the lower row. **c.** Experimental set-up of DMBA/TPA 2-stage carcinogenesis protocol with induction of CIN. One dose of DMBA was used for initiation and seven days later, biweekly treatments with TPA started for tumour promotion. CIN was induced on back skin ten days after DMBA treatment (before tumorigenesis) (1), or on tumours (2). **d.** H&E stained examples of DMBA/TPA-induced hyperplasia (left), papilloma (middle), and invasive carcinoma (right).

relapsed after 7 to 42 days after 4-OHT treatment (Fig. 2B and example of very high CIN induction in Fig. 2C, D, S2B), with the exception of 2 out of 19 of the tumours with highest CIN level induced (KD/KD) (Fig. S2A). Also, two out of three CIN groups showed extended average survival compared to the wild-type control group (Fig. S2C). Taken together, induction of CIN in DMBA/TPA skin tumours caused tumour regression that positively correlated with the level of CIN, and increased average survival.

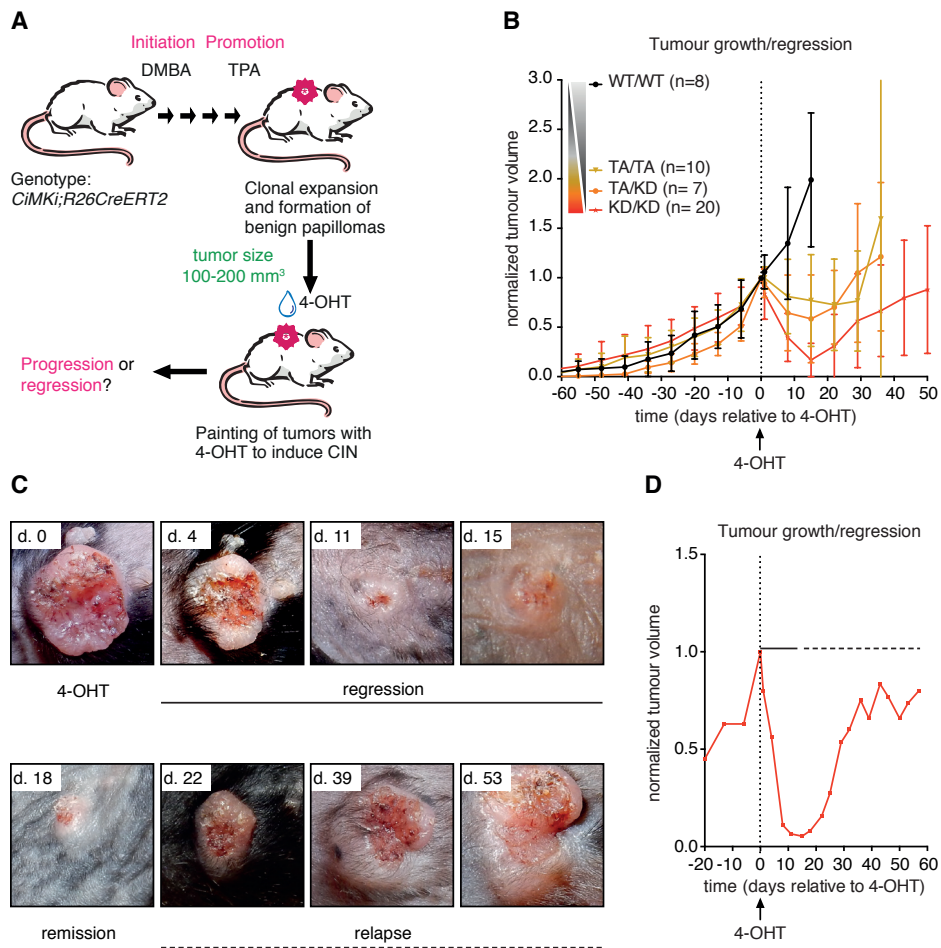


Figure 2: The extent of tumour regression positively correlates with CIN levels. a. *CiMKi;R26CreERT2* mice were treated topically with DMBA (1x) and TPA (biweekly) to induce skin tumours on the back skin. Tumours sized 100-200 mm³ were painted with 4-OHT on five consecutive days to induce the *CiMKi* alleles specifically in the tumours. b. Average tumour volume plotted against time. Data are averages of different tumours. Volumes are relative to normalized volume at the start of 4-OHT treatment. Error bars indicate SD *Legend continues on next page*

Continued from previous page c. Example of regressing and relapsing tumour after 4-OHT treatment. Regression is almost immediate, and complete at 8 days. Relapse is apparent 22 days after 4-OHT. d. Plot of relative tumour volume to normalized volume at start of treatment for the tumour shown in c. Solid line indicates regression, dotted line indicates relapse.

Various CIN levels have differential effects on tumour initiation and growth

For CIN induction to be successful in cancer treatments, negative effects on surrounding tissues should preferably be minimal to none. As we and others have reported CIN to be able to promote tumorigenesis in different tissues, we tested the effects of various CIN levels on skin tumorigenesis in the DMBA/TPA background when CIN was induced before tumour onset. We hypothesized that low to moderate CIN levels would support tumour formation, as this could trigger a faster selection for a beneficial karyotype^{9,47}. Higher levels of CIN were expected to cause less or no tumour formation, as these high CIN levels generally lead to cell death in tissue culture^{45,48}, decreased tumour formation⁴⁸, and caused tumour regression in this study (Fig. 2).

To test this hypothesis in the two-stage carcinogenesis protocol, mice were topically treated with 4-OHT on their backs to induce CIN one week after initiation with DMBA, before tumorigenesis started (Fig. 3A). The results were striking: tumorigenesis unexpectedly took place at all CIN levels, including the highest. Moreover, moderate to very high CIN levels caused significant earlier onset of tumorigenesis (Fig. 3B). Overall, average tumour onset of all *CiMKi* groups inversely correlated with CIN levels as measured in the *CiMKi* MEFS (Fig. 3C). A fraction of tumours also showed increased growth rates when moderate to high CIN levels were induced (Fig. 3D). Concurrently, a bigger fraction of the moderate to very high CIN tumours grew larger than tumours in the control mice (Fig. 3E). Furthermore, very low to moderate CIN levels increased the number of tumours, whereas the higher CIN levels did so to a lesser extent (Fig. 3E). Finally, lesions in the moderate to high CIN groups were more often graded as papilloma and CS, compared to lesions low CIN groups. (Fig. S3A, B). Thus, whereas moderate to very high CIN levels affected tumour onset and growth rate, only the lower and moderate CIN levels increased the chance of tumour initiation. This therefore shows that various CIN levels have distinct effects on tumorigenesis in the skin.



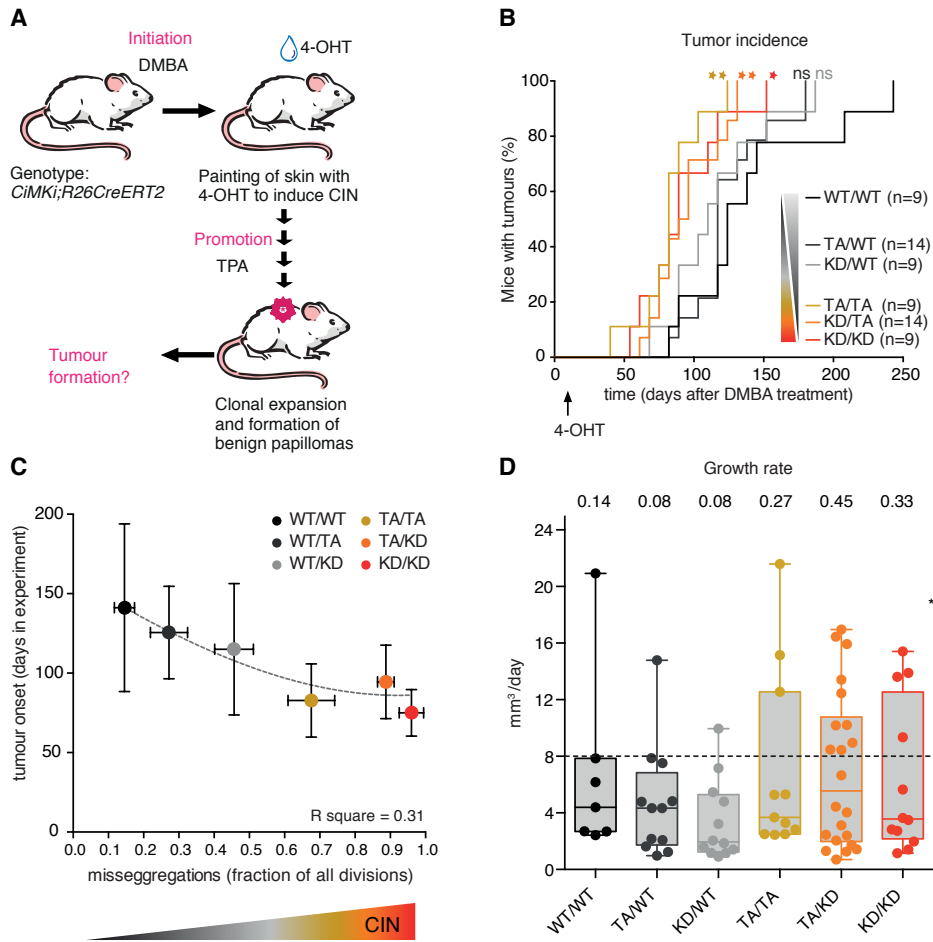
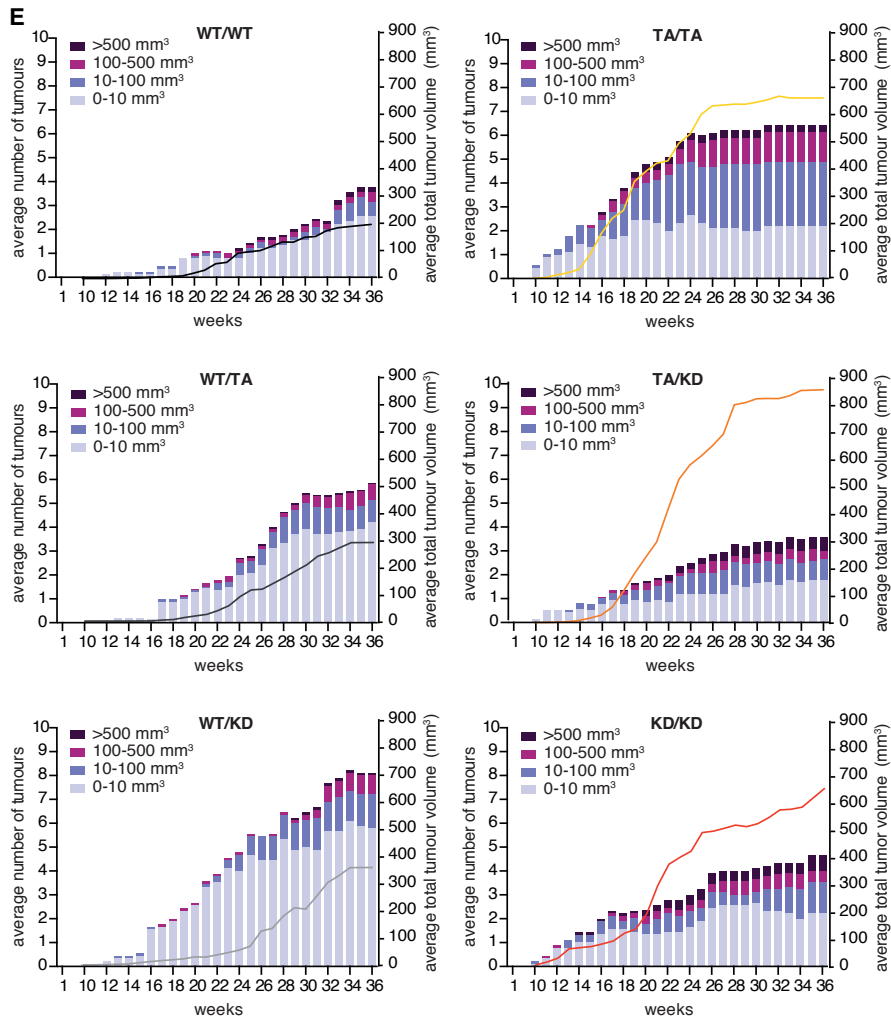


Figure 3: Early induced various CIN levels have differential effects on tumour initiation and growth
a. *CiMKi;R26CreERT²* mice were treated topically with DMBA (1x) and TPA (biweekly), and ten days after DMBA treatment, the back skin of the mice was treated for five consecutive days with 4-OHT to induce the *CiMKi* alleles specifically in the back skin. **b.** Kaplan-Meier curves of DMBA/TPA-induced tumour incidence with various early-induced CIN levels (see Fig. 3A). Asterisks indicate significance (* $p < 0.05$, ** $p < 0.005$). **c.** Correlation plot of tumour onset against the fraction of missegregations in the *CiMKi* genotypes as measured in *CiMKi* MEFs (see Chapter 2 of this thesis) (third order polynomial fit, R square= 0.31; Spearman correlation = -0.94; $p = 0.0167$). **d.** Box and whisker plot showing tumour growth rates for all tumours. Each data point represents one tumour. Boxes indicate 25th to 75th percentiles with median and error bars indicate min to max values. Above each box, the fraction of tumours that on average grew more than 8 mm³ per day after exceeding 100 mm³ is indicated. **e.** Quantification of the average number and size of the DMBA/TPA promoted tumours in time in *CiMKi;R26CreERT²* mice with aggravating levels of CIN (WT/WT to KD/KD). Average tumour numbers were binned by size in four categories (0-10 mm³, 10-100 mm³, 100-500 mm³, and > 500 mm³) for each genotype (left y-axis). Lines represent the average total tumour volume per mouse (right y-axis).

Figure continues on next page

3



High CIN levels cause a non-cell intrinsic benefit for tumorigenesis

Tumour formation at the highest CIN levels (TA/KD and KD/KD) was unexpected, since full inhibition of Mps1 is known to cause cell death^{45,49}. It is unlikely for these high CIN cells to be able to initiate tumorigenesis. We therefore checked if the *CiMKi* mutations were fully induced in these tumours. For this, targeted sequencing for the *Mps1* point mutations was done on bulk cDNA obtained from the tumours (Fig. 4A). Remarkably, tumours that arose on skin of TA/KD or

KD/KD mice never carried the expected two mutated alleles. In fact, all tumours from KD/KD and TA/KD mice contained a mix of mutant and wild-type *Mps1* cDNA (Fig. 4B, S4A). Since none of the tumours from TA/KD mice contained both TA and KD mutations, but always one of them in combination with wild-type *Mps1* cDNA, we reasoned that most probably cells with only one recombined *CiMKi* allele were tumour initiating cells. In support hereof, the tumours that relapsed after initial CIN-induced regression (Fig. 2C) revealed a similar pattern (Fig. S4B). Tumours from heterozygous *CiMKi* mice (low CIN) and homozygous TA/TA mice (moderate CIN) did have the expected cDNA sequence (Fig. S4A), suggesting efficient recombination. Most probably therefore, low to moderate CIN levels cause a cell-intrinsic benefit for tumour initiation (WT/TA and WT/KD), and for initiation and growth (TA/TA).

Even though the *CiMKi* cDNA in tumours of TA/KD and KD/KD mice was similar to that of tumours from heterozygous *CiMKi* mice, the growth pattern was remarkably different. This indicated that outgrowth of tumour cells with very high CIN levels (TA/KD or KD/KD) is highly unlikely, but death of high CIN cells could provide cell extrinsic benefits for the not fully induced, low CIN cells. To further explain the difference between tumours originating from high and low CIN mice, we compared chromosome compositions between the different tumours. We subjected three tumours and one piece of normal looking (DMBA/TPA/4-OHT-treated) skin of each genotype to whole genome sequencing to reveal possible copy numbers alterations (CNA) of (parts of) chromosomes. Trisomy of chromosome 6 and 7 have been described to occur spontaneously in the DMBA/TPA model^{33,50} and these were also observed in most of the low and all of the higher CIN tumours. Furthermore, a subset of the tumours had a gain of chromosome 10. Gain of chromosome 16 seemed specific for moderate to high CIN. Finally, no obvious changes were present in copy numbers for all chromosomes in normal looking skin for all genotypes, indicating that aneuploidies are indeed related to tumorous skin. So even though the *CiMKi* mutations are not fully expressed in tumours from the TA/KD and KD/KD mice, tumour karyotypes differ from the low CIN genotypes, indicating differential environmental influences on evolving and surviving karyotypes.

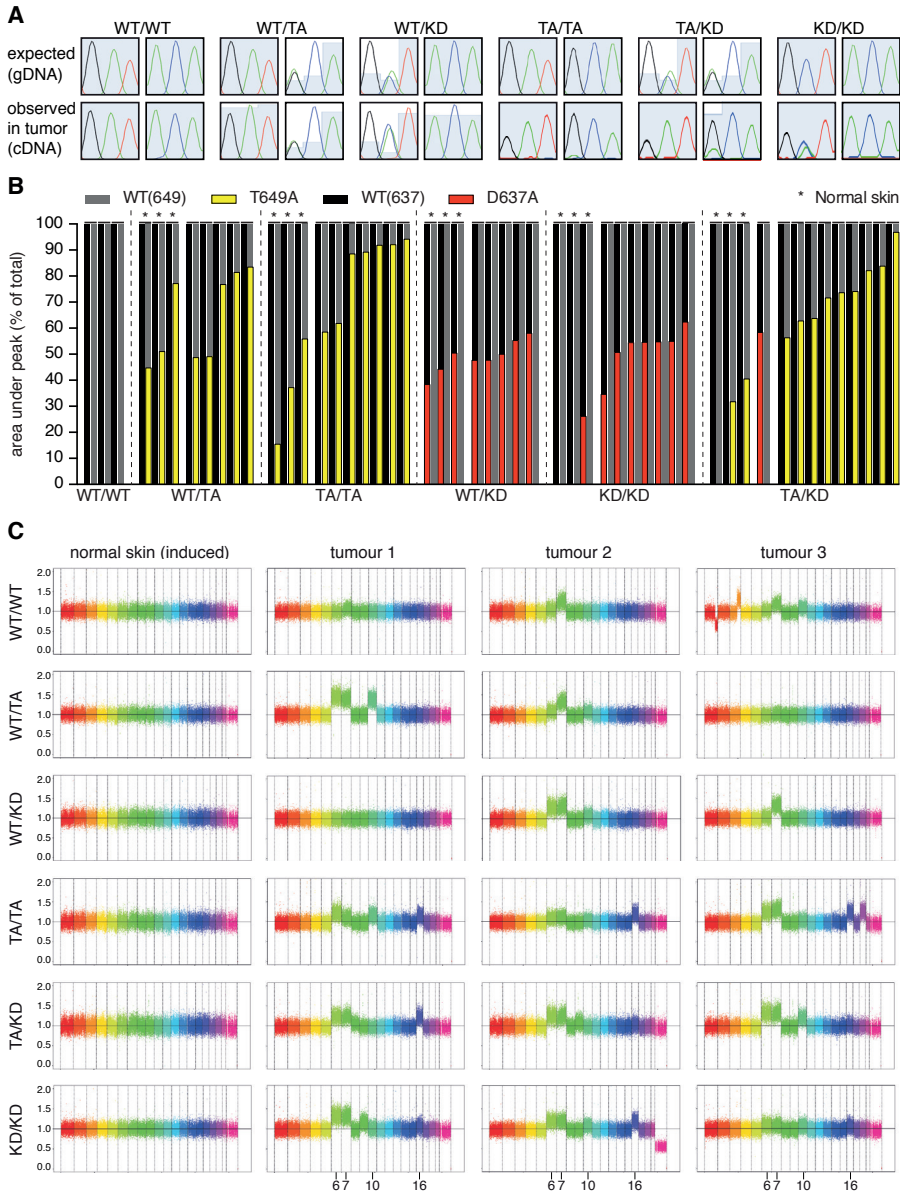


Figure 4: High CIN levels cause a non-cell intrinsic benefit for tumorigenesis **a.** cDNA sequences of CiMKi mutation sites in *Mps1* from end-stage tumours of CiMKi;R26CreER^{T2} mice. For each genotype, upper panels show expected sequences on gDNA level, and bottom panels show examples of the cDNA sequences of one tumour per genotype. **b.** Quantification of areas under sequence peaks for wild-type and mutant bases as proxy of recombination efficiency, in a panel of tumours and normal induced skin (*) of all CiMKi genotypes. Grey and yellow represent wild-type and mutant base 649, black and orange represent wild-type and mutant base 637. **c.** Rainbow plots of whole genome sequencing data for copy number alterations in induced normal skin and three tumours for each CiMKi genotype. Each colour represents one chromosome (from left to right: 1-19, X). Deviations from 1 indicates increase (>1) or decrease (<1) of copy number for that chromosome.

Discussion

Aneuploidy and CIN are hallmarks of cancer, still it has proven difficult to evaluate its impact on tumorigenesis. This is partly due to the lack of models that have the possibility to timely induce various levels of CIN and combine this with the ability to follow tumour growth or regression over time. In this study, we assessed the effect of various CIN levels on tumorigenesis and regression in the two-stage DMBA/TPA induced skin carcinogenesis model.

We revealed clear, differential effects between low, moderate, and high CIN on tumorigenesis. Tumours regressed when moderate to very high CIN levels were induced, with the most prominent response to the highest CIN levels. Moreover, most tumours relapsed, and our data imply that the relapsing, fast growing tumours in high and very high CIN mice (TA/KD and KD/KD) were probably initiated from inefficiently targeted (and thereby low CIN) cells, as they always carried approximately 50% wild-type *Mps1* cDNA (modelled in Fig. 5). It is unlikely that this amount of wild-type cDNA would originate from non-tumour and non-targeted stromal material, as the combination of TA and KD (together with wild-type) would then also have been found in TA/KD mice, which was never the case. Therefore, we conclude that the highest possible CIN has to be reached in all cells to effectively eradicate tumours, and if this does not occur, lower CIN levels initiate a fast relapse.

This inefficient recombination in a fraction of cells after 4-OHT treatment could also explain the differential response in tumorigenesis when CIN is induced before tumour onset. While the *CiMKi* cDNA expression was similar in the end-stage tumours, the differences in initiation, growth and CNAs are striking. While low CIN increased the number of tumours, it is the background of high CIN in which the heterozygously targeted cells thrive and form fast-growing, large tumours. The specific phenotypes caused by high and low CIN, can be attributed to cell-intrinsic and -extrinsic factors, or a combination hereof. Low CIN could induce the right amount of adaptability and give an advantage over wild-type cells to propagate in a background of hyperproliferation and inflammation caused by repetitive TPA treatments. This effect could be enhanced in a high CIN background

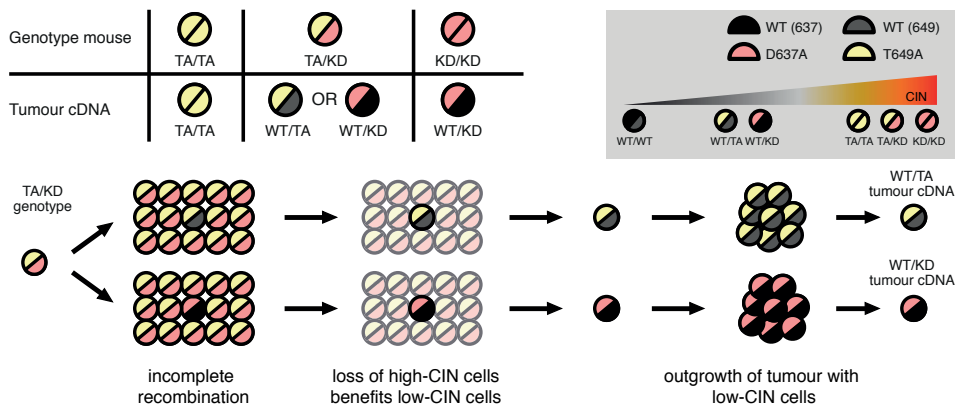


Figure 5: Model for outgrowth of heterozygous tumours. Tumours from high CIN mice (TA/KD and KD/KD) never show mutant induction on both alleles. It is therefore unlikely that these high CIN levels are compatible with cell survival. If not all cells in the population have efficiently switched both alleles, these lower CIN cells may benefit from extrinsic factors instigated by massive cell death in the high CIN population. These can include activation of proliferation and immune responses, especially in -but not limited to- TPA related stimulation. Together with cell intrinsic benefits that low CIN seems to exert in this background, tumours are prone to develop from inefficiently recombined, low CIN, cells. Lower cartoon shows outgrowth of tumours with either 50% TA or 50% KD cDNA, next to WT cDNA, in a TA/KD mouse.

3

where initial massive cell death of the high CIN, followed by hyperproliferation and immune system activation would stimulate outgrowth of lower CIN cells, though these possible effects of high CIN should be studied independent of TPA in this case. Still, high levels of CIN are not sufficient to induce skin tumorigenesis at 45 weeks (n=3 for WT, n=8-10 for other genotypes), contrary to what we observed in intestine (see Chapter 2 of this thesis). This indicates that a mutagenic hit and/or the effects of TPA are required here to collaborate with CIN to drive tumour development, but the exact effect of the various CIN levels on normal skin should be studied further.

Similar to what we described in the intestine (Chapter 2 of this thesis), moderate CIN is most potent level for tumour development in chemically induced cSSC. *CiMKi^{TA/TA}* mice show the most severe phenotype in terms of initiation and tumour growth. Interestingly, these tumours do predominantly express mutant *Mps1* cDNA, indicating that here no selection for inefficiently targeted cells has happened. We hypothesize that this CIN level is less detrimental than the higher levels, and surviving cells can thrive through the combination of cell-intrinsic and -extrinsic effects.

Altogether, CIN is a major contributor to cutaneous tumorigenesis in the two-stage carcinogenesis protocol. The extent of the effect is highly dependent on the level of CIN, as we described previously for intestinal tumorigenesis. As a treatment strategy, there is potential for induction of high CIN in tumour cells, though local, repetitive treatment will be required to minimize adverse effects on surrounding tissue and potential relapse.

Acknowledgements

We thank Wigard Kloosterman and the Utrecht Sequencing Facility for providing sequencing service and data. Utrecht Sequencing Facility is subsidized by the University Medical Center Utrecht, Hubrecht Institute and Utrecht University. This project was funded by grants from the Dutch cancer society (KWF), Oncode, and Cancer Genomics Centre.

References

1. Baker, D. J., Jin, F., Jegathan, K. B. & van Deursen, J. M. Whole Chromosome Instability Caused by Bub1 Insufficiency Drives Tumorigenesis through Tumor Suppressor Gene Loss of Heterozygosity. *Cancer Cell* **16**, 475–486 (2009).
2. Foijer, F. et al. Chromosome instability induced by Mps1 and p53 mutation generates aggressive lymphomas exhibiting aneuploidy-induced stress. *Proc. Natl. Acad. Sci.* **111**, 13427–13432 (2014).
3. Thompson, S. L. & Compton, D. a. Chromosomes and cancer cells. *Chromosome Res.* **19**, 433–444 (2011).
4. Burrell, R. A. et al. Replication stress links structural and numerical cancer chromosomal instability. *Nature* **494**, 492–496 (2013).
5. Crasta, K. et al. DNA breaks and chromosome pulverization from errors in mitosis. *Nature* **482**, 53–58 (2012).
6. Janssen, A., van der Burg, M., Szuhai, K., Kops, G. J. P. L. & Medema, R. H. Chromosome Segregation Errors as a Cause of DNA Damage and Structural Chromosome Aberrations. *Science (80-.)*. **333**, 1895–1898 (2011).
7. Zhang, C.-Z. et al. Chromothripsis from DNA damage in micronuclei. *Nature* **522**, 179–184 (2015).
8. Liu, S. et al. Nuclear envelope assembly defects link mitotic errors to chromothripsis. *Nature* **561**, 551–555 (2018).
9. Burrell, R. A., McGranahan, N., Bartek, J. & Swanton, C. The causes and consequences of genetic heterogeneity in cancer evolution. *Nature* **501**, 338–345 (2013).
10. Hanahan, D. & Weinberg, R. A. Hallmarks of Cancer: The Next Generation. *Cell* **144**, 646–674 (2011).
11. Lengauer, C., Kinzler, K. W. & Vogelstein, B. Genetic instabilities in human cancers. *Nature* **396**, 643–649 (1998).
12. Ree, J. H. Van, Jegathan, K. B., Malureanu, L. & Deursen, J. M. Van. Overexpression of the E2 ubiquitin-conjugating enzyme UbcH10 causes chromosome missegregation and tumor formation. **188**, 83–100 (2010).
13. Weaver, B. A. A., Silk, A. D., Montagna, C., Verdier-Pinard, P. & Cleveland, D. W. Aneuploidy acts both oncogenically and as a tumor suppressor. *Cancer Cell* **11**, 25–36 (2007).
14. Babu, J. R. et al. Rae1 is an essential mitotic checkpoint regulator that cooperates with Bub3 to prevent chromosome missegregation. **2**, 341–353 (2003).
15. Iwanaga, Y. et al. Heterozygous deletion of mitotic arrest-deficient protein 1 (MAD1) increases the incidence of tumors in mice. *Cancer Res.* **67**, 160–166 (2007).
16. Michel, L. S. et al. MAD2 haplo-insufficiency causes premature anaphase and chromosome instability in mammalian cells. *Nature* **409**, 355–359 (2001).
17. Rao, C. V et al. Colonic tumorigenesis in BubR1+/- ApcMin/+ compound mutant mice is linked to premature separation of sister chromatids and enhanced genomic instability. 1–6 (2005).
18. Remeseiro, S. et al. Cohesin-SA1 deficiency drives aneuploidy and tumourigenesis in mice due to impaired replication of telomeres. **31**, 2076–2089 (2012).
19. Ricke, R. M., Jegathan, K. B. & Deursen, J. M. Van. Bub1 overexpression induces aneuploidy and tumor formation through Aurora B kinase hyperactivation. **193**, (2011).
20. Sercin, Ö. et al. Transient PLK4 overexpression accelerates tumorigenesis in p53-deficient epidermis. **18**, (2016).
21. Sotillo, R. et al. Mad2 Overexpression Promotes Aneuploidy and Tumorigenesis in Mice. *Cancer Cell* **11**, 9–23 (2007).
22. Baker, D. J. et al. BubR1 insufficiency causes early onset of aging-associated phenotypes and infertility in mice. **36**, 744–749 (2004).
23. Simon, J. E., Bakker, B. & Foijer, F. CINcere modelling: what have Mouse Models for Chromosome Instability Taught Us? *Recent results cancer Res.* 39–60 (2015). doi:10.1007/978-3-319-20291-4
24. Diepgen, T. L. & Mahler, V. Epidemiology of non-melanoma skin cancer. *Br. J. Dermatology* 2002; **146**, 1–6 (2002).
25. Greinert, R. et al. European Code against Cancer 4th Edition: Ultraviolet radiation and cancer. *Cancer Epidemiol.* **39**, S75–S83 (2015).
26. Carless, M. A. & Griffiths, L. R. Cytogenetics of Melanoma and Nonmelanoma Skin Cancer. (2008).
27. Ratushny, V. et al. From keratinocyte to cancer: the pathogenesis and modeling of cutaneous squamous cell carcinoma Find the latest version : Review series From keratinocyte to cancer : the pathogenesis and modeling of cutaneous squamous cell carcinoma. **122**, 464–472 (2012).
28. Abel, E. L., Angel, J. M., Kiguchi, K. & DiGiovanni, J. Multi-stage chemical carcinogenesis in mouse skin: fundamentals and applications. *Nat. Protoc.* **4**, 1350–62 (2009).
29. Balmain, A. & Yuspa, S. H. Milestones in Skin Carcinogenesis: The Biology of Multistage Carcinogenesis. 2–7 (2014). doi:10.1038/skinbio.2014.2
30. Lee, C. S. et al. Recurrent point mutations in the kinetochore gene KNSTRN in cutaneous

- squamous cell carcinoma. **46**, 1060–1062 (2015).
31. Jin, C. et al. Karyotypic heterogeneity and clonal evolution in squamous cell carcinomas of the head and neck. **132**, 85–96 (2002).
 32. Huang, P. Y. & Balmain, A. Modeling cutaneous squamous carcinoma development in the mouse. *Cold Spring Harb. Perspect. Med.* **4**, 1–24 (2014).
 33. Aldaz, C. M., Conti, C. J., Klein-szanto, A. J. P. & Slaga, T. J. Progressive dysplasia and aneuploidy are hallmarks of mouse skin papillomas: Relevance to malignancy (cancer/tumor. **84**, 2029–2032 (1987).
 34. Aldaz, C. M. et al. Sequential Development of Aneuploidy , Keratin Modifications , and Expression in Mouse Skin Papillomas1. 3253–3257 (1988).
 35. Jin, Y. et al. Nonrandom Karyotypic Features in Squamous Cell Carcinomas of the Skin. **303**, 295–303 (1999).
 36. Schwarz, M., Münzel, P. A. & Braeuning, A. Non-melanoma skin cancer in mouse and man. *Arch. Toxicol.* **87**, 783–798 (2013).
 37. Maia, A. R. R. et al. Inhibition of the spindle assembly checkpoint kinase TTK enhances the efficacy of docetaxel in a triple-negative breast cancer model. *Ann. Oncol.* **26**, 2180–2192 (2015).
 38. Wengner, A. M. et al. Novel Mps1 Kinase Inhibitors with Potent Antitumor Activity. *Mol. Cancer Ther.* **15**, 583–592 (2016).
 39. Colombo, R. et al. Targeting the Mitotic Checkpoint for Cancer Therapy with NMS-P715, an Inhibitor of MPS1 Kinase. *Cancer Res.* **70**, 10255–10264 (2010).
 40. Maia, A. R. R. et al. Mps1 inhibitors synergise with low doses of taxanes in promoting tumour cell death by enhancement of errors in cell division. *Br. J. Cancer* **118**, 1586–1595 (2018).
 41. Jemaà, M. et al. Characterization of novel MPS1 inhibitors with preclinical anticancer activity. *Cell Death Differ.* **20**, 1532–1545 (2013).
 42. Tannous, B. A., Kerami, M., Van der Stroop, P. M. & al, et. effects of the Selective MPS1 inhibitor MPS1-iN-3on Glioblastoma Sensitivity to Antimitotic Drugs. 1–10 (2013).
 43. Sheltzer, J. M. & Amon, A. The aneuploidy paradox: costs and benefits of an incorrect karyotype. *Trends Genet.* **27**, 446–453 (2011).
 44. Kops, G. J. P. L., Foltz, D. R. & Cleveland, D. W. Lethality to human cancer cells through massive chromosome loss by inhibition of the mitotic checkpoint. 1–6 (2004).
 45. Jelluma, N. et al. Chromosomal Instability by Inefficient Mps1 Auto-Activation Due to a Weakened Mitotic Checkpoint and Lagging Chromosomes. *PLoS One* **3**, e2415 (2008).
 46. Roylance, R. et al. Relationship of Extreme Chromosomal Instability with Long-term Survival in a Retrospective Analysis of Primary Breast Cancer. *Cancer Epidemiol. Biomarkers Prev.* **20**, 2183–2194 (2011).
 47. Nicholson, J. M. & Cimini, D. Cancer karyotypes : survival of the fittest. **3**, 1–9 (2013).
 48. Silk, A. D. et al. Chromosome missegregation rate predicts whether aneuploidy will promote or suppress tumors. *Proc. Natl. Acad. Sci.* **110**, E4134–E4141 (2013).
 49. Kwiatkowski, N. et al. Small-molecule kinase inhibitors provide insight into Mps1 cell cycle function. *Nat. Chem. Biol.* **6**, 359–368 (2010).
 50. Aldaz, C. M., Trono, D., Larcher, F., Slaga, T. J. & Conti, C. J. Sequential trisomization of chromosomes 6 and 7 in mouse skin premalignant lesions. *Mol. Carcinog.* **2**, 22–26 (1989).

<https://www.who.int/uv/faq/skincancer/en/index1.html>
<https://clinicaltrials.gov/ct2/show/NCT02366949?term=Mps1>

Methods

Animals

All animal experiments were approved by Animal Experimental Committee Utrecht under license number 2014.III.08.071. All animals were bred and housed under standard conditions at the animal facility of the Gemeenschappelijk Dieren Laboratorium (GDL), Utrecht, the Netherlands. *CiMKi* mice were generated as described in Hoevenaar et al. (Chapter 2 of this thesis). *Rosa26-CreER^{T2}* (B6.129Gt(ROSA)26Sor^{tm1(cre/ERT2)Tyj/J}, stock number 008463) were purchased at JAX® mice. All mice were maintained in C57BL/6 background. Mice were genotyped using standard PCR and targeted sequencing procedures. For primers see Table 1.

Treatment and analysis

3 The classical DMBA/TPA skin carcinogenesis protocol²⁹ was applied in combination with induction of various levels of CIN at two timepoints. Back skin of 5- to 6-weeks old female mice was shaven and topically treated with a single dose of 7,12-dimethylbenz[a]-anthracene (DMBA) (800 nmol/0.2 ml acetone, Sigma). One week later, biweekly treatment with 12-O- tetradecanoylphorbol-13-acetate (TPA) (4 µg/0.2 ml acetone, Sigma) was issued until the end of the experiment. CIN was induced by applying 4-hydroxytamoxifen (4-OHT) (1 mg/0.2 ml DMSO, Sigma) for five consecutive days. To induce CIN in tumours, 4-OHT was applied when tumours were 100-200mm³ in size and in the early induction group, treatment started ten days after DMBA application.

To monitor tumour growth, the backs of the mice were shaven as often as necessary and tumour volume was calculated by taking length and width measurements with a caliper every week. The average of these values was divided by two and taken as radius (volume = $4/3\pi r^3$).

Mice were euthanized when total tumour volume exceeded 1500 mm³, or maximally when 45 weeks in experiment. At dissection, tumours, normal skin and internal organs were isolated and divided to be snap-frozen or fixed in formalin.

For identification and assessment of tumours 4-µm sections of paraffin-

embedded tissue were cut and stained with hematoxylin/eosin (H&E). Grading of tumours was done by pathologists from the Dutch Molecular Pathology Centre.

Assessment of mutant induction and ploidy

To confirm recombination, RNA was isolated from tumours and normal skin with a quick RNA kit (Zymo Research). cDNA was prepared using standard procedures, subjected to PCR and subsequently sequenced to determine the presence of T649A or D637A. For primers see Table 1.

For whole genome sequencing, gDNA was isolated from tumours and normal skin with a DNeasy Blood and Tissue kit (Qiagen) according to the manufacturer's instruction. Sequencing and analysis were done at the Utrecht Sequencing Facility according to standardized processes.

Statistical analysis

Power analysis dictated the number of animals that had to be used in each group to detect differences with 80% power and 95% confidence. Animals were not randomized, but assigned to the experimental groups based on their genotype. Statistical analyses were done in GraphPad Prism. Statistical tests that were used as indicated in the figure legends. Data is presented as mean \pm SD unless otherwise stated in legends.

3

Supplemental figures

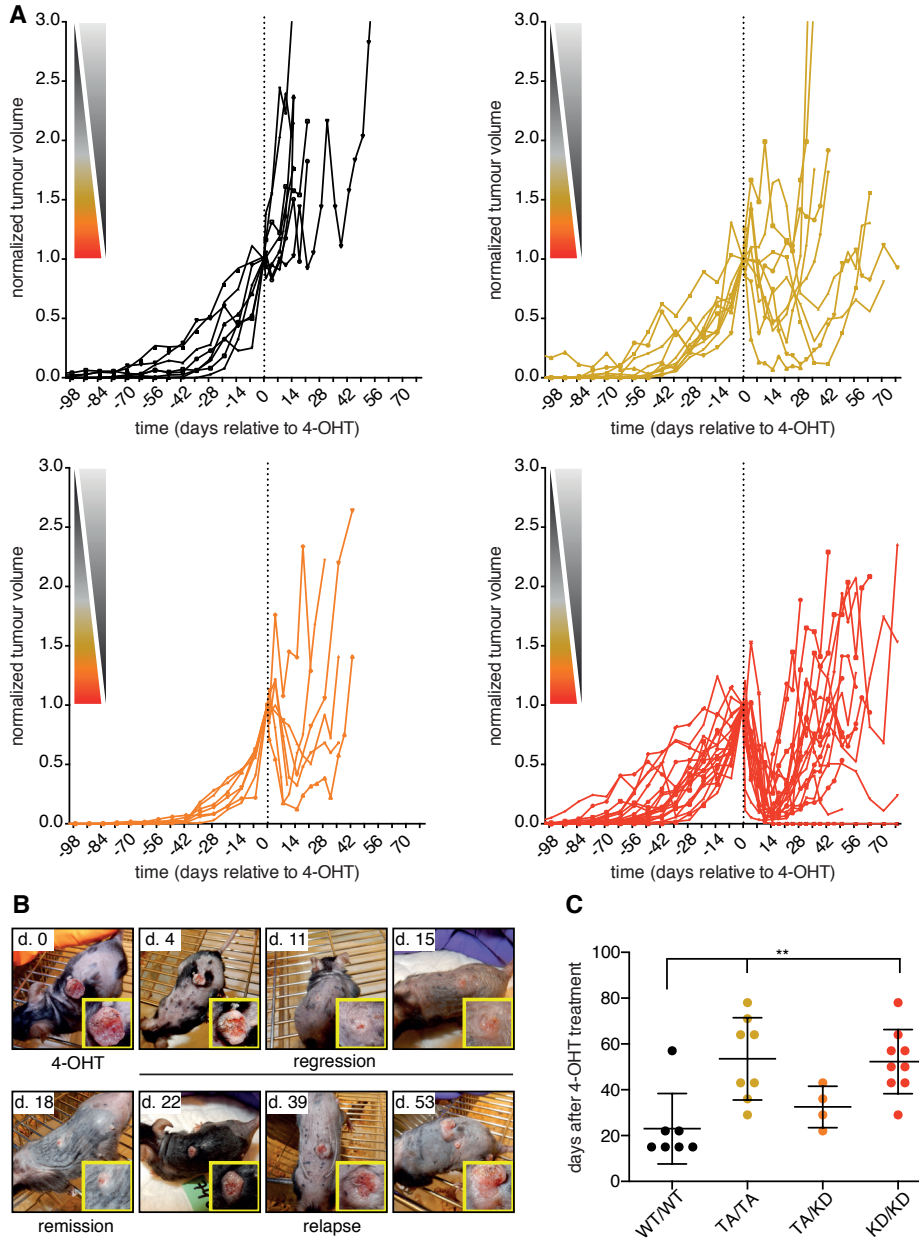


Figure S2: The extent of tumour regression positively correlates with CIN levels. **a.** Plot of relative tumour volume to normalized volume at start of treatment for each tumour treated with 4-OHT. Two of the KD/KD tumours did not grow back until the end of the experiment. **b.** Whole-mouse overview example of regressing and relapsing tumour after 4-OHT treatment. Regression is almost immediate, and complete at 8 days. Relapse is apparent 22 days after 4-OHT. **c.** Average survival of each mouse in days after 4-OHT treatment. Student's t-test was used to compare CIN groups to wild-type, asterisks indicate significance (** $p < 0.005$). Error bars indicate SD.

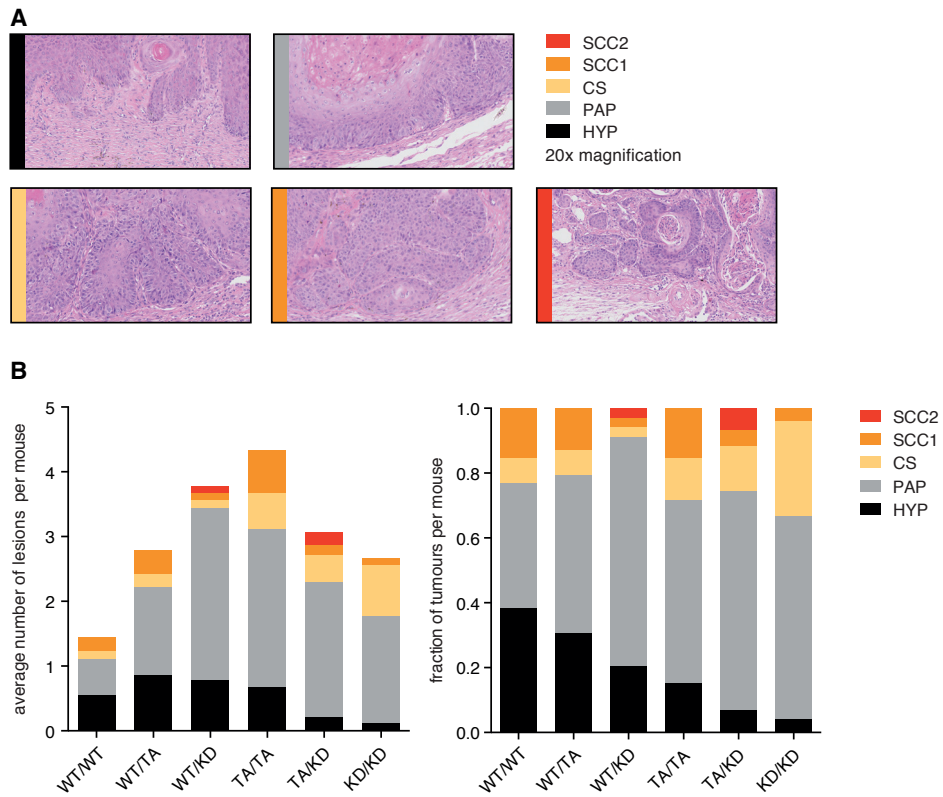


Figure S3: Early induced various CIN levels have differential effects on tumour initiation and growth. a. H&E examples of the various stages of skin tumorigenesis in DMBA/TPA and CIN promoted tumorigenesis (classified as hyperplastic (HYP), papilloma (PAP), carcinoma in situ (CS), squamous cell carcinoma 1 and 2 (SCC1 and SCC2)). **b.** The average number and fraction of the various stages of lesions per mouse for each *CiMKi* genotype at the moment sacrifice, classified as in A.

3

3

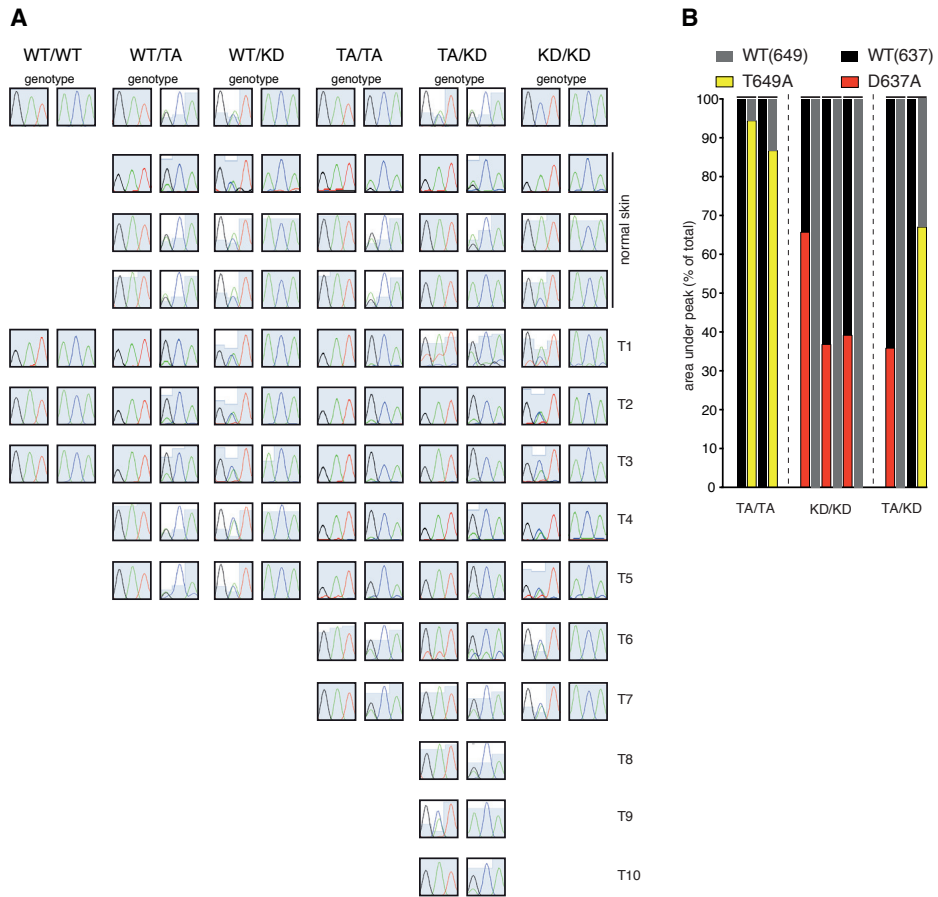
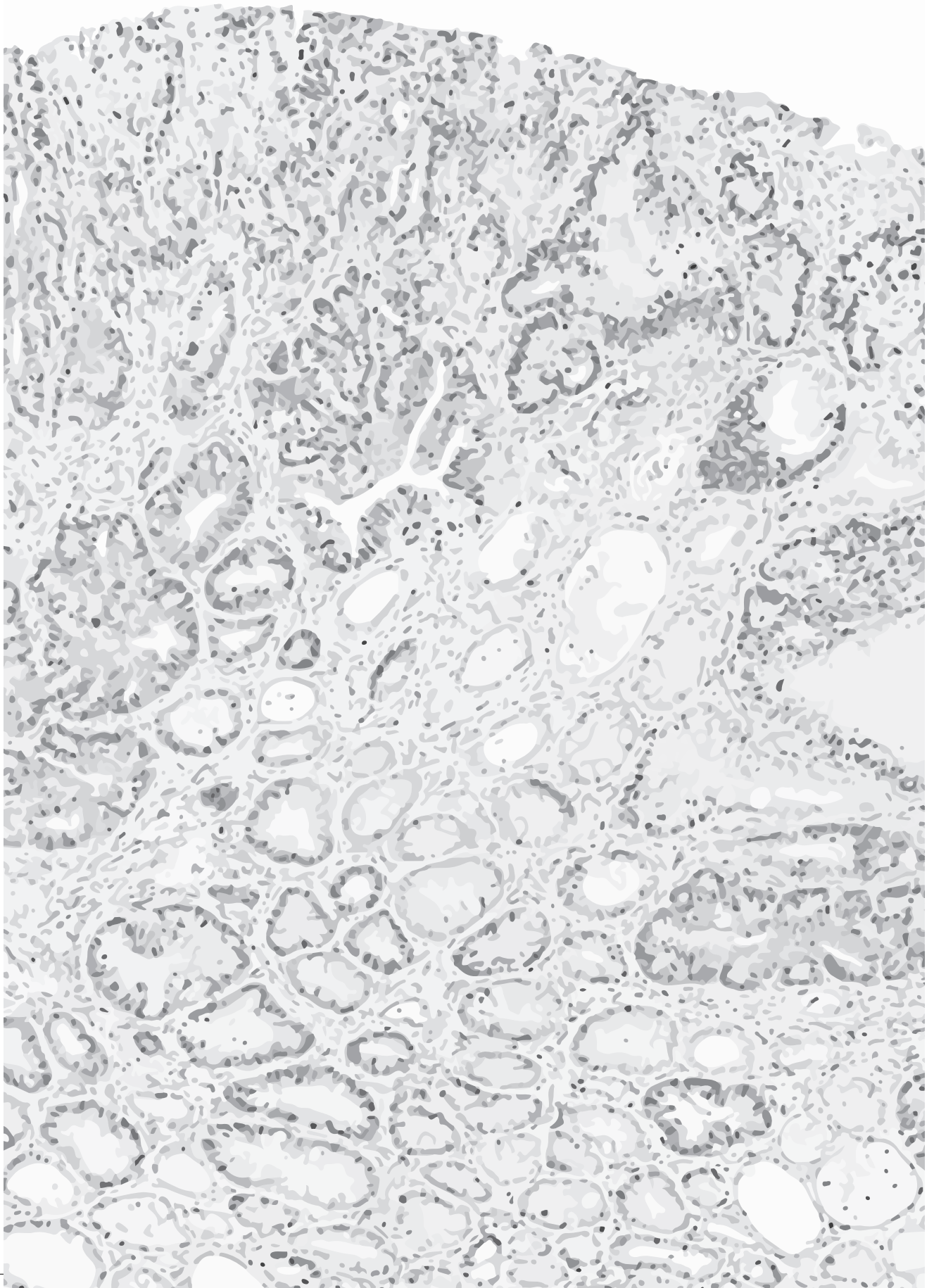


Figure S4: High CIN levels cause a non-cell intrinsic benefit for tumorigenesis. a. cDNA sequences of *CiMKi* mutation sites in *Mps1* from end-stage tumours (T) of *CiMKi;R26CreER^{T2}* mice, as quantified in Fig. 4B. **b.** Quantification of area under the sequence peak for wild-type and mutant bases as proxy of recombination efficiency in relapsed tumours. Grey and yellow represent wild-type and mutant base 649, black and orange represent wild-type and mutant base 637.

Table S1: Primers for genotyping and cDNA analysis

Gene	Forward primer	Reverse primer	Expected band size	Sequence primer	Mutation sequence
<i>CIMKi</i> (mutation)	GTGTCCTCACCTG AAAATG	CAAAGCACAGCTG GGCTGTAGAG	~1000 bp	CGGATTTTATTTTG AAGGTATTG	T649A: ACA <u>A</u> /GCA D637A: TTGG <u>A</u> /CT
<i>CIMKi</i> cDNA (mutation)	CCTAGAAGACGCC GATAGCC	GTCTCTGATTGCTT CTGGGGC	~400 bp	GATAAGATCATCC GCCTCTATG	T649A: ACA <u>A</u> /GCA D637A: TTGG <u>A</u> /CT
<i>Rosa26-CreER^{T2}</i> (mut)	GGCAGGAAGCACT TGCTCTCCC	CCTGATCCTGGCAA TTTCG	~825 bp	NA	NA
<i>Rosa26-CreER^{T2}</i> (wt)	GGCAGGAAGCACT TGCTCTCCC	GGAGCGGGAGAA ATGGATATG	~650 bp	NA	NA



Chapter 4

Drug screening to identify synergy between chromosomal instability and anti-cancer drugs in organoids

Wilma H.M. Hoevenaar¹, Antoinette Teixeira¹, Ana C. Bolhaqueiro¹, Ajit I. Quirindongo¹, Geert J.P.L Kops¹, Nannette Jelluma¹

¹Oncode Institute, Hubrecht Institute-KNAW and University Medical Center Utrecht, Utrecht, The Netherlands.

Abstract

Colorectal cancer (CRC) ranks second as deadliest cancer, and treatment falls short for higher grade and metastatic disease. Drug resistance and general lack of efficiency of clinically used cancer drugs are major problems. A factor that could alter a tumour's response to cancer treatment is chromosomal instability (CIN), which causes continuous changes in the genetic landscape of tumours. CIN can confer resistance, but on the other hand can also decrease cell vitality and therefore synergise with chemotherapy.

Here we investigated via an unbiased screening approach if CIN could synergise with chemotherapeutic drugs. For this, drugs were tested for efficacy to kill small intestinal adenoma organoids in which we can induce various levels of CIN. A wide range of clinically approved drugs or drugs currently in clinical trials were tested for their potential to synergise with CIN in a semi-automated screen setup. We found that 10 percent of tested drugs had more potent killing potential when organoids had a moderate CIN level. These drugs, including microtubule poisons and mitotic kinase inhibitors, are known to interfere with chromosome segregation and thus likely provided synergistic cell killing by further elevating CIN to lethal levels. A more thorough investigation of these compounds narrowed the hits to taxanes only. In a more relevant setting, however, paclitaxel was unable to differentiate between human tumour organoids with low or high CIN levels.

Altogether, this study shows the potential of finding synergistic actions between CIN and taxanes in mouse intestinal adenoma organoids, but also highlight the challenges in using CIN levels as a predictor of killing potential of anti-cancer drugs in human tumour cultures.

4

Introduction

Colorectal cancer (CRC) is one of the most prevalent cancers in the Western world affecting 1.8 million-, and killing 862.000 patients each year (WHO). Hereditary types like familial adenomatous polyposis (FAP) and Lynch syndrome^{1,2} account for ~15% of the cases, but the majority of CRC originate spontaneously. The latter can be divided in microsatellite unstable (MIN/MSI) and chromosomally unstable (CIN) subtypes³⁻⁵. In the consensus molecular subtypes (CMS) classification for CRC, the subtypes with increased CIN are distinguished by their predominantly distal location in the colon and their worse prognosis⁶. Furthermore, CIN tumours are more aggressive and have worse therapy response⁷. Common therapy strategies are (partial) resection of the tumour and/or colon, and, depending on the stage and genetic make-up of the cancer, (combinations of) chemotherapy or immune- or targeted therapy^{8,9}. These strategies work well on early stage (0-2) cancer, however for later stage tumours, therapies are now aimed more at increasing life span and reducing discomfort than at curing the disease^{8,10}.

Many CRC tumours are aneuploid, meaning that they have aberrant chromosome numbers¹¹⁻¹³, caused by missegregations of chromosomes during mitosis. For various reasons, the cells may fail to correctly align, attach or separate their chromosomes during cell division, leading to chromosomal instability (CIN)¹⁴. While aneuploidy is rare in healthy cells¹⁵, it is a common feature of tumour cells¹¹, where aneuploidy levels are correlated to tumour aggressiveness and bad prognosis in many cancers^{12,13,16-24}. CIN can benefit tumorigenesis by facilitating adaptation to changing environments and increasing loss of heterozygosity (LOH) rates of tumour suppressor genes²⁵⁻²⁷ (Chapter 2 of this thesis). Furthermore, CIN can influence therapy response; the genetic changes render tumour cells unresponsive to therapies and can give rise to resistant clones^{18,22,28,29}, which is one of the major challenges in cancer treatment.

While CIN can have substantial benefits for tumour cells, it is inherently detrimental to cell physiology^{30,31}. Aneuploidy can for example negatively affect cells by proteotoxicity resulting from differential expression of genes of gained

or lost chromosomes, which disturbs the protein balance in cells^{32,33}. Also, CIN aggravates genomic instability in a broader way by inducing DNA damage³⁴ and chromosome fragmentation^{35,36}, thereby putting more stress on repair machinery and cell cycle checkpoints. It is thought that tumour cells need to overcome these negative effects, but CIN levels can be too high even for cancer cells to cope with. Moreover, we and others have shown that induction of high levels of CIN can kill tumour cells^{21,30,37-39} (Chapter 3 of this thesis). The lethality of high CIN levels lead to the proposal to exploit CIN to kill tumour cells⁴⁰. Inhibitors of the spindle checkpoint kinase MPS1, which cause CIN, are in clinical trials. They have shown promise in preclinical models when combined with paclitaxel, which resulted in massive chromosome missegregations and lead to tumour (cell) death^{29,41-46}. Additionally, since aneuploidy and CIN are distinctive features of tumour cells, targeting specifically these cells by exploiting their CIN-related vulnerabilities in combination with anti-cancer drugs has been proposed as treatment strategy⁴⁷. Though it may seem counter-intuitive that CIN can both be a therapeutic target and a causative factor for therapy resistance, the eventual outcome could heavily depend on the level of CIN induced in tumour cells and the tolerance these cells have for high aneuploidy levels (see Chapter 3, reviewed in^{48,49}). By inducing sufficiently high levels of CIN, synergy with other anti-cancer drugs may be achieved in an efficient manner^{50,51}, thereby preventing resistance.

4

Our recently developed mouse model for CIN (*CiMKi*, see Chapter 2 of this thesis) provides an *in vitro* system to find drugs that synergise with various levels of CIN. We established adenoma organoid lines from the intestines of 10-week-old *CiMKi;Apc^{Min/+};VillinCreER^{T2}* mice, in which various CIN levels can be induced. We opted to use adenoma organoids from young mice, so as to study the effect of CIN irrespective of confounding effects of accumulated mutations that are usually present in end stage tumours, and to do this in a system that closely mimics tumour tissue^{52,53}. Using these lines, we screened a small drug library to identify compounds/pathways that synergise with CIN in killing tumour cells.

Results

CiMKi;Apc^{Min/-};VillinCreER^{T2} organoids as a system to study drug sensitivity

To establish a reliable *in vitro* system for screening of compounds in combination with various CIN levels, organoids were established from small intestines of *CiMKi;Apc^{Min/+};VillinCreER^{T2}* mice as described in Chapter 2 of this thesis. The organoids were selected for loss of *Apc* function by excluding the Wnt ligand R-spondin from the growth medium^{54,55} (Fig. 1). Effective induction of *CiMKi* mutations was confirmed by targeted sequencing of cDNA obtained 72 hours after addition of 4-hydroxytamoxifen (4-OHT) (Fig. S1). The various CIN levels after induction in these organoid lines were previously verified (see Chapter 2 of this thesis). For screening, we selected three distinct CIN levels (low (WT/TA, moderate (TA/TA), and high (TA/KD)) that could potentially affect drug sensitivity (Fig. 1).

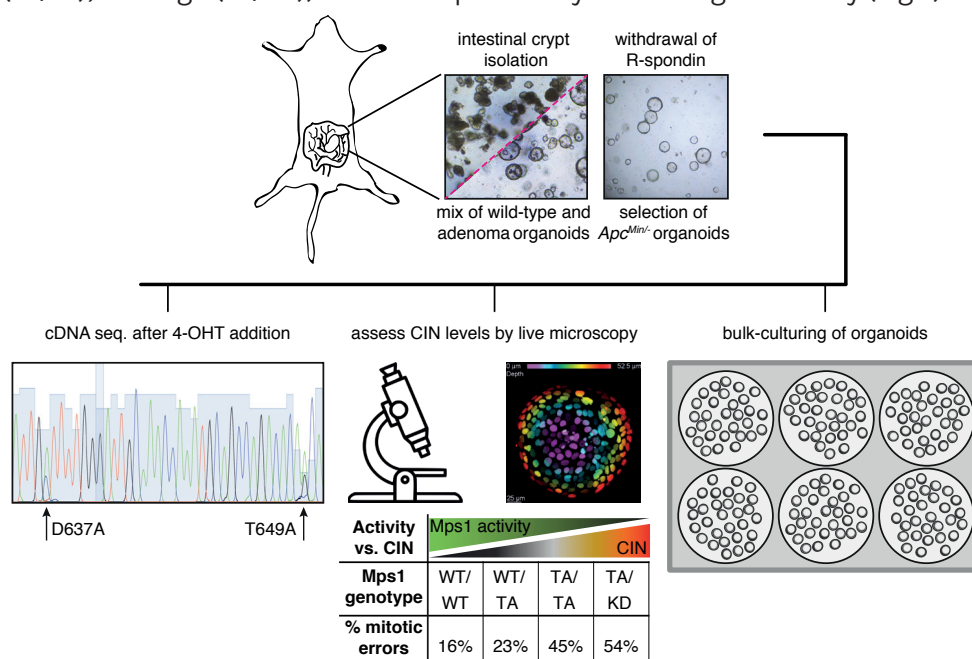


Figure 1: *CiMKi;Apc^{Min/-};VillinCreER^{T2}* organoids as system to study drug sensitivity. Schematic overview of organoid culture and selection procedure. Small intestine adenoma organoids were derived from 10-week old *CiMKi;Apc^{Min/+};VillinCreER^{T2}* mice and cultured in Matrigel & medium without Wnt ligands to select organoids with *Apc* LOH. 72 hours after 4-OHT addition, cDNA of these organoids was sequenced to confirm mutant induction, and CIN levels were assessed by live cell imaging (see Chapter 2, average percentage of missegregations is indicated). For screening experiments, selected organoid lines were cultured in bulk.

Drug screening to identify synergy between chromosomal instability and anti-cancer drugs in organoids | 99

Sequoia/ENZO library screen of anti-cancer drugs

We first set up an initial screen for a set of drugs that are either clinically approved or (currently) tested in clinical trial. Two libraries were obtained from the High-Throughput Screening facility of the Princess Maxima Center; The Anti-Neoplastic KIT (Sequoia), containing 165 (recently) approved drugs used in cancer treatment, and The Screen-Well® Epigenetics Library (Enzo), containing 43 drugs with defined activity against epigenetics-modifying enzymes. Many different pathways, such as DNA damage (repair), metabolism, and mitotic spindle formation are targeted by the combined 208 compounds in these libraries (table 1). Some of the compounds (e.g. 5-Fluorouracil and irinotecan) are used for CRC treatment^{7,17}. We supplemented these libraries with a selection of drugs that were tested in pilot experiments based on their described effect on aneuploid or CIN cells (AICAR⁵⁰), on interference with kinetochore-microtubule interactions (Lonafarnib^{56,57}), or because they aggravate CIN by Mps1 inhibition (CPD5⁵⁸).

Organoids with no, low, moderate, and high CIN were cultured in bulk and CIN was induced by adding 4-OHT 56 hours before the start of the experiment. Organoids were mechanically sheared on the day before the experiment, and left for recovery in Matrigel overnight. The next morning, all organoids were harvested and filtered through a 70 µm strainer to assure seeding of organoids of comparable sizes. Organoids were counted to seed similar densities of approximately 150 organoids per well (Fig. S2). Organoids of each line were seeded in six 384 well plates, and three concentrations (10, 100, or 1000nM) of the compounds were added in duplicate immediately after seeding. Cell viability was assessed 72 hours later with CellTiter Glo (Fig. 2A), and data were normalised to the DMSO controls.

50 to 60 drugs caused at least 50% decrease in viability at the 1000nM concentration in all lines regardless of genotype (Fig. 2B). When comparing the relative effect of drugs in the moderate and high CIN lines (TA/TA and TA/KD) to the no CIN line (WT/WT), most of these drugs showed no synergy with CIN. We found that 22 compounds, including gemcitabine, CPD5 and various taxanes, slightly decreased viability specifically in moderate (but not high) CIN organoids

(Fig. 2C). We cannot exclude that the compounds that had no effect in this screen would be effective at other concentrations, and whether this would depend on CIN level. In conclusion, while the screen performed in this set-up was unable to identify compounds with strong synergy with CIN, it identified several with weak synergy.

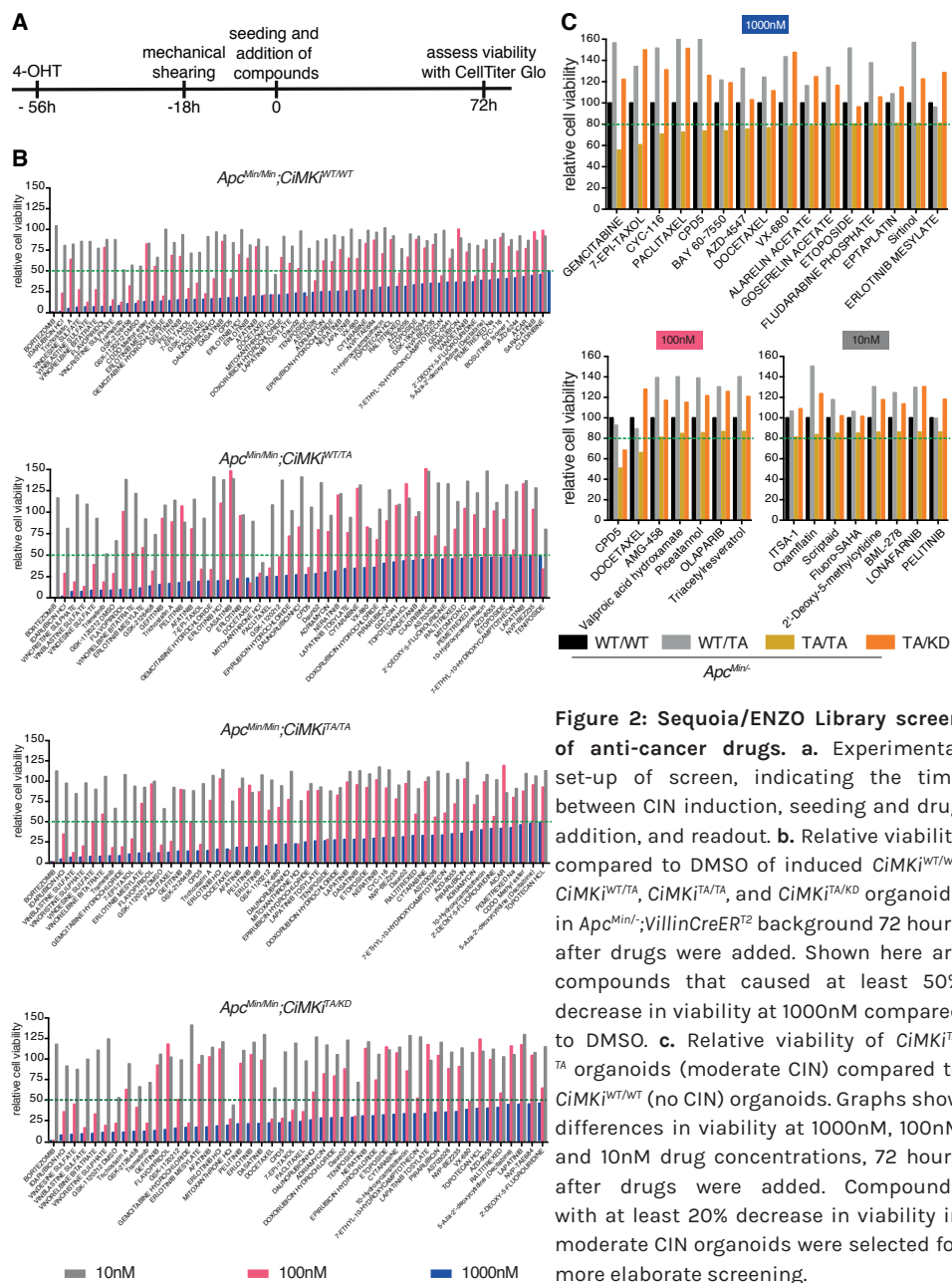


Figure 2: Sequoia/ENZO Library screen of anti-cancer drugs. a. Experimental set-up of screen, indicating the time between CIN induction, seeding and drug addition, and readout. b. Relative viability compared to DMSO of induced $CiMKI^{WT/WT}$, $CiMKI^{WT/TA}$, $CiMKI^{TA/TA}$, and $CiMKI^{TA/KD}$ organoids in $Apc^{Min/-}; VillinCre^{ER2}$ background 72 hours after drugs were added. Shown here are compounds that caused at least 50% decrease in viability at 1000nM compared to DMSO. c. Relative viability of $CiMKI^{TA/TA}$ organoids (moderate CIN) compared to $CiMKI^{WT/WT}$ (no CIN) organoids. Graphs show differences in viability at 1000nM, 100nM and 10nM drug concentrations, 72 hours after drugs were added. Compounds with at least 20% decrease in viability in moderate CIN organoids were selected for more elaborate screening.

Drug screening to identify synergy between chromosomal instability and anti-cancer drugs in organoids | 101

An expanded set-up to screen a small selection of drugs

To further assess potential synergy of CIN with compounds that had a slightly increased effect on moderate CIN organoids in the initial screen, we expanded the concentration range of compounds to seven concentrations (from 0.1nM to 100µM). Furthermore, we now used two independent organoid lines per genotype and added a wild-type line that did not carry the *Apc* mutation, to assess the effect of the compounds on healthy tissue (Fig. 3A). Finally, the number of organoids was increased to 200 per well to reduce variation. In addition to the 22 drugs that were selected from the first screen, the combination Trifluridine + tipiracil (known as Lonsurf) was added to the compound list, as it was approved for metastatic colorectal cancer⁵⁹.

Despite a more elaborate screen set-up, the variation between lines of the same genotype was quite high and some of the compounds identified as potential hits in the initial screen (BAY-60-7550, alarelin, ITSA, goserelin, fludarabine, eptaplatin, oxaliplatin) displayed no effect in this second screen, suggesting they were false positives (Fig. 3B, S3A). Also, AICAR and Lonsurf were not effective in this screen (Fig. 3B, S3A), so these nine drugs were excluded from further experiments. For a subset of compounds, we were able to deduce suitable concentrations for follow-up, even if the dose-response curves were not optimal (AZD-4547, sirtinol, lonafarnib, and irinotecan) (Fig. 3C, S3). Proper dose-response curves could be plotted for another set of compounds (gemcitabine, oxamflatin, CYC-116, paclitaxel, CPD5, docetaxel, VX-680, etoposide, erlotinib, and 5-Fluorouracil) (Fig. 3D, S3C). Among these compounds were agents that are currently used as CRC treatment (5-Fluorouracil, gemcitabine and erlotinib), but also CIN-inducing drugs, such as taxanes and CPD5. With the obtained results we adapted and elaborated concentration ranges based on IC50 values of 14 compounds of this screen (Fig. 3C, D, S3B, C).

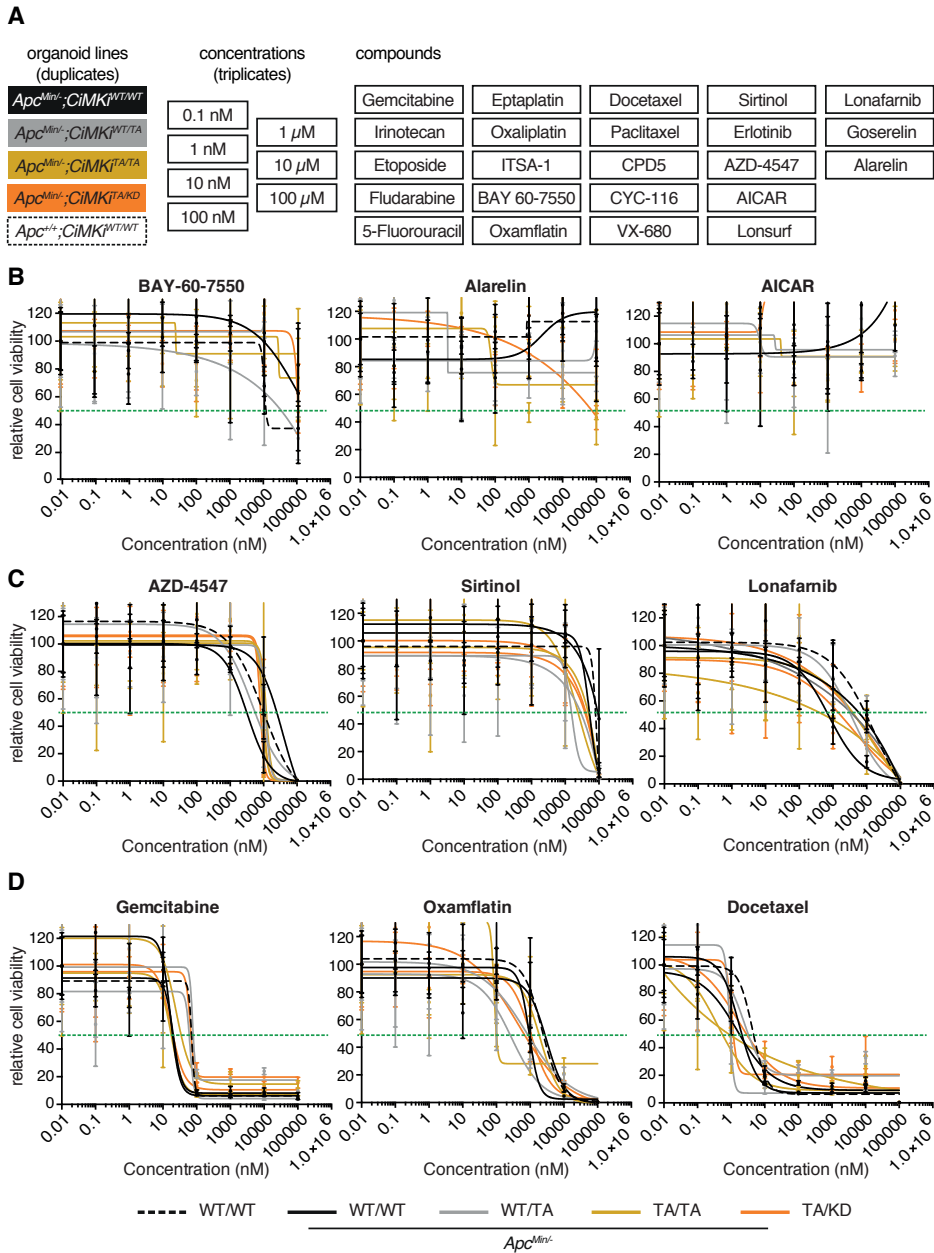


Figure 3: Detailed approach to screen small selection of drugs. a. Overview of organoid lines, concentrations and compounds selected for a more elaborate screen of possible synergistic effects of CIN and anti-cancer drugs. b. Three examples out of nine of dose-response curves showing viability 72 hours after drugs were added. Values were normalised to DMSO controls and relative viability is plotted as percentages of DMSO values. Compounds shown here were not effective in this concentration range (see also S3A). c. As B, but for three out of four compounds for which concentration range had to be adapted (see also S3B). d. As B, but for three out of ten compounds with suitable concentration range (see also S3C).

Tailored concentration range for selection of drugs

Using the IC50 values derived from the previous screen, we tailored the concentrations specifically to each of the 14 drugs and decreased the interval between the concentrations by adding intermediate steps between the log10 concentrations (i.e. 5nM between 1nM and 10nM). By using a TECAN liquid printer (Lifesciences) we were able to add drugs to final concentrations ranging from 0.005nM to 100µM (Fig. 4A) -with adjusted DMSO concentrations- in a fast and reproducible manner. The normalised values were calculated for each line and the average of the two lines per genotype were plotted. We now obtained good dose-response curves for most compounds (Fig. 4B), although there were still drugs for which the highest concentrations were not enough to kill all the cells (Fig. S4). The only two compounds showing synergy with CIN were the taxanes docetaxel and paclitaxel, and the sensitivity to these taxanes increased with increasing CIN levels (Fig. 4B, S4). In the CiMKi organoids CIN levels are related to Mps1 activity, which is decreased even further by CPD5, therefore it is surprising that CPD5 did not synergise with increasing CIN levels of the organoids.

Taxane response is not dependent on CIN level in human CRC organoids

4

So far, we used mouse small intestinal organoids from *Apc^{Min/+}* mice, that were not confounded by accumulated mutations that are present in end stage tumours. The *CiMKi* model is a clean system to assess if CIN synergises with anti-cancer drugs, but it has to be noted that many chromosomally unstable tumours may have acquired mutations that allow for CIN tolerance⁶⁰ and therapy resistance^{58,61}. To test if CIN synergises with taxanes in human tumours, we examined taxane sensitivity of human CRC organoids with known CIN levels. CIN levels were analysed in a set of human CRC organoids (Bolhaquero et al., unpublished data) and six lines with low, medium or high CIN phenotypes were selected (Fig. 5A). These CRC organoids were treated with various concentrations of paclitaxel for 72 hours before cell viability was measured. Response to paclitaxel treatment did not correlate to CIN level in the CRC organoid lines, and especially the high CIN lines responded significantly different from one other (Fig. 5B). The

A

organoid lines (duplicates)	concentrations (triplicates)	compounds
<i>Apc^{Msi1};CimK1^{WT/WT}</i>	0.005 nM - 100 nM	Gemcitabine
<i>Apc^{Msi1};CimK1^{WT/TA}</i>	0.05 nM - 100 nM	Docetaxel
<i>Apc^{Msi1};CimK1^{TA/TA}</i>	0.05 nM - 10 μM	Sirtinol
<i>Apc^{Msi1};CimK1^{TA/KD}</i>	0.5 nM - 1 μM	Irinotecan
<i>Apc^{Msi1};CimK1^{WT/WT}</i>	0.5 nM - 100 μM	Paclitaxel
	5 nM - 10 μM	Erlotinib
	5 nM - 100 μM	Etoposide
	50 nM - 100 μM	CPD5
		AZD-4547
		5-Fluorouracil
		CYC-116
		Lonafanib
		Oxamflatin
		VX-680

B

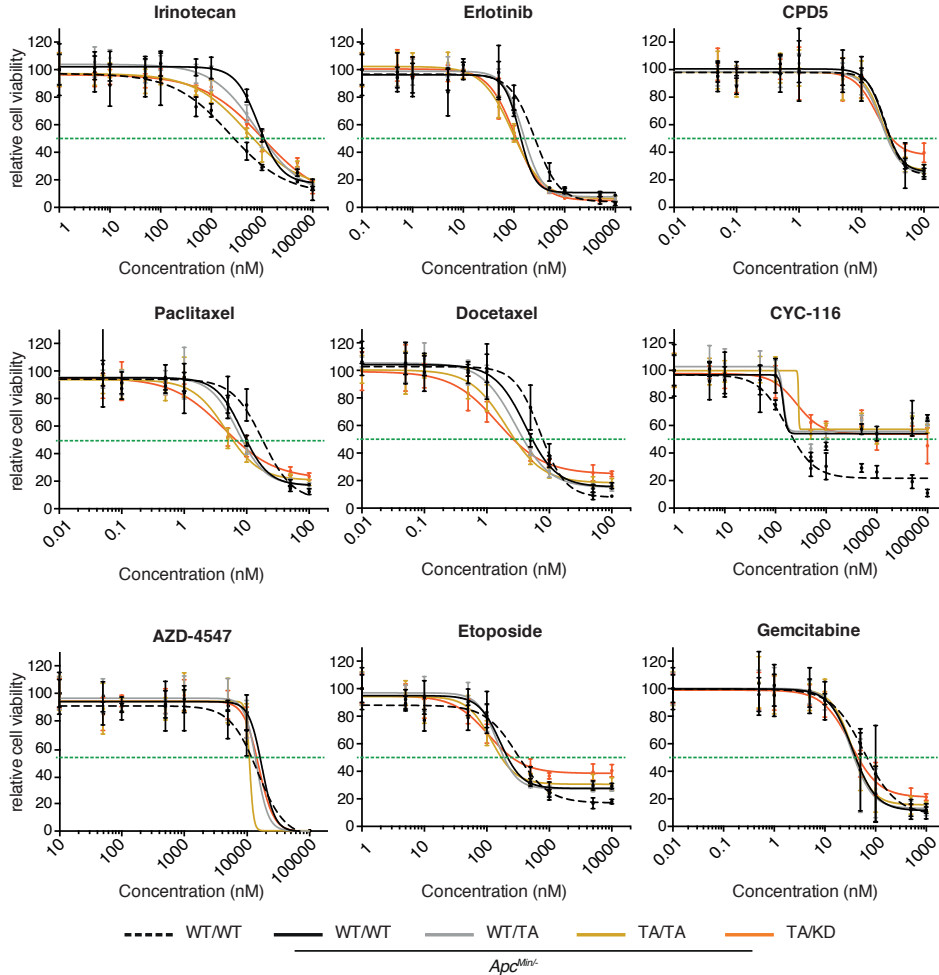
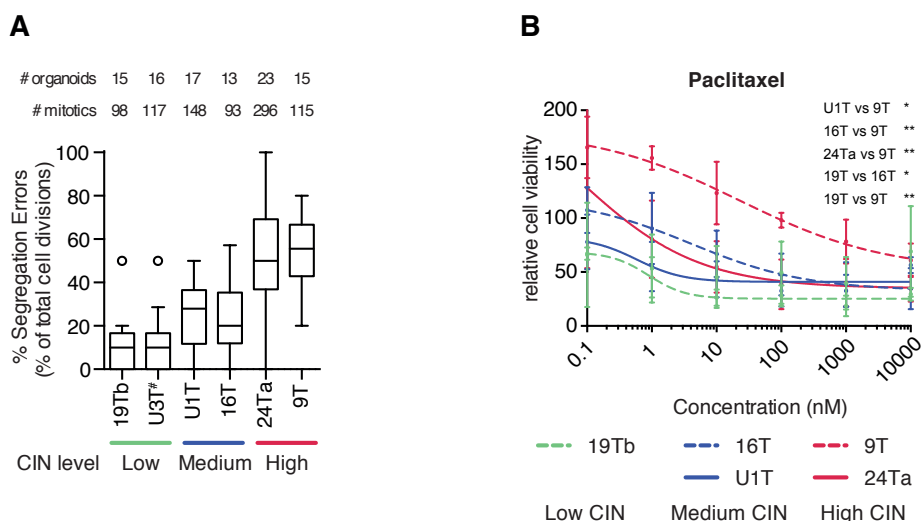


Figure 4: Tailored concentration range for selection of drugs. a. Overview of organoid lines, tailored concentrations ranges and compounds selected for a more detailed screen of possible synergistic effects of CIN and anti-cancer drugs. **b.** Dose-response curves showing viability 72 hours after drugs were added. Values were normalised to DMSO controls and relative viability is plotted as percentages of DMSO values.

variability between duplicates in one of the low CIN lines (U3T#) was so substantial that no dose response curve could be plotted. Since taxanes synergised with CIN in defined mouse organoids but not in human CRC organoids (although only a small set was used), our data do not support CIN levels as a reliable marker to predict taxane treatment response.



4

Figure 5: Taxane response is not dependent on CIN level in human CRC organoids. **a.** Quantification of segregation errors per organoid observed in tumour PDOs as determined in (Bolhaqueiro et al., unpublished data). Tumour PDOs were subdivided into hypermutated MSI (19Tb, U1T and U3T#), hypermutated (24Ta) or non-hypermutated (9T and 16T) depending on the frequency of mutations per Mb (>10 mutations/Mb vs < 10 mutations/Mb, respectively)⁵³ and lack of expression of MLH1 and PMS2 as determined by immunohistochemistry. U3T# is a metastasis (Bolhaqueiro et al., unpublished data). Data are represented as a box-and-whisker plot with the location of the whiskers based on the Tukey method. **b.** Dose-response plot of five human tumour PDOs with different CIN levels treated for 3 days with increasing concentrations of paclitaxel. Absolute values are normalized to DMSO-treated condition. Tumour PDOs were classified in low CIN (green), medium CIN (purple) or high CIN (pink). Each dot represents the mean of three independent experiments \pm SD. (** $p < 0.01$, * $p < 0.05$, repeated measures ANOVA).

Discussion

Therapy resistance remains one of the biggest challenges in treating cancer, urging for better predictors to choose the right treatment regime. Here, we screened organoids with various, inducible CIN levels for possible synergy between CIN and a broad selection of anti-cancer drugs to assess if CIN level could serve as a biomarker for treatment success. More evolved tumours display a wide variety in mutation spectra, which complicates the assessment of CIN as marker for therapy response. By using mouse small intestine adenoma organoids inducible for various CIN levels, we aimed to attribute differences between the lines in sensitivity to drugs exclusively to CIN. In this screen, no new compounds/pathways that synergised with (certain levels of) CIN were identified. However, only a relatively small drug library of 211 compounds was used, which is not a comprehensive reflection of all drugs available. New targets could possibly be identified in large-scale screens (>10.000 compounds), but handling large amounts of organoids would be a major challenge, as well as overcoming significantly higher related costs to organoid culturing compared to 2D cultures.

The only hits in our CIN mouse organoid screens were taxanes, which is interesting since a dual relationship between CIN and taxanes has been described. On the one hand, taxanes have been described to synergise with CIN by elevating missegregation levels⁴¹⁻⁴⁶, while on the other hand, CIN has been linked to taxane resistance^{29,62}. Our results in mouse organoids support the view that taxanes and CIN can synergise, but this was not confirmed in human CRC organoids with various CIN levels. The different response between human and mouse organoids could be explained by the time of onset of CIN; in the mouse organoids, induction took place just before treatment, simulating a combination therapy. In the human tumour organoids, CIN has been an ongoing process, so it is likely that these organoid lines developed various genomic landscapes, with possible consequences for e.g. transcriptomic and metabolomic processes. Overcoming the negative consequences of CIN and (partial) insensitivity to taxanes could have resulted from these ongoing adaptations⁶³⁻⁶⁵. Altogether, the method of screening described here is unlikely to pinpoint CIN as an unequivocal biomarker

for taxanes response. And since taxanes were the clearest hits, this notion of CIN being a poor biomarker for treatment selection may be true more generally.

Even though our screen could not identify a clear relationship between CIN levels and drug sensitivity, the use of (human) organoids in this screen underlines how heterogeneous tumours are and how important this can be for choosing the right therapy. Due to its closer resemblance to tumours and tissues, organoids are a more reliable tissue model than using 2D cell lines to screen for screening potential therapies for patients⁵². Establishment of organoids makes it possible to determine mutational status as well as CIN level of tumours, opening opportunities to generate more knowledge on how the combined effects of CIN and mutational background can be utilised to develop personalized treatments^{53,66,67}. Unfortunately, the screening method we have set up here could not directly contribute to improve efficiency by predefining CIN levels as biomarkers. However, since CIN is such a widespread feature of many cancers, it may be worthwhile to set up larger screens with CiMKi organoids of various tumour types and follow up on compounds that show strong synergy.

4

Acknowledgements

We thank Emmy Dolman and Anke Essing from the High Throughput Screening facility of the Princess Maxima Center in Utrecht for their input and assistance. This project was funded by grants from the Dutch cancer society (KWF), Oncode, and Cancer Genomics Centre.

References

1. Half, E., Bercovich, D. & Rozen, P. Familial adenomatous polyposis. *Orphanet J. Rare Dis.* 4, (2009).
2. Lynch, H. T. & de la Chapelle, A. Hereditary Colorectal Cancer. *N. Engl. J. Med.* 348, 919–932 (2003).
3. Grady, W. M. & Carethers, J. M. Genomic and Epigenetic Instability in Colorectal Cancer Pathogenesis. *Gastroenterology* 135, 1079–1099 (2008).
4. Fleming, M., Ravula, S., Tatishchev, S. F. & Wang, H. L. Colorectal carcinoma: Pathologic aspects. *J. Gastrointest. Oncol.* 3, 153–73 (2012).
5. Fearon, E. R. Molecular Genetics of Colorectal Cancer. *Annu. Rev. Pathol. Mech. Dis.* 6, 479–507 (2011).
6. Guinney, J. et al. The consensus molecular subtypes of colorectal cancer. *Nat. Med.* 21, 1350–1356 (2015).
7. De Sousa E Melo, F. et al. Poor-prognosis colon cancer is defined by a molecularly distinct subtype and develops from serrated precursor lesions. *Nat. Med.* 19, 614–8 (2013).
8. Labianca, R. et al. Early colon cancer: ESMO Clinical Practice Guidelines for diagnosis, treatment and follow-up. *Ann. Oncol.* 24, vi64–vi72 (2013).
9. Iqbal, A. & George, T. J. Randomized Clinical Trials in Colon and Rectal Cancer. *Surg. Oncol. Clin. N. Am.* 26, 689–704 (2017).
10. Schmoll, H. J. et al. Esmo consensus guidelines for management of patients with colon and rectal cancer. A personalized approach to clinical decision making. *Ann. Oncol.* 23, 2479–2516 (2012).
11. Duijf, P. H. G., Schultz, N. & Benezra, R. Cancer cells preferentially lose small chromosomes. *Int. J. Cancer* 132, 2316–2326 (2012).
12. Walther, A., Houlston, R. & Tomlinson, I. Association between chromosomal instability and prognosis in colorectal cancer: A meta-analysis. *Gut* 57, 941–950 (2008).
13. Orsetti, B. et al. Impact of chromosomal instability on colorectal cancer progression and outcome. *BMC Cancer* 14, 1–13 (2014).
14. Kops, G. J. P. L., Weaver, B. A. A. & Cleveland, D. W. On the road to cancer: aneuploidy and the mitotic checkpoint. *Nat. Rev. Cancer* 5, 773–785 (2005).
15. Knouse, K. A., Wu, J., Whittaker, C. A. & Amon, A. Single cell sequencing reveals low levels of aneuploidy across mammalian tissues. *Proc. Natl. Acad. Sci.* 111, 13409–13414 (2014).
16. Taylor, A. M. et al. Genomic and Functional Approaches to Understanding Cancer Aneuploidy. *Cancer Cell* 33, 676–689 (2018).
17. Lee, A. J. X. et al. Chromosomal Instability Confers Intrinsic Multi-Drug Resistance. *Cancer Res.* 71, 1858–1870 (2011).
18. McClelland, S. E., Burrell, R. A. & Swanton, C. Chromosomal instability: A composite phenotype that influences sensitivity to chemotherapy. *Cell Cycle* 8, 3262–3266 (2009).
19. Choi, C. M. et al. Chromosomal instability is a risk factor for poor prognosis of adenocarcinoma of the lung: Fluorescence in situ hybridization analysis of paraffin-embedded tissue from Korean patients. *Lung Cancer* 64, 66–70 (2009).
20. Carter, S. L., Eklund, A. C., Kohane, I. S., Harris, L. N. & Szallasi, Z. A signature of chromosomal instability inferred from gene expression profiles predicts clinical outcome in multiple human cancers. *Nat. Genet.* 38, 1043–1048 (2006).
21. Roylance, R. et al. Relationship of Extreme Chromosomal Instability with Long-term Survival in a Retrospective Analysis of Primary Breast Cancer. *Cancer Epidemiol. Biomarkers Prev.* 20, 2183–2194 (2011).
22. Birkbak, N. J. et al. Paradoxical relationship between chromosomal instability and survival outcome in cancer. *Cancer Res.* 71, 3447–3452 (2011).
23. Duijf, P. H. G. & Benezra, R. The cancer biology of whole-chromosome instability. *Oncogene* 32, 4727–4736 (2013).
24. Bielski, C. M. et al. Genome doubling shapes the evolution and prognosis of advanced cancers. *Nat. Genet.* 50, 1189–1195 (2018).
25. Lengauer, C., Kinzler, K. W. & Vogelstein, B. Genetic instabilities in human cancers. *Nature* 396, 643–649 (1998).
26. Michor, F., Iwasa, Y., Lengauer, C. & Nowak, M. A. Dynamics of colorectal cancer. *Semin. Cancer Biol.* 15, 484–493 (2005).
27. Baker, D. J., Jin, F., Jegannathan, K. B. & van Deursen, J. M. Whole Chromosome Instability Caused by Bub1 Insufficiency Drives Tumorigenesis through Tumor Suppressor Gene Loss of Heterozygosity. *Cancer Cell* 16, 475–486 (2009).
28. Bakhoun, S. F. & Cantley, L. C. The Multifaceted Role of Chromosomal Instability in Cancer and Its Microenvironment. *Cell* 174, 1347–1360 (2018).
29. Swanton, C. et al. Chromosomal instability determines taxane response. *Proc. Natl. Acad. Sci. U.*

Drug screening to identify synergy between chromosomal instability and anti-cancer drugs in organoids | 109

S. A. 106, 8671–8676 (2009).

30. Sheltzer, J. M. & Amon, A. The aneuploidy paradox: costs and benefits of an incorrect karyotype. *Trends Genet.* 27, 446–453 (2011).
31. Simonetti, G., Bruno, S., Padella, A., Tenti, E. & Martinelli, G. Aneuploidy: cancer strenght or vulnerability. *Int. J. Cancer* (2018).
32. Ohashi, A. et al. Aneuploidy generates proteotoxic stress and DNA damage concurrently with p53-mediated post-mitotic apoptosis in SAC-impaired cells. *Nat. Commun.* 6, 1–16 (2014).
33. Ried, T. et al. The consequences of chromosomal aneuploidy on the transcriptome of cancer cells. *Biochim. Biophys. Acta - Gene Regul. Mech.* 1819, 784–793 (2012).
34. Janssen, A., van der Burg, M., Szuhai, K., Kops, G. J. P. L. & Medema, R. H. Chromosome Segregation Errors as a Cause of DNA Damage and Structural Chromosome Aberrations. *Science (80-.)*. 333, 1895–1898 (2011).
35. Crasta, K. et al. DNA breaks and chromosome pulverization from errors in mitosis. *Nature* 482, 53–58 (2012).
36. Stephens, P. J. et al. Massive genomic rearrangement acquired in a single catastrophic event during cancer development. *Cell* 144, 27–40 (2011).
37. Kops, G. J. P. L., Foltz, D. R. & Cleveland, D. W. Lethality to human cancer cells through massive chromosome loss by inhibition of the mitotic checkpoint. 1–6 (2004).
38. Jelluma, N. et al. Chromosomal Instability by Inefficient Mps1 Auto-Activation Due to a Weakened Mitotic Checkpoint and Lagging Chromosomes. *PLoS One* 3, e2415 (2008).
39. Silk, A. D. et al. Chromosome missegregation rate predicts whether aneuploidy will promote or suppress tumors. *Proc. Natl. Acad. Sci.* 110, E4134–E4141 (2013).
40. Janssen, A., Kops, G. J. P. L. & Medema, R. H. Elevating the frequency of chromosome missegregation as a strategy to kill tumor cells. *PNAS* 106, 1–6 (2009).
41. Maia, A. R. R. et al. Inhibition of the spindle assembly checkpoint kinase TTK enhances the efficacy of docetaxel in a triple-negative breast cancer model. *Ann. Oncol.* 26, 2180–2192 (2015).
42. Wengner, A. M. et al. Novel Mps1 Kinase Inhibitors with Potent Antitumor Activity. *Mol. Cancer Ther.* 15, 583–592 (2016).
43. Colombo, R. et al. Targeting the Mitotic Checkpoint for Cancer Therapy with NMS-P715, an Inhibitor of MPS1 Kinase. *Cancer Res.* 70, 10255–10264 (2010).
44. Maia, A. R. R. et al. Mps1 inhibitors synergise with low doses of taxanes in promoting tumour cell death by enhancement of errors in cell division. *Br. J. Cancer* 118, 1586–1595 (2018).
45. Jemaà, M. et al. Characterization of novel MPS1 inhibitors with preclinical anticancer activity. *Cell Death Differ.* 20, 1532–1545 (2013).
46. Tannous, B. A., Kerami, M., Van der Stroop, P. M. & al, et. effects of the Selective MPS1 inhibitor MPS1-IN-3on Glioblastoma Sensitivity to Antimitotic Drugs. 1–10 (2013).
47. Shaukat, Z. et al. Chromosomal instability causes sensitivity to metabolic stress. *Oncogene* 34, 4044–4055 (2015).
48. Funk, L. C., Zasadil, L. M. & Weaver, B. A. Living in CIN: Mitotic Infidelity and Its Consequences for Tumor Promotion and Suppression. *Dev. Cell* 39, 638–652 (2016).
49. Tanaka, K. & Hirota, T. Chromosomal instability: A common feature and a therapeutic target of cancer. *Biochim. Biophys. Acta - Rev. Cancer* 1866, 64–75 (2016).
50. Tang, Y.-C., Williams, B. R., Siegel, J. J. & Amon, A. Identification of aneuploidy-selective antiproliferation compounds. *Cell* 144, 499–512 (2011).
51. Lee, H.-S. et al. Effects of Anticancer Drugs on Chromosome Instability and New Clinical Implications for Tumor-Suppressing Therapies. *Cancer Res.* 76, (2016).
52. Liu, Y. & Chen, Y.-G. 2D- and 3D-Based Intestinal Stem Cell Cultures for Personalized Medicine. *Cells* 7, 225 (2018).
53. van de Wetering, M. et al. Prospective Derivation of a Living Organoid Biobank of Colorectal Cancer Patients. *Cell* 161, 933–945 (2015).
54. Sato, T. et al. Long-term Expansion of Epithelial Organoids From Human Colon, Adenoma, Adenocarcinoma, and Barrett's Epithelium. *YGAST* 141, 1762–1772 (2011).
55. Schwank, G. et al. Functional repair of CFTR by CRISPR/Cas9 in intestinal stem cell organoids of cystic fibrosis patients. *Cell Stem Cell* 13, 653–658 (2013).
56. George Njoroge, F. et al. (+)-4-[2-[4-(8-chloro-3,10-dibromo-6,11-dihydro-5H- benzo[5,6] cyclohepta[1,2-b]pyridin-11(R)-yl)-1-piperidinyl]-2-oxo-ethyl]-1- piperidinecarboxamide (SCH-66336): A very potent farnesyl protein transferase inhibitor as a novel antitumor agent. *J. Med. Chem.* 41, 4890–4902 (1998).
57. Sacristan, C. et al. Dynamic kinetochore size regulation promotes microtubule capture and chromosome biorientation in mitosis. *Nat. Cell Biol.* 20, 800–810 (2018).
58. Koch, A., Maia, A., Janssen, A. & Medema, R. H. Molecular basis underlying resistance to Mps1/TTK inhibitors. *Oncogene* 35, 2518–2528 (2016).

59. Martinez-Perez, J., Riesco-Martinez, M. C. & Garcia-Carbonero, R. The safety of trifluridine and tipiracil for the treatment of metastatic colorectal cancer. *Expert Opin. Drug Saf.* 17, 643–650 (2018).
60. Gronroos, E. & López-García, C. Tolerance of Chromosomal Instability in Cancer: Mechanisms and Therapeutic Opportunities. *Cancer Res.* 78, 6529–6535 (2018).
61. Lee, A. J. X. & Swanton, C. Tumour heterogeneity and drug resistance: Personalising cancer medicine through functional genomics. *Biochem. Pharmacol.* 83, 1013–1020 (2012).
62. Swanton, C., Tomlinson, I. & Downward, J. Chromosomal Instability, Colorectal Cancer and Taxane Resistance. *Cell Cycle* 5, 818–823 (2006).
63. Burrell, R. A. et al. Targeting chromosomal instability and tumour heterogeneity in HER2-positive breast cancer. *J. Cell. Biochem.* 111, 782–790 (2010).
64. Roberts, J. R., Rowinsky, E. K., Donehower, R. C. & Allison, D. C. Development of Polyploidization in Taxol-resistant Human Leukemia Cells in Vitro. *Cancer Res.* 50, 710–716 (1990).
65. Bouchet, B. P. et al. Paclitaxel resistance in untransformed human mammary epithelial cells is associated with an aneuploidy-prone phenotype. *Br. J. Cancer* 97, 1218–1224 (2007).
66. Vlachogiannis, G. et al. Patient-derived organoids model treatment response of metastatic gastrointestinal cancers. *Science* (80-.). 359, 920–926 (2018).
67. Verissimo, C. S. et al. Targeting mutant RAS in patient-derived colorectal cancer organoids by combinatorial drug screening. *Elife* 5, 1–26 (2016).
68. Sato, T. et al. Single Lgr5 stem cells build crypt-villus structures in vitro without a mesenchymal niche. *Nature* 459, 262–265 (2009).
69. Drost, J. et al. Sequential cancer mutations in cultured human intestinal stem cells. *Nature* 521, 43–47 (2015).
70. Roerink, S. F. et al. Intra-tumour diversification in colorectal cancer at the single-cell level. *Nature* 556, 457–462 (2018).

<https://www.who.int/en/news-room/fact-sheet/detail/cancer>
<https://clinicaltrials.gov/ct2/show/record/NCT02366949>

Methods

Isolation and expansion of organoid lines

Organoids were isolated from *CiMKi;Apc^{Min/+};VillinCreER^{T2}* mice as described in Sato et al⁶⁸ and chapter 2 of this thesis. In brief, intestines of ten-week-old sacrificed mice were removed, cleaned with PBS, and incubated in 0.5 mM EDTA on ice for 30 minutes, and transferred to 25 ml PBS in 50 ml tubes. After harsh shaking to release the crypts, the suspension was filtered through a 70µm strainer (Greiner Bio-one). After centrifugation, the pelleted crypts were seeded in Matrigel (Corning, 356231) and covered with culture medium containing advanced DMEM/F12 medium (Invitrogen, 126334-010), Hepes Buffer (Sigma, H0887, 1 mM), Pencilin/Strep (Sigma, P0781, 1%), Ala-Glu (Sigma, G8541, 0.2 mM), Noggin conditioned medium (10%) (Thermo/Life Technologies, PHC1506, 1x), B27 (Thermo/Life Technologies, 17504001, 1x), N-acetylcysteine (Sigma-Aldrich, A7250, 1.25 mM), EGF 0,1% (Invitrogen/Life Technologies, 53003-018) and Primocin 0.5% (Invivogen, ant-pm1). For passaging, organoids were sheared by repetitive pipetting and re-plated in Matrigel in a pre-warmed 24-well plate. Since growth medium did not contain Wnt ligands, only adenoma-like organoids (with deregulated Wnt signalling) survived and proliferated^{54,55}.

4

Verification of CIN

To confirm induction of the *CiMKi* mutations, RNA was isolated from organoids 72 hours after induction with 4-Hydroxytamoxifen (4-OHT, 1µM, Sigma H6278) using an RNA miniprep kit (Zymo) following manufacturer's protocol. cDNA was produced and amplified by standard RT-PCR (Forward: CCTAGAAGACGCCGATAGCC, Reverse: GTCTCTGATTGCTTCTGGGGC) and the PCR product was sequenced (sequence primer GATAAGATCATCCGCCTCTATG) for presence of the point mutations. CIN levels were determined by live microscopy of pLV-H2B-mNEON transduced organoids as described in chapter 2.

Selection of drugs

For screening, we utilized a compound library assembled by the High-Throughput Screening facility of the Princess Maxima Center in Utrecht from

drugs of the Sequoia and Enzo libraries, (www.sequoiasciences.com, www.enzolifesciences.com) containing approved, clinical trial, and pre-clinical drugs. Compounds in these libraries include, but are not limited to, nucleotide analogues, microtubule drugs and growth factor inhibitors, and epigenetic drugs like HDAC inhibitors and DNA methyl transferases, (overview in table 1). Here, we opted for this library because of the variety of targets, but many other options are available. Some are aimed at specific tumour types or targets like DNA damage pathways, and it is also possible to design a bespoke library. Master plates of the compounds were kept in liquid nitrogen and thawed only shortly before the start of the experiment. As controls, 30 wells with DMSO were distributed throughout the plates.

Seeding and induction of organoids

Organoids of the four *CiMKi;Apc^{Min/-};VillinCreER^{T2}* genotypes (WT/WT, WT/TA, TA/TA, and TA/KD) were seeded in 384-well plates at a density of 200 organoids per well. Organoids were cultured in bulk and CIN was induced 72 hours before the start of the experiment by adding 4-OHT. The organoids were mechanically sheared one day before the start of the experiment. For reproducibility of amounts of viable organoids after seeding, organoids were allowed to recover overnight. Organoids were harvested the next morning by extensive resuspension in cold DMEM/F12 and cooling on ice for at least 30 minutes, followed by repetitive centrifugation/washing. Organoids were then filtered through a 70 μ m strainer to assure organoids of equal size were seeded. It was important to remove the Matrigel meticulously because remainders of Matrigel clog the strainers and cause loss of organoids. The number of organoids was counted and adjusted to reach 150 or 200 organoids per well in the final, 5% Matrigel in growth medium suspension. Based on optimisation experiments, 200 organoids per well yielded most reproducible outcomes; numbers were high enough to compensate for small deviations between wells, but not too high to deplete nutrients in the medium during the experiment. For accurate seeding, 35 μ L organoid suspension (first screen) or 40 μ L organoid suspension (follow-up screens) in 5% Matrigel in growth medium was suspended in each well by using the Multidrop Combi

(Thermo). During seeding, organoid suspensions were kept on ice at all times. Tubes were rinsed between each line with ice cold ethanol and PBS. After seeding, the plates were centrifuged briefly to make sure the organoid suspension was at the bottom of the well and any air bubbles were removed.

Addition of drugs for library screen

For the library screen, drugs were added to the organoids using the Caliper Sciclone ALH 3000 liquid handling robot. The library plate contained drugs at a 200 μ M concentration, so dilutions were made in three deep well plates (Costar #3965) containing 90 μ L of growth medium. First, 4 μ L the library plate, together with 6 μ L H₂O (added by the robot) was added to the first plate (8000nM solution). From this plate, 10 μ L was transferred to the next plate (800nM) and from this solution, again 10 μ L was transferred to the last dilution plate (80nM). Of these dilution plates, 5 μ L was added to the organoid suspension to reach the final concentrations 1000nM, 100nM and 10nM. The robot was equipped with fixed needles that were extensively rinsed ice-cold ethanol and PBS between plates. Furthermore, a Liconic STX-44 automated tissue culture incubator was attached to the robot, adequately transporting the appropriate plates to the pipetting deck and thereby minimizing time outside the incubator.

4

For the follow-up screens, the number of drugs was drastically lower, but instead of only three, seven to twelve concentrations were added, supplemented by DMSO control wells. For this, the Tecan HPD 300 liquid printer was now used to add the selected compounds to ten organoid lines (two independent lines for each CIN level, plus two wild-type lines). Use of the Tecan printer allowed for testing a wide range of final drug concentrations, as it is able to dispense volumes in the picoliter range. All drugs were added in triplicate and DMSO was corrected to 1% in all wells. Plates were kept in incubators for 72 hours before viability readout. This timepoint was chosen since it should give enough time for most compounds to exert their effect, but not enough to cause nutrient depletion.

Read-out of screen

Cell viability was measured 72 hours after drug addition by CellTiter Glo® 3D Cell Viability Assay (Promega). CellTiter Glo® 3D was equilibrated to room temperature and added to the organoid suspension in a 1:1 ratio. The organoids were incubated for 30 minutes, of which five minutes were on shaker. Luminescence was measured on an MDC Spectramax M5e as readout for ATP levels and thereby cell viability. For each line, consistency of seeding density was assessed by measuring cell viability at the day of seeding (T0).

All values were normalized to DSMO controls of the same organoid line to calculate percentage viability after 72 hours or growth compared to T0. The normalized values of the CIN lines were compared to those of wild-type lines (CIN line/wild-type*100) to assess potential differences in drug effects. If the difference in viability was more than 20% between high CIN and wild-type, the drug was selected for follow-up experiments. In these follow-up screens normalization was done in the same way, and since two lines of each genotype were used, the average of the normalised values for each genotype was calculated and compared to *CiMKi* wild-type adenoma organoids and wild-type small intestinal organoids. Dose-response curves were made by performing a log transformation on the data, followed by non-linear fitting of this transformation, using GraphPad Prism software.

Human Tumour Organoid Culture

Origins and maintenance of tumour PDOs used in this study were described previously^{53,69,70} (Bolhaqueiro et al, unpublished data). We used the nomenclature of the organoids obtained from Wetering et al⁵³. Organoids obtained from UMCU and the HUB foundation: HUB-02-C2-098 (U3T) and CRC29 (UIT). In summary, tumour PDOs were cultured in medium containing advanced DMEM/F12 medium (Invitrogen), Hepes Buffer (Sigma-Aldrich, 1 mM), Pencilin/Strep (Sigma-Aldrich, 1%), Ala-Glu (Sigma-Aldrich, 0.2 mM), R-Spondin conditioned medium (20%), Noggin conditioned medium (10%), B27 (Thermo/Life Technologies, 1x), nicotinamide (Sigma-Aldrich, 10 mM), N-acetylcysteine (Sigma-Aldrich, 1.25 mM), A83-01 (Tocris, 500 nM), EGF (Invitrogen/Life Technologies, 50 ng/ml) and

Drug screening to identify synergy between chromosomal instability and anti-cancer drugs in organoids | 115

SB203580 (Invitrogen/Life Technologies, 3 μ M). For passaging, tumour PDOs were dissociated with Tryple (Gibco) and re-plated in matrigel in a pre-warmed plate.

Dose-Response Assays in Human Tumour PDOs

96-well plates were pre-coated with 15 μ L of a mix of 25% Matrigel (Corning) and 75% advanced DMEM/F12 medium (Invitrogen) containing Hepes Buffer (Sigma-Aldrich, 1 mM), Pencilin/Strep (Sigma-Aldrich, 1%), Ala-Glu (Sigma-Aldrich, 0.2 mM). Organoids were dissociated to single cells with Tryple (Gibco) for 5-10 minutes. After washout of Tryple with advanced DMEM/F12 medium (Invitrogen) containing Hepes Buffer (Sigma-Aldrich, 1 mM), Pencilin/Strep (Sigma-Aldrich, 1%), Ala-Glu (Sigma-Aldrich, 0.2 mM), cells were counted using a Countess II FL (Life Technologies). 2000 cells were plated per well (12.5 μ L organoids in matrigel). Tumour PDOs were cultured in medium with Paclitaxel (Sigma Aldrich, 1mM stock) for 3 days. Cell viability was measured using CellTiter Glo® 3D Cell Viability Assay (Promega) as described above, except here CellTiter Glo® 3D was diluted in advanced DMEM/F12 medium (Invitrogen) containing Hepes Buffer (Sigma-Aldrich, 1 mM), Pencilin/Strep (Sigma-Aldrich, 1%), Ala-Glu (Sigma-Aldrich, 0.2 mM) (1:1 ratio) and incubated for 20 minutes. The values were calculated by normalizing the absolute values to the DMSO condition.

4

Supplemental figures

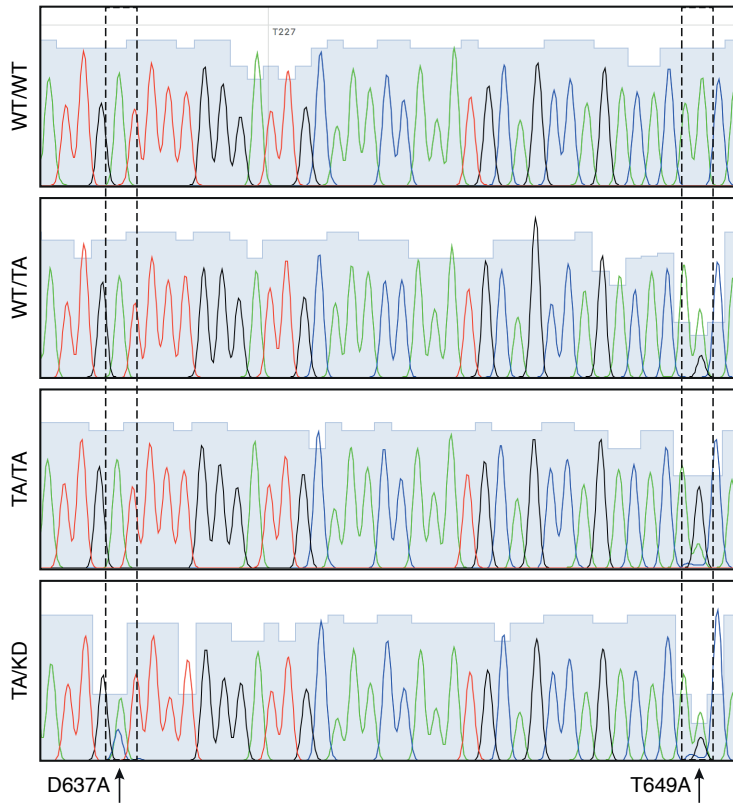


Figure S1: Mutant induction in *CiMKi*; *Apc^{Min/-}*; *VillinCreER^{T2}* organoids. cDNA sequences of *CiMKi* mutation sites (D637A=KD and T649A=TA) in *Mps1* from *CiMKi*; *Apc^{Min/-}*; *VillinCreER^{T2}* organoids 72 hours after CIN induction.

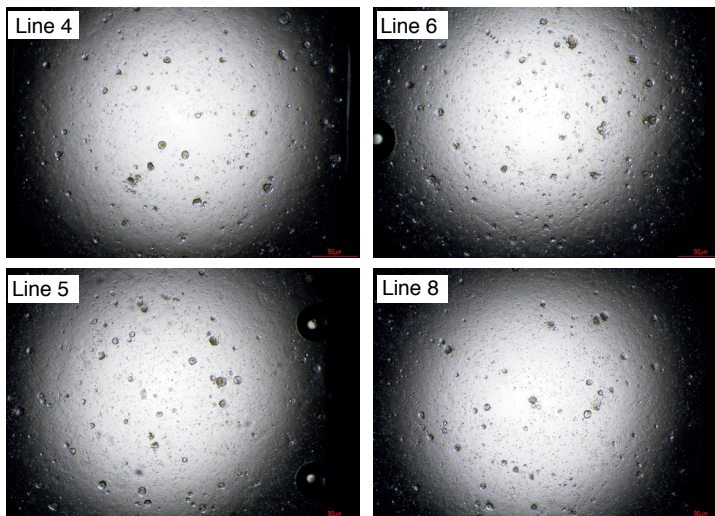


Figure S2: Equal seeding of mouse small intestine adenoma organoids for screening. Examples of organoid density directly after seeding of various *CiMKi*; *Apc^{Min/-}*; *VillinCreER^{T2}* lines

4

Drug screening to identify synergy between chromosomal instability and anti-cancer drugs in organoids | 117

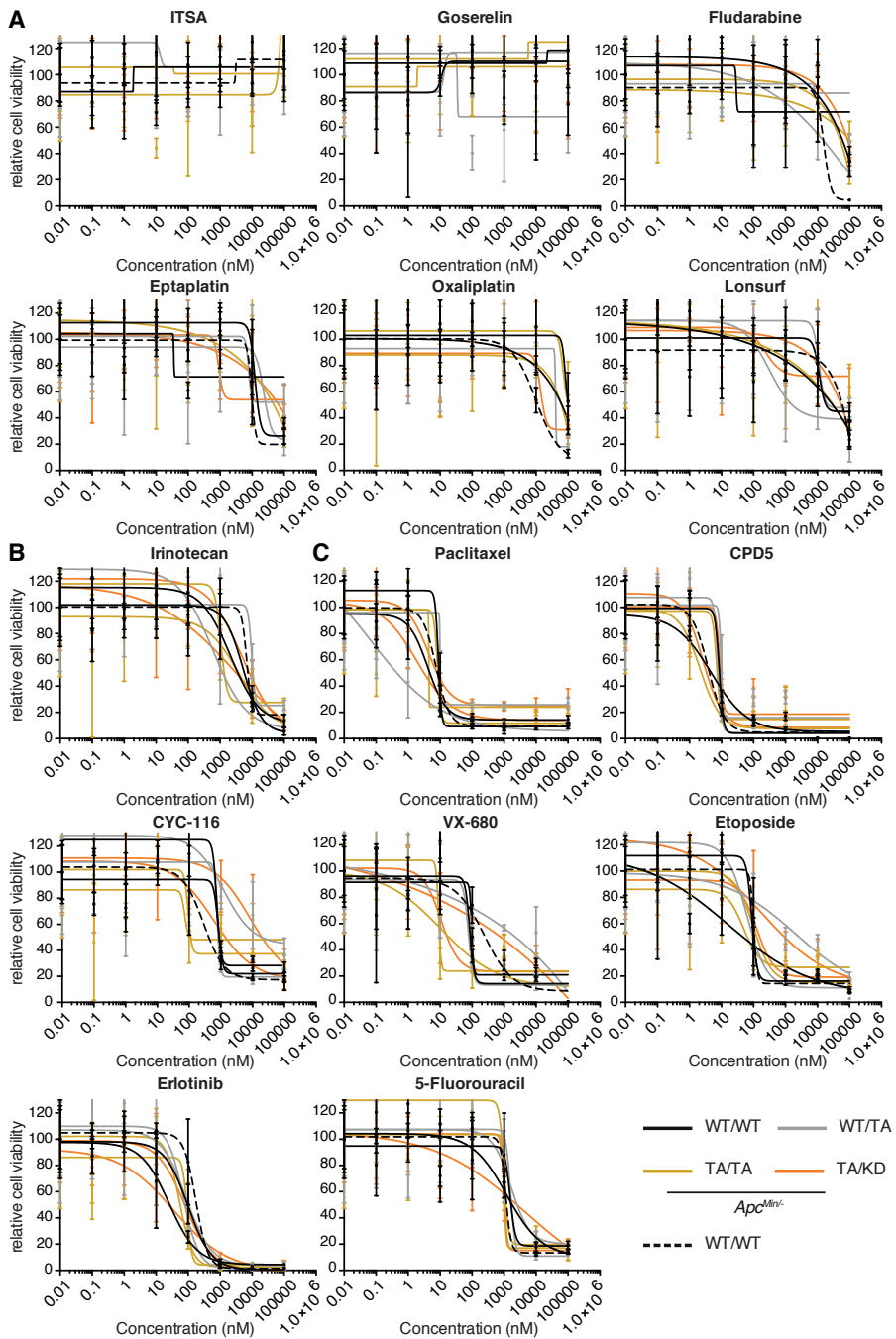


Figure S3: Detailed approach to screen small selection of compounds. a. Dose-response curves showing viability 72 hours after drugs were added. Values were normalised to DMSO controls and relative viability is plotted as percentage of DMSO values. Compounds shown here were not effective in this concentration range. b. As A, but for compounds for which concentration range had to be adapted. c. As A, but for compounds with suitable concentration range.

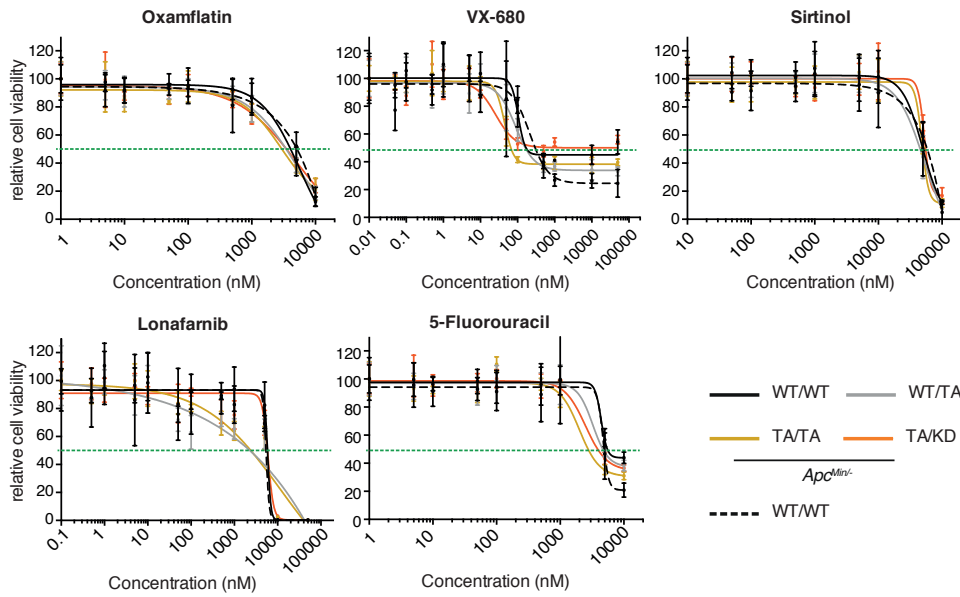


Figure S4: Tailored concentration range for selection of drugs. Dose-response curves showing viability 72 hours after drugs were added. Values were normalised to DMSO controls.

Table S1: Sequoia/ENZO library of drugs and their targets

Well Address 384	Drug Name	Target
C10	ANASTROZOLE	Aromatase
C11	BUSERELIN ACETATE	GnRH analog
C12	MELPHALAN	DNA alkylating agent
C14	MITOMYCIN C	DNA alkylating agent
C15	DOVITINIB LACTATE	Receptor tyrosine kinases
C16	10-Hydroxycamptothecin	DNA topoisomerase I
C17	ZOSUQUIDAR	P-glycoprotein
C18	7-ETHYL-10-HYDROXYCAMPTOTHECIN	DNA topoisomerase I
C19	SARACATINIB	Src, Abl
C20	ERLOTINIB HCl	EGFR
C21	ESTRAMUSTINE SODIUM PHOSPHATE	Microtubule polymerization
C22	CEDIRANIB	VEGFR1/2/3, c-Kit, PDGFR- α/β , FGFR-1
C3	DOCETAXEL	Microtubule depolymerization
C4	5'-DEOXY-5-FLUOROCYTOSINE	DNA/RNA/ribosomal protein synthesis
C9	VINBLASTINE SULFATE	Microtubule polymerization
D10	Resveratrol	SIRT1 activator
D11	Daun02	DNA topoisomerase II, DNA intercalator
D12	Valproic acid hydroxamate	HDAC
D13	LEUPROLIDE ACETATE	GnRH analog
D14	BIX-01294-3HCl	G9a histone methyltransferase
D15	Regorafenib	Receptor tyrosine kinases
D16	BML-278	SIRT1 activator
D17	SATRAPLATIN	Induces intra- & interstrand DNA and DNA-protein cross-links
D18	Triacetyresveratrol	SIRT1 activator
D19	MK-0822	Cathepsin K
D20	NVP-BEZ235	PI3K $\alpha/\gamma/\delta/\beta$, mTOR
D21	AMG-458	c-Met
D22	LEE011	CDK4/6
D3	PIRARUBICIN	DNA topoisomerase II, DNA intercalator
D4	Trichostatin A	HDAC
D5	VALRUBICIN	DNA topoisomerase II
D6	Suberoyl bis-hydroxamic acid	HDAC

4

D8	Isonicotinamide	Nicotinamide antagonist
E10	EXEMESTANE	Aromatase
E11	GOSERELIN ACETATE	LH-RH analog
E12	LY-294002	PI3K $\alpha/\delta/\beta$
E13	AFATINIB	EGFR, HER2
E14	LBH-589	HDAC
E15	GSK-2126458	PI3K $\alpha/\gamma/\delta/\beta$, mTORC1/2
E16	FLUDARABINE PHOSPHATE	Adenosine and deoxyadenosine analog
E17	NILOTINIB	Bcr-Abl
E18	RUBITECAN	DNA topoisomerase I
E19	NERATINIB	HER2, EGFR
E20	AS703026	MEK1/2
E21	ENOCITABINE	Antimetabolite (inhibitor nucleic acid synthesis)
E22	CCG-63802	G-protein signaling protein
E4	2'-DEOXY-5- FLUOROURIDINE	Antimetabolite (inhibitor thymidylate synthase)
E9	VINCRIStINE SULPHATE	Microtubule polymerization
F10	M-344	HDAC
F11	TARIQUIDAR	P-glycoprotein
F12	AGK2	SIRT2 inhibitor
F13	TENIPOSIDE	DNA topoisomerase II
F14	Butyrolactone 3	Gcn5 histone methyltransferase
F15	IRINOTECAN HCl (trihydrate)	DNA topoisomerase I
F16	NCH-51	HDAC
F17	MONENSIN SODIUM	Na ⁺ ionophore; blocks glycoprotein
F18	MDV-3100	Androgen receptor modulator
F19	GSK-1120212 DMSO	MEK1/2
F20	EPTAPLATIN	Induces intra- & interstrand DNA and DNA-protein cross-links
F21	PACLITAXEL	Microtubule depolymerization
F22	ABT263	Bcl-2, Bcl-xL, Bcl-w
F3	DAUNORUBICINHC I	DNA topoisomerase II, DNA intercalator
F4	2,4- Pyridinedicarboxyl ic Acid	inhibitor of the histone lysine demethylases
F5	LAPATINIB	(HER2/ERBB2) and epidermal growth factor receptor (HER1/EGFR/ERBB1) tyrosine kinases inhibitor.
F6	Scriptaid	HDAC
F7	FORETINIB	HGFR, VEGFR2
F8	ITSA-1	Trichostatin A inhibitor (HDAC activator)
F9	SORAFENIB TOLSYLATE	Raf-1, B-Raf, B-Raf V599E, VEGFR2
G10	NELARABINE	Purine antimetabolite

Drug screening to identify synergy between chromosomal instability and anti-cancer drugs in organoids | 121

4

G11	TRIPTORELIN ACETATE	GnRH agonist
G12	NIMUSTINE HCl	DNA alkylating and crosslinking agent
G13	ERLOTINIB MESYLATE	EGFR
G14	ABIRATERONE	Androgen synthesis inhibitor
G15	CDDO Methyl ester	Antioxidant Inflammation Modulator (AIM)
G16	CYC-116	Aurora kinases A/B
G17	BOSUTINIB Isomer 1	Chk1, Wee1
G18	ERLOTINIB	EGFR
G19	CANERTINIB DIHCl	EGFR, HER2, ErbB-4
G20	OLAPARIB	PARP1/2
G21	NILOTINIB HCl	Bcr-Abl
G22	ST-836 HCl	Dopamine receptor ligand
G3	7-EPI-TAXOL	Microtubule depolymerization
G4	DOXIFLURIDINE	Pyrimidine antimetabolite
G9	LAPATINIB TOSYLATE	EGFR, HER2
H10	Nicotinamide	SIRT inhibitor
H11	MASITINIB	c-Kit, PDGFR α/β , FGFR3
H12	Salermide	SIRT inhibitor
H13	MITOXANTHRONE HCl	DNA topoisomerase II, intercalates into and crosslinks DNA
H14	CTPB	HAT inhibitor
H15	APREPITANT	Substance P antagonists (SPA; blocks neurokinin 1 receptor)
H16	CI-994	HDAC1
H17	ELACRIDAR	P-glycoprotein
H18	VX-680	Aurora kinases A/B/C
H19	EPIRUBICIN HYDROCHLORIDE	DNA topoisomerase II
H20	Trametinib	MEK1/2
H21	TRAMETINIB	MEK1/2
H22	ABT199	Bcl-2
H4	Garcinol	HAT inhibitor
H6	Nullscript	Scriptaid Neg control
H7	ALARELIN ACETATE	Synthetic GnRH agonist
H8	Phenylbutyrate-Na	HDAC
H9	BAY 60-7550	PDE2
I10	GEMCITABINE HYDROCHLORIDE	Deoxycytidine analog, cytidine-5'-triphosphate Synthase (CTPS) inhibitor
I11	NAFARELIN ACETATE	GnRH agonist
I12	CP-690550	JAK3 > JAK2 > JAK1
I13	PLX-4032	B-Raf V600E
I14	IDOXURIDINE	Thymidine analog
I15	DASATINIB	Abl, Src, c-Kit (WT), c-Kit D816V

I16	MOTESANIB	VEGFR1/2/3, c-Kit, PDGFR, Ret
I17	PONATINIB	Abl, PDGFR α , VEGFR2, FGFR1, Src
I18	OXALIPLATIN	Induces intra- & interstrand DNA and DNA-protein cross-links
I19	NVP-BGJ398	FGFR1/2/3
I20	PAZOPANIB	VEGFR1/2/3, PDGFR, FGFR, c-Kit, c-Fms
I21	SU-11274	c-Met
I22	CCG-63808	Regulator of G-protein signaling (RGS) proteins
I3	ACLARUBICIN HCL	DNA topoisomerase II, DNA and RNA intercalator, inhibits nucleic acid synthesis
I4	PROCARBAZINE HCl	DNA alkylating agent, MAO inhibitor
I9	ABT-263	Bcl-2, Bcl-xL, Bcl-w
J10	BML-266	SIRT2 inhibitor
J11	NVP-TAE684	ALK
J12	MC-1293	HDAC1, maize histone deacetylase HD2
J13	GSK-1120212	MEK1/2
J14	Oxamflatin	HDAC
J15	TEGAFUR	Antimetabolite
J16	NSC-3852	HDAC
J17	CYTARABINE	Antimetabolite, DNA synthesis inhibitor
J18	AZD-8055	mTOR
J19	CLADRIBINE	Adenosine deaminase inhibitor
J20	LDK378	ALK
J21	CLOFARABINE	Ribonucleotide reductase and DNA polymerase.
J22	RG7388	MDM2 antagonist
J3	ETOPOSIDE	DNA topoisomerase II, complexates with DNA
J4	Splitomicin	SIRT2 inhibitor
J5	IMATINIB MESYLATE	v-Abl, c-Kit and PDGFR
J6	5-Aza-2'-deoxycytidine (Decitabine)	DNA methyltransferase
J7	TOREMIFENE CITRATE	Estrogen-receptor modulator (SERM)
J8	Tranylcpromine hemisulfate	Lysine demethylase inhibitor
J9	ELACRIDAR HCl	P-glycoprotein
K10	CISPLATIN	Induces intra- & interstrand DNA and DNA-protein cross-links
K11	BLEOMYCIN SULPHATE	inhibits DNA-, RNA- and protein synthesis
K12	ABT-888	PARP
K13	GSK 2118436	B-Raf V600E, B-Raf, C-Raf
K14	SB-408124	OX1 receptor antagonist
K15	BMS-777607	c-Met, Axl, Ron, Tyro3
K16	BORTEZOMIB	20S proteasome
K17	SUNITINIB MALATE	VEGFR2, PDGFR β , c-Kit
K18	SUNITINIB	VEGFR2, PDGFR β , c-Kit
K19	MGCD-265	c-Met, VEGFR1/2/3, Ron, Tie

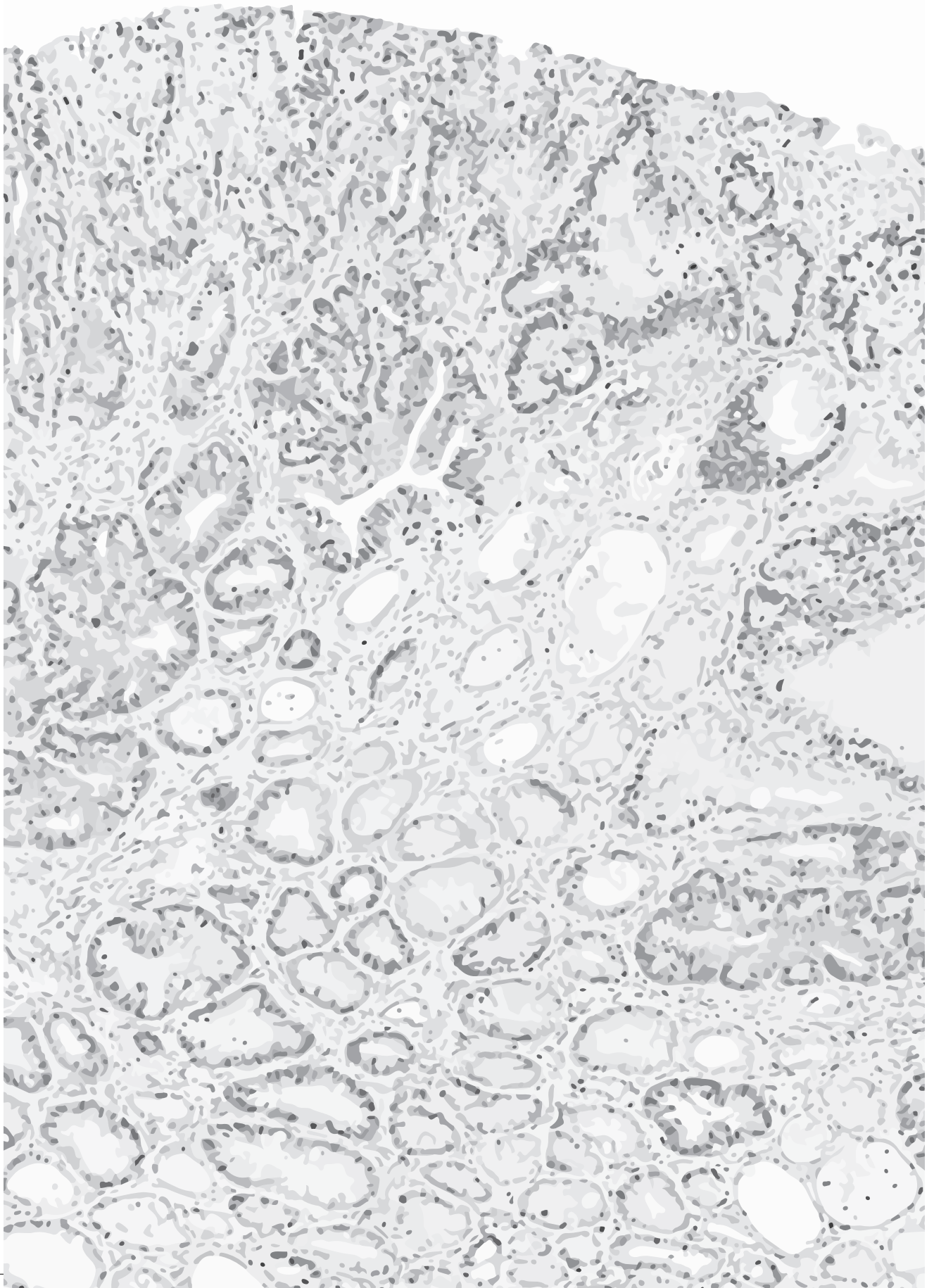


Drug screening to identify synergy between chromosomal instability and anti-cancer drugs in organoids | 123

4

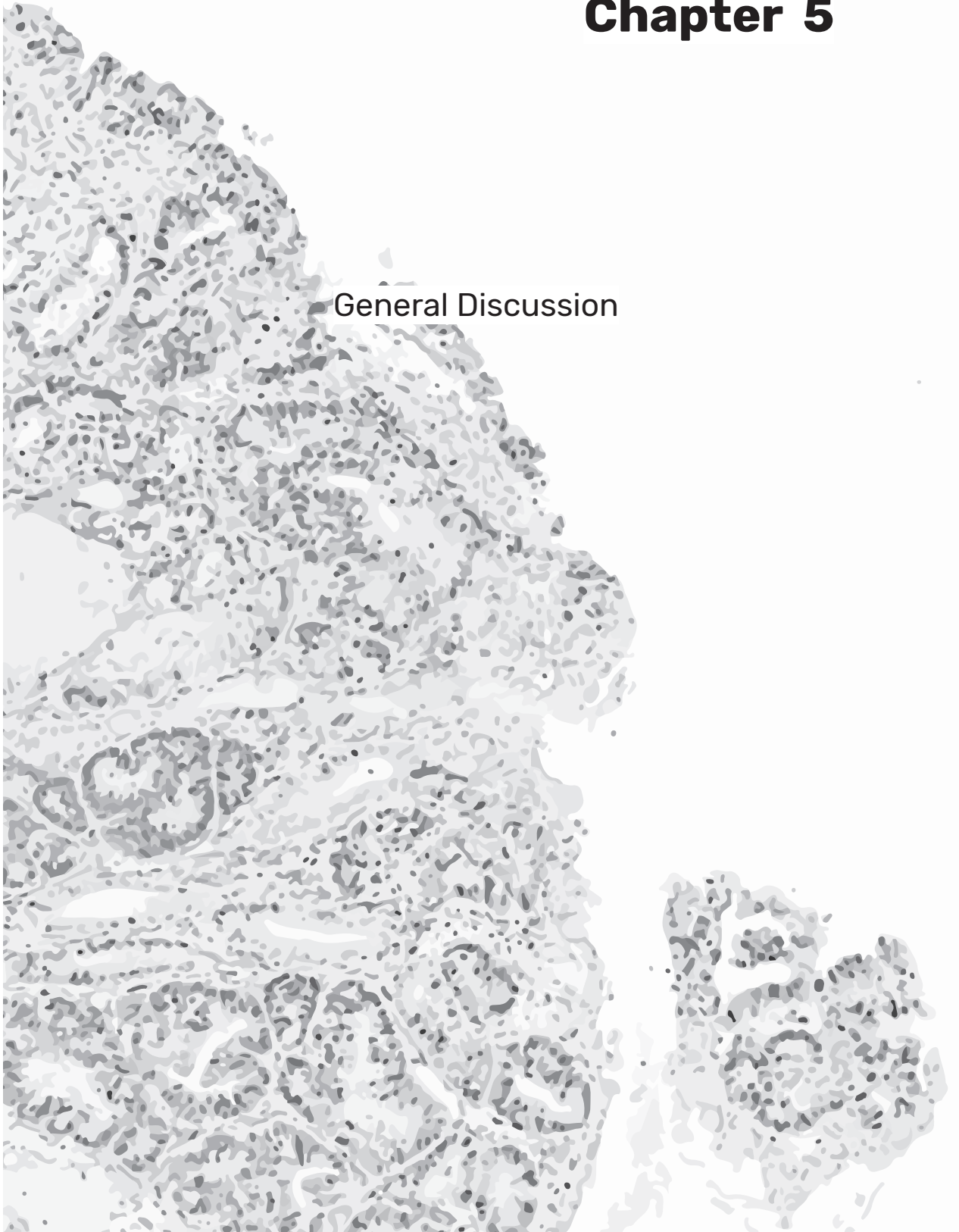
K20	BRIVANIB ALANINATE	VEGFR2/1, FGFR1
K21	ADRIAMYCIN	DNA topoisomerase II
K22	AZD-6244	MEK1, ERK1/2 phosphorylation
K3	GSK-1904529A	IGF-1R, IR
K4	LENALIDOMIDE	TNF- α secretion inhibitor
K9	PEMETREXED Na	Antimetabolite
L10	Piceatannol	SIRT activator
L11	CRIZOTINIB	ALK, c-Met
L12	Anacardic acid	HAT inhibitor
L13	AZD-4547	FGFR
L14	Sirtinol	SIRT inhibitor
L15	Dideoxycytidine	Nucleoside analog reverse transcriptase inhibitor (NRTI)
L16	Aminoresveratrol sulfate	SIRT1 activator
L17	CARMUSTINE	DNA alkylating agent
L18	PELITINIB	EGFR
L19	LOMUSTINE	DNA alkylating agent
L20	AT7519	CDK1/2/3/4/6/7/9
L21	LY-404039	mGluR1/2, dopamine receptor
L22	CYC-065	CDK 2/5/9 inhibitor
L3	FASUDIL HCl	ROCK-II, PKA, PKG, PKC, MLCK
L4	BML-210	HDAC
L5	LY-450139	γ -secretase blocker for A β 42, A β 40 and A β 38, Notch
L6	Zebularine	DNA methyltransferase
L7	ABIRATERONE ACETATE	CYP17
L8	Valproic acid	HDAC
L9	VATALANIB HCl	VEGFR2 > VEGFR1 > VEGFR3
M10	FORMESTANE	Aromatase
M11	VANDETANIB	VEGFR2
M12	LONIDAMINE	Hexokinase inactivator
M13	IMATINIB BASE	v-Abl, c-Kit, PDGFR
M14	NOLATREXED 2HCl	Antimetabolite (inhibitor thymidylate synthase)
M15	GDC-0941	PI3K α , δ
M16	AXITINIB	VEGFR2/3 phosphorylation
M17	IDARUBICIN HCl	DNA topoisomerase II
M18	FLAVOPIRIDOL	CDK1/2/4/6/7
M19	TANDUTINIB	FLT3, PDGFR, c-Kit
M20	GEFITINIB	EGFR
M21	DOXORUBICIN HYDROCHLORIDE	DNA topoisomerase II
M22	TOPOTECAN HCl	DNA topoisomerase I
M3	VINDESINE SULFATE	Microtubule polymerization
M4	VADIMEZAN	DT-diaphorase
M9	VINORELBINE BITATRATE	Microtubule polymerization
N10	Fluoro-SAHA	HDAC

N11	LOMEGUATRIB	O(6)-alkylguanine-DNA alkyltransferase (MGMT)
N12	B2	SIRT2 inhibitor
N13	A-769662	AMPK activator
N14	Suramin-6Na	Inhibits calmodulin binding to ryanodine receptor-1, G protein coupling to GPCRs and P2 purinergic receptors
N15	TOK-001	CYP17, androgen receptor
N16	BML-281	HDAC-6
N17	CYT387	JAK1/2
N18	BMS-794833	Met, VEGFR2, Ron, Axl, Flt3
N19	PF-2341066 (Crizotinib)	ALK, c-Met
N20	YM155	Survivin
N21	RALTITREXED	Antimetabolite
N22	JQ1	MYCN
N3	2'-Deoxy-5-methylcytidine	pyrimidine analog that integrates into chromatin to inhibit DNA methylation
N4	Apicidin	HDAC
N5	O6-BENZYLGUANINE	O(6)-alkylguanine-DNA alkyltransferase (MGMT)
N6	Vorinostat (SAHA)	HDAC
N7	FLUDARABINE	Adenosine and deoxyadenosine analog
N8	EX-527	SIRT1 inhibitor
N9	NEDAPLATIN	Induces intra- & interstrand DNA and DNA-protein cross-links



Chapter 5

General Discussion



Summary

Chromosomal instability (CIN) is at the heart of genome destabilisation, but so far, many questions about its role in tumorigenesis remained unanswered. This was partly due to technical limitations and difficulties to accurately study the effects of CIN in organisms. Here we present a novel mouse model for CIN in which various levels of CIN can be induced in a time and tissue specific manner.

In **chapter 2** we describe that a specific level of CIN causes early onset tumorigenesis in the small intestine. In the tumour prone *Apc^{Min/+}* background, moderate CIN caused increased tumorigenesis in both small intestine and colon, but high CIN had this effect only in colon. Finally, we confirmed that loss of heterozygosity (LOH) of the *Apc* gene is not caused by whole chromosome 18 loss. Most likely, double non-disjunction events or somatic recombination lead to the presence of two mutant alleles and either of these processes can be induced by CIN. Our follow-up experiments described in **appendix of chapter 2** showed that CIN had little effect on tumorigenesis when induced at tumour onset or after tumour establishment in *Apc^{Min/+}* mice. The impact of CIN on intestinal tumorigenesis thus dependent on the level, site and timing of CIN induction.

The CiMKi alleles can be induced in any tissue, making it an attractive model to study CIN in specific tissues, and tumour types and stages. In **chapter 3** we show that in a DMBA/TPA-induced skin tumorigenesis model, tumour free survival was decreased in moderate to very high CIN mice. Also, tumour numbers were increased in low to moderate CIN mice, revealing distinct effects of the various CIN levels on skin tumorigenesis. Induction of moderate to high CIN in skin tumours caused rapid regression of the tumours (followed by relapse), confirming that sufficiently high CIN levels can indeed kill tumour cells. Analyses of induced CiMKi expression suggested that tumour initiation and growth is influenced by both cell intrinsic and cell extrinsic factors.

Since CIN and aneuploidy are unique features of tumour cells and high CIN is lethal to cells, it has been proposed that aggravating CIN could be a treatment strategy and/or that CIN levels in tumours could be used to predict treatment response. In **chapter 4** we performed a small drug library screen and revealed the potential of finding synergistic actions between CIN and taxanes in mouse intestinal adenoma organoids, but also high-light the challenges in using CIN levels as a predictor of killing potential of anti-cancer drugs in human tumour cultures.

Discussion

CiMKi as new tool to study CIN and aneuploidy

The presence of CIN and aneuploidy in cancer has been acknowledged for a long time, but its contribution to various phases of tumorigenesis has been poorly understood. The aneuploidy paradox summarises the fact that aneuploidy is very negative for normal cells, but very common in cancer cells that seem to be less affected by an aneuploid state¹. On the one hand, aneuploid cells have to deal with proteotoxic and metabolic stress as well as pressure imposed on repair and checkpoint pathways, but on the other hand, aneuploidy is the most common genomic aberrancy in cancer cells. It is postulated that cancer cells can benefit from aneuploidy and CIN because they are more adaptable to changing environments because of their instability. We are only beginning to understand the impact of CIN on all different levels of cell regulation. Various models of CIN have been difficult to compare the different models with their variety in backgrounds, CIN inducing mutations and organs that were assessed (table 1, introduction). With the CiMKi model, we now have a system in which various CIN levels can be accurately studied *in-vivo* and *in-vitro*. We can now directly compare various levels of CIN in different tissues and in chapter 2 and 3 we demonstrated the potential of our model in intestinal and skin tumorigenesis. We now show for the first time in one model that the effects of CIN depend on its level, site and moment of induction.

5

This research could now easily be extended to investigate how CIN and aneuploidy impact other tumour types known to be highly aneuploid in humans, like for example brain, pancreatic, or breast cancer². Furthermore, CIN and aneuploidy have not only been implicated in tumorigenesis, but also in accelerated aging^{3,4}. The aging phenotype is prominent in BubR1 hypomorph and Bub1/Rae1 double mutant mice, but not in heterozygous knock-outs^{3,4}, so one can assume that a particular level of CIN has to be reached to cause this phenotype. Since no other CIN models have shown an ageing phenotype, it is not clear if the phenotype is caused by aneuploidy or is *Bub1/BubR1* related. Therefore, the CiMKi mouse model could be well suited to investigate the aging phenotype further,

due to the possibility of inducing a range of low to very high CIN levels (in various genetic backgrounds).

The aging phenotype in CIN mice has been attributed to induction of senescence in a P53 mediated manner^{3,4}. This P53 dependency underscores the importance of the genetic background of cells for the fate for these cells after missegregations. For example, P53 activation is necessary to induce senescence and apoptosis (reviewed in^{5,6}), while loss of P53 function facilitates CIN tolerance^{7,8}. All in all, the effects of CIN can be plentiful and dependent on cellular context, which is why a controlled model for CIN will greatly contribute to unravelling the ins and outs of CIN.

The impact of CIN during various stages of tumour development

In the CiMKi mice, we assessed the effect of CIN during various stages of tumorigenesis. In the skin, we were able to follow tumour development over time and found that low level CIN was sufficient to increase tumour initiation in a DMBA/TPA background. Also, more of these tumours were classified as more advanced papilloma or as carcinoma when CIN levels were high. In the intestine, early onset CIN caused a dramatic increase in colon tumour numbers in moderate and high CIN *Apc^{Min/+}* mice, but we were not able to conclude whether tumours initiated earlier, grew faster, or both, since the age of sacrifice varied between groups. Interestingly, induction of *CiMKi^{TA/KD}* caused increased tumorigenesis in the colon, but not in the small intestine of the same mice. Even though CIN levels were somewhat different between colon and small intestine, this did not explain the difference in tumorigenesis. High CIN increased the proliferative potential in the colon, but not small intestine, which could partly explain the different phenotypes (chapter 2), though potentially other factors play a role as well. Colon and small intestinal tissues differ greatly in their make-up and function; the small intestine has villi where nutrient absorption takes place, but colon lacks these structures and is mainly involved in reabsorbing fluids. Importantly, small intestine and colon also differ in their numbers of stem cells and basal Wnt signaling, as colon lacks the Wnt-secreting Paneth cells⁹. These physiological aspects can contribute the different phenotypes between colon and

small intestine in sense of tolerance of high CIN and propagation of CIN cells. Since the impact of CIN on these different tissues in the same mouse is poorly understood, future research could focus on the responses CIN elicits in different tissues.

Tumours in the intestine did not progress beyond the adenoma stage regardless of the CIN level, while skin tumours did progress with increasing CIN levels. It is possible that the $Apc^{Min/+}$ mice did not live long enough due to high tumour burden to allow for progression. This could be overcome by using other types of Apc mutated mice with lower tumour burden and increased life span. The Apc^{1638N} model, for example, shows tumour progression, and could be used for such studies¹⁰. So far, we did not observe tumour regression in the colon when high CIN levels were induced, while skin tumours showed a rapid decrease in tumour volume after CIN induction (chapter 3). It is possible that regression did not happen, but also that we missed it since we cannot monitor internal tumours over time. Another option is that the lack of effect in the intestine could be due to incomplete induction of the $CiMKi$ alleles. A single intraperitoneal injection with tamoxifen was the maximum tolerated dose in $Apc^{Min/+}$ mice with the higher CIN mutations, which may not have been enough to accomplish tissue-wide recombination. In the skin, 4-hydroxy tamoxifen was applied directly on the skin tumours on five consecutive days to assure maximal effects.

To better study the impact of CIN on various stages of intestinal tumorigenesis, it is necessary to follow the development of the tumours over time and to manipulate them *in vivo*. We showed that CIN induction before tumour onset greatly enhances tumour formation in the colon, but we are also interested in studying the impact of CIN on metastasis and in exploring CIN-based treatment options for colorectal cancer (CRC). The use of endoscopy applications would be very useful for these purposes¹¹, as it allows for orthotopic implantation of tumour organoids, or local injection of tamoxifen. Location of CIN and number of tumours can be controlled and this would prevent premature health issues and lethality due to general induction of CIN and massive amounts of adenomas. Furthermore, tumour development could be followed over time by repetitive imaging sessions.

5

By implanting fluorescently tagged organoids, (preferably organoids that switch colours upon Cre-recombination, as it would control for efficient recombination) we can assess the potential of CIN cells to establish tumours in-vivo and if these would be the cells that eventually metastasise.

Ways of CIN to promote tumorigenesis

An exciting result was that skin tumours from high CIN mice did not carry the fully induced *CiMKi* mutations, but nevertheless had a clearly distinct phenotype from low CIN mice with similar *CiMKi* mutations in the tumours. Tumours from *CiMKi^{TA/KD}* or *CiMKi^{KD/KD}* mice always carried one non-recombined allele, indicating that the tumours are populated by cells that were not efficiently recombined. In *CiMKi^{TA/TA}* mice, we did find highly efficient recombination in tumours. This argues that efficient recombination is likely, but that there may be an optimal level of CIN for tumour outgrowth. This observation made us speculate about the possible effects that CIN can have on cell autonomous and non-cell autonomous levels. In tissues as well as in tumours, cells compete for space, nutrients and oxygen and the fittest cells will eventually populate tissue compartments¹². Since the tumours in the high CIN mice were never homozygous mutant or wild-type for the *Mps1* allele, it is likely that the low CIN cells have an advantage over no- or high CIN cells to initiate tumours in the skin. Again, these effects will depend on the tissue in which CIN is induced, since we did observe increased small intestine tumorigenesis in high CIN *Apc^{Min/+}* mice.

Cell-autonomous effects of CIN

Even though it is shown that aneuploid and CIN cells can have decreased fitness and proliferative disadvantage over diploid cells (reviewed in¹³), this is not necessarily true in cells where other genomic alterations or environmental stresses are present. For example in yeast strains, some aneuploid strains do better in context of DNA damage¹⁴ and trisomic colon epithelial cells outcompete diploid cells in serum free culture conditions¹⁵. Even though these results cannot directly be extrapolated to tumour cells, the adaptive potential of low CIN cells may be beneficial in the hostile tumour environment where nutrient and oxygen

supplies can be low and the immune system is present to eradicate suspicious cells. The genetic evolution and adaptive potential of CIN cells can now be better studied over time by assessing genomic changes in tumours. Single-cell karyosequencing and whole genome exon sequencing of tumour biopsies during various stages of development would provide more information on the dynamics of how cells adapt to the tumour environment. Moreover, the potential selective advantage of certain CIN levels can be studied *in-vitro* by co-culturing organoids with different CiMKi genotypes (and thereby CIN levels). If a given level of CIN is beneficial, the organoids with this level will outcompete the others, which could easily be assessed by tagging the different lines with different fluorescent tags. This set-up could also include co-culture with immune cells and assessment of which CIN levels are most beneficial under stresses as low oxygen or nutrient supply.

Non-cell autonomous effects of CIN

As we have shown that the impact of CIN on tumorigenesis varies greatly between tissues, is it highly likely that not only the cell-intrinsic effects of CIN are important. Tissues vary greatly in their function, environment, proliferation rate etc. so this context has to be considered when making assumptions on the role of CIN. Moreover, CIN changes the microenvironment in (tumour) tissue for example by inducing apoptosis and senescence, thereby triggering activation of inflammatory responses that are in place to clear apoptotic cells¹⁶. Furthermore, the presence of cytosolic DNA (a characteristic of CIN and aneuploid cells), can activate the cGAS-STING (cyclic GMP-AMP synthase-stimulator of interferon genes) pathway^{17,18}, fuelling the inflammatory response even further. The consequent upregulation of proliferative programs¹⁹ may aid the outgrowth of tumour cells and the fast tumour relapse we saw in these animals. It would therefore be interesting to study the interplay between direct consequences of CIN induction (apoptosis, senescence) and the associated tissue response (upregulation of proliferation, immune infiltration). This can probably best be achieved by repetitive tumour biopsies, as it would allow to follow the response over time.

5

Aneuploidy and CIN cells have been described to respond differently to the immune system, as there seems to be a switch from CIN cells attracting immune cells to evading the immune system. CIN cells have been shown to produce pro-inflammatory signals and to be cleared by immune cells²⁰. Also, it has been reported that aneuploid cells have reduced expression of neoantigens and of genes specific for cytotoxic activities mediated by CD8+ T-cells and Natural Killer immune cells. This makes these cells less visible for the immune system enabling immune evasion²¹. Hence, there might be a benefit over diploid cells when immune system is triggered. Moreover the microenvironment set up by inflammatory responses may facilitate to dissemination and metastasising of CIN tumour cells¹⁷. Since the interplay between the immune system and CIN cells is obviously there, it would be very insightful to establish expression profiles of immune factors in CIN tumours over time to be able to link CIN to the changes in immune response. With this information, it would then be possible to assess if reversal of immune evasion would also decrease the metastatic potential of CIN cells.

To conclude, it is highly likely that a combination of cell autonomous and non-cell autonomous factors causes the phenotype of high CIN. For example, in our skin tumour experiment where high CIN was induced in the tumours, cell autonomous responses would have included cell death and genetic adaptation of cells that were not fully recombined. Together with the non-cell autonomous responses that can be triggered by massive cell death, an environment was created in which the low CIN cells benefitted most and grew as relapsed tumour.

CIN in cancer treatment

Since high levels of CIN are detrimental for cells^{1,22-24}, the induction of severe missegregations in tumour cells seems an attractive treatment strategy. Indeed, high CIN levels cause quick and almost complete tumour regression in DMBA/TPA-induced skin tumours (chapter 3), but tumours relapsed again. Only two of the tumours on mice with the most severe CiMKi genotype did not relapse, indicating that CIN levels must be high throughout the tumour to sustain elimination of tumour cells. To achieve such high levels of CIN for tumour treatment, the potential of MPS1 inhibitors (in combination with taxanes) is now tested in clinical trials²⁵⁻³⁰(clinicaltrials.gov

trial numbers NCT02366949, NCT03411161, NCT03328494). The notion that CIN can synergise with taxanes prompted us to set up a drug screen to assess if CIN could also have this effect with other drugs. In mouse adenoma organoids, we did indeed find synergy between increasing CIN levels and taxanes, but this finding did not extend to human colorectal cancer (CRC) organoids. Also, in other studies, CIN and aneuploidy are linked to taxanes resistance in patients^{31,32}. One has to keep in mind that tumours (organoids) have accumulated mutations, may have ongoing instability and can therefore be very heterogeneous³³⁻³⁶. The effect of CIN as an ongoing event may have a very different influences on cell viability than acute increases in CIN levels, like the induction in the mouse organoids. In that sense, I suggest to invest in combination screens where elevation of CIN levels can re-sensitise CRC organoids to chemotherapeutic agents. Use of e.g. MPS1 inhibitors can increase CIN to a level where even tumour cells have difficulties coping with, and this could be titrated specifically to the pre-existing CIN levels in CRC organoids from the patient. Combining this treatment with anti-cancer drugs could provide the synergy that is needed to effectively kill the tumour cells. Finally, with the advent of techniques that can assess heterogeneity in (organoids from) tumours at the single cell level, it will become possible to integrate mutational status, CIN level and probability of resistance to certain drugs to optimise treatment regimes.

Concluding remarks

The research described in this thesis provides new insights on the effects of CIN in normal cells and during various stages of tumorigenesis. Our approach resulted in more detailed knowledge of how time of onset, level and tissue of CIN induction are all key in the eventual outcome for tumours. We developed the CiMKi model to allow for more precise studies of CIN, and combined with improved technologies for tissue culture and single-cell analysis we are now able to study this hallmark of cancer in a better controlled way. In this thesis, I describe the first studies with CiMKi, but the possibilities for this model are plentiful. CiMKi provides excellent opportunity to further study open questions in the field regarding the impact of CIN and aneuploidy metastasis and immune regulation and how tissues can differ in their response to CIN.

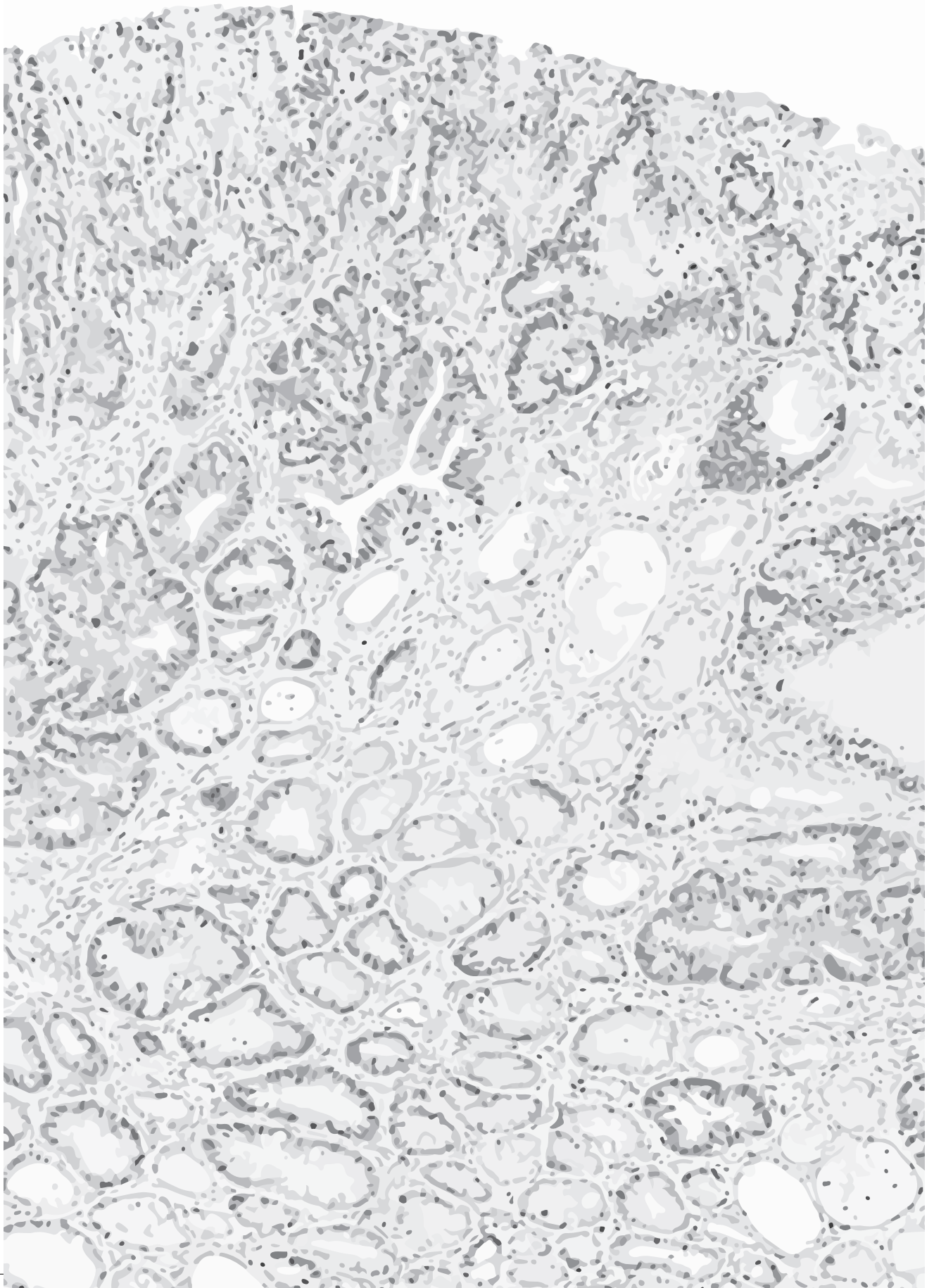
5

References

1. Sheltzer, J. M. & Amon, A. The aneuploidy paradox: costs and benefits of an incorrect karyotype. *Trends Genet.* **27**, 446–453 (2011).
2. Duijf, P. H. G., Schultz, N. & Benezra, R. Cancer cells preferentially lose small chromosomes. *Int. J. Cancer* **132**, 2316–2326 (2012).
3. Baker, D. J. et al. BubR1 insufficiency causes early onset of aging-associated phenotypes and infertility in mice. **36**, 744–749 (2004).
4. Baker, D. J. et al. Early aging-associated phenotypes in Bub3/Rae1 haploinsufficient mice. *J. Cell Biol.* **172**, 529–540 (2006).
5. Tomasini, R., Mak, T. W. & Melino, G. The impact of p53 and p73 on aneuploidy and cancer. *Trends Cell Biol.* **18**, 244–252 (2008).
6. Zuckerman, V., Wolyniec, K., Sionov, R. V., Haupt, S. & Haupt, Y. Tumour suppression by p53: the importance of apoptosis and cellular senescence. *J. Pathol.* **219**, 3–15 (2009).
7. Drost, J. et al. Sequential cancer mutations in cultured human intestinal stem cells. *Nature* **521**, 43–47 (2015).
8. Manning, A. L., Benes, C. & Dyson, N. J. Whole chromosome instability resulting from the synergistic effects of pRB and p53 inactivation. *Amity.* **33**, 2487–2494 (2014).
9. Leedham, S. J. et al. A basal gradient of Wnt and stem-cell number influences regional tumour distribution in human and mouse intestinal tracts. *Gut* **62**, 83–93 (2013).
10. Fodde, R. et al. A targeted chain-termination mutation in the mouse Apc gene results in multiple intestinal tumors. *Proc. Natl. Acad. Sci. U. S. A.* **91**, 8969–8973 (1994).
11. Zigmund, E. et al. Utilization of murine colonoscopy for orthotopic implantation of colorectal cancer. *PLoS One* **6**, 1–7 (2011).
12. Merino, M. M., Levayer, R. & Moreno, E. Survival of the Fittest: Essential Roles of Cell Competition in Development, Aging, and Cancer. *Trends Cell Biol.* **26**, 776–788 (2016).
13. Santaguida, S. & Amon, A. Short- and long-term effects of chromosome mis-segregation and aneuploidy. **16**, 473–485 (2015).
14. Pavelka, N. et al. Aneuploidy confers quantitative proteome changes and phenotypic variation in budding yeast. *Nature* **468**, 321–325 (2010).
15. Ly, P. et al. Characterization of Aneuploid Populations with Trisomy 7 and 20 Derived from Diploid Human Colonic Epithelial Cells. *Neoplasia* **13**, 348–IN17 (2015).
16. Rock, K. L. & Kono, H. The Inflammatory Response to Cell Death. *Annu. Rev. Pathol. Dis.* **3**, 499–522 (2008).
17. Bakhom, S. F. et al. Chromosomal instability drives metastasis through a cytosolic DNA response. *Nature* **553**, 467–472 (2018).
18. Sun, L., Wu, J., Du, F., Chen, X. & J, C. Z. Cyclic GMP-AMP Synthase Is. *Science (80-)*. **339**, 786–791 (2013).
19. Kizil, C., Kyritsis, N. & Brand, M. Effects of inflammation on stem cells: together they strive? *EMBO Rep.* **16**, 416–426 (2015).
20. Santaguida, S. et al. Chromosome Mis-segregation Generates Cell-Cycle-Arrested Cells with Complex Karyotypes that Are Eliminated by the Immune System. *Dev. Cell* **41**, 638–651.e5 (2017).
21. Davoli, T., Uno, H., Wooten, E. C. & Elledge, S. J. Tumor aneuploidy correlates with markers of immune evasion and with reduced response to immunotherapy. *Science (80-)*. **355**, (2017).
22. Kops, G. J. P. L., Foltz, D. R. & Cleveland, D. W. Lethality to human cancer cells through massive chromosome loss by inhibition of the mitotic checkpoint. **1–6** (2004).
23. Jelluma, N. et al. Chromosomal Instability by Inefficient Mps1 Auto-Activation Due to a Weakened Mitotic Checkpoint and Lagging Chromosomes. *PLoS One* **3**, e2415 (2008).
24. Roylance, R. et al. Relationship of Extreme Chromosomal Instability with Long-term Survival in a Retrospective Analysis of Primary Breast Cancer. *Cancer Epidemiol. Biomarkers Prev.* **20**, 2183–2194 (2011).
25. Maia, A. R. R. et al. Inhibition of the spindle assembly checkpoint kinase TTK enhances the efficacy of docetaxel in a triple-negative breast cancer model. *Ann. Oncol.* **26**, 2180–2192 (2015).
26. Wengner, A. M. et al. Novel Mps1 Kinase Inhibitors with Potent Antitumor Activity. *Mol. Cancer Ther.* **15**, 583–592 (2016).
27. Colombo, R. et al. Targeting the Mitotic Checkpoint for Cancer Therapy with NMS-P715, an Inhibitor of MPS1 Kinase. *Cancer Res.* **70**, 10255–10264 (2010).
28. Maia, A. R. R. et al. Mps1 inhibitors synergise with low doses of taxanes in promoting tumour cell death by enhancement of errors in cell division. *Br. J. Cancer* **118**, 1586–1595 (2018).
29. Jemaà, M. et al. Characterization of novel MPS1 inhibitors with preclinical anticancer activity. *Cell Death Differ.* **20**, 1532–1545 (2013).
30. Tannous, B. A., Kerami, M., Van der Stroop, P. M. & al, et. effects of the Selective MPS1 inhibitor

- MPS1-IN-3on Glioblastoma Sensitivity to Antimitotic Drugs. 1-10 (2013).
31. Swanton, C., Tomlinson, I. & Downward, J. Chromosomal Instability , Colorectal Cancer and Taxane Resistance. *Cell Cycle* **5**, 818–823 (2006).
 32. Burrell, R. A. et al. Targeting chromosomal instability and tumour heterogeneity in HER2-positive breast cancer. *J. Cell. Biochem.* **111**, 782–790 (2010).
 33. van de Wetering, M. et al. Prospective Derivation of a Living Organoid Biobank of Colorectal Cancer Patients. *Cell* **161**, 933–945 (2015).
 34. Roerink, S. F. et al. Intra-tumour diversification in colorectal cancer at the single-cell level. *Nature* **556**, 457–462 (2018).
 35. Lee, A. J. X. & Swanton, C. Tumour heterogeneity and drug resistance: Personalising cancer medicine through functional genomics. *Biochem. Pharmacol.* **83**, 1013–1020 (2012).
 36. Mcgranahan, N. & Swanton, C. Review Clonal Heterogeneity and Tumor Evolution : Past , Present , and the Future. *Cell* **168**, 613–628 (2017).
- <https://clinicaltrials.gov/ct2/show/NTC02366949>
<https://clinicaltrials.gov/ct2/show/NTC03411161>
<https://clinicaltrials.gov/ct2/show/NTC03328494>





Addendum

Nederlandse samenvatting
Nederlands curriculum Vitae
Dankwoord

Nederlandse samenvatting

Introductie

Celdeling

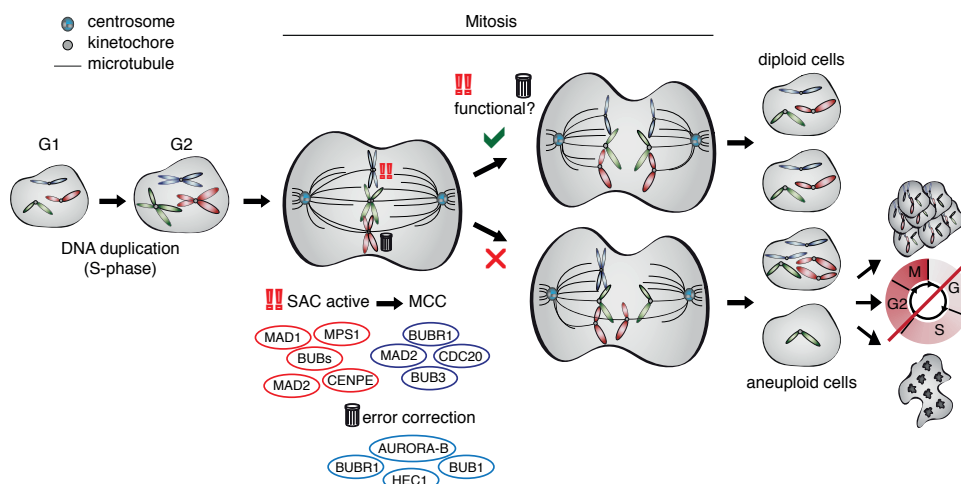
Cellen zijn de bouwstenen van mensen, dieren en planten. Om van bevruchte eicel naar volwassen mens met biljoenen cellen te groeien, vinden enorm veel celdelingen plaats. Deze delingen worden strikt gereguleerd zodat alleen gezonde cellen delen op momenten dat groei of herstel nodig is. Tumoren kunnen ontstaan als cellen ongecontroleerd delen en daarom kan kanker gezien worden als celdelingsziekte. Dat cellen deze controle verliezen, kan komen door mutaties in het DNA, dat alle genetische informatie bevat. Het menselijke DNA is georganiseerd in 23 paren (een set van de moeder, een set van de vader) van lange strengen, chromosomen genaamd. Deze chromosomen bevatten de genen die voor eiwitten coderen en deze eiwitten voeren de cel functies uit. Fouten in het DNA kunnen dus leiden tot veranderde eiwit expressie en functie. Veranderingen in het DNA kunnen op verschillende manieren ontstaan: voordat een cel gaat delen, moet eerst het hele genoom gekopieerd worden zodat beide dochtercellen een volledige set chromosomen krijgen. Er kunnen fouten ontstaan tijdens dit kopieer proces in de vorm van mutaties, of tijdens de deling zelf waarin door verschillende oorzaken hele (stukken van) chromosomen verkeerd verdeeld worden. Als cellen na deling niet de normale hoeveelheid chromosomen hebben, zijn ze aneuploid. Wanneer er herhaaldelijk delingsfouten gemaakt worden, zijn de cellen chromosomaal instabiel en stapelen fouten zich op. Aneuploidie en chromosomale instabiliteit (CIN) zijn erg zeldzaam in gezonde cellen. De enige numerieke afwijkingen in autosomale chromosomen (dus niet het X- of Y-chromosoom) die niet direct tot embryonale sterfte leiden, zijn trisomieën van chromosoom 13, 18 of 21, al veroorzaken deze wel ernstige afwijkingen. Opvallend is dat veel kankercellen chromosomale afwijkingen vertonen; wel 70% van de tumoren bevat cellen met afwijkende chromosoomaantallen. Hierdoor zijn aneuploidie en chromosomale instabiliteit onderscheidende kenmerken van



kanker. Het is echter niet bekend in hoeverre deze kenmerken bijdragen aan de ontwikkeling van tumoren en of ze ook een zwakke plek kunnen zijn waartegen therapieën ontwikkeld kunnen worden. In dit proefschrift is het onderzoek naar het belang van delingsfouten in de ontwikkeling van tumoren beschreven.

Het belang van correcte celdeling

Zoals genoemd is celdeling een strikt gereguleerd proces. Om ervoor te zorgen dat de deling correct verloopt en alle chromosomen in de juiste dochtercel terecht komen, zijn verschillende controlesystemen actief. Voordat de cel kan delen, worden alle chromosomen gekopieerd tijdens S-fase en wanneer de mitotische fase begint, bewegen alle chromosomen naar het midden van de cel waar ze een metafaseplaat vormen. Hier worden de chromosomen via eiwitcomplexen (kinetochoren) op de centromeer verbonden aan microtubuli, welke vanuit tegenoverliggende polen van de cel komen. Het is de bedoeling dat de chromosoomparen in een bipolaire manier verbonden worden, zodat wanneer



Figuur 1: Verdeling van chromosomen tijdens mitose. Voor correcte verdeling van het DNA worden de chromosomen verdubbeld tijdens S-fase (links). Tijdens mitose gaan deze chromosoomparen naar de metafase plaat in de cel waar ze worden verbonden met microtubuli. Als er geen (blauwe chromosomen) of foute (rode chromosomen) connecties zijn, blijven het SAC en error correctie mechanisme actief zodat de cel nog niet deelt en tijd heeft om correcte verbindingen te maken, waarna alsnog gedeeld wordt (bovenste cellen). Als dit mechanisme niet goed functioneert, kan een cel toch delen met ontbrekende of verkeerde kinetochoor-microtubule verbindingen, waardoor aneuploïde cellen kunnen ontstaan (onderste cellen). Afhankelijk van de ernst van de fouten en de toestand van de cel zijn er verschillende mogelijkheden, waaronder celdood, stoppen van de celcyclus of juist doorgroeien met verkeerde DNA inhoud.



de micotubuli de paren uit elkaar trekken, beide dochtercellen een volledige set chromosomen krijgen. Het spindle assembly checkpoint (SAC) monitort of alle chromosomen verbonden zijn en remt verdere progressie door mitose zolang dit niet het geval is. Dit SAC bestaat uit verschillende eiwitten die elkaar kunnen activeren en uiteindelijk het mitotisch checkpoint complex produceren waardoor anafase niet ingezet kan worden. Het is ook mogelijk dat chromosomen niet op de juiste manier verbonden zijn aan de microtubuli, bijvoorbeeld als een van de centromeren aan beide polen verbonden wordt. Om dit te corrigeren is het er nog een controlemechanisme dat foute connecties destabiliseert (zie figuur 1 voor een overzicht van mitose en functie van het SAC). Een van de belangrijkste eiwitten in de SAC en error correctie is monopolar spindle 1 (Mps1) kinase. Als dit eiwit niet goed functioneert, maakt de cel delingsfouten, welke erger worden naar mate de activiteit van Mps1 verder afneemt. De gevolgen van deze fouten voor de cel kunnen uiteenlopend zijn; cellen kunnen doodgaan, de celcyclus stoppen of verder delen met het verkeerde chromosoompakket. Dit laatste is wat de heterogeniteit in tumoren kan veroorzaken, wanneer fout op fout gestapeld wordt, ontstaan er verschillende klonen in de tumor met elk aparte genomische veranderingen. Daarnaast kan de doorlopende chromosomale instabiliteit voor versnelde aanpassing aan de omgeving en therapie resistentie zorgen. Dit kan uiteindelijk leiden tot uitzaaiingen van de tumor en een slechte prognose voor de patiënt.

Chromosomale instabiliteit en kanker

Aneuploïdie en chromosomale instabiliteit zijn specifieke kenmerken voor tumoren en correleren met tumor agressiviteit, resistentie voor chemotherapie en slechte prognose voor patiënten, zoals bijvoorbeeld in colorectaal kanker. In huidkanker worden verhoogde aneuploïdie levels gevonden in hooggradige tumoren en metastases. Ondanks dat er een klaarblijkelijke connectie is tussen aneuploïdie, CIN en kanker, is het nog niet duidelijk hoe tumorontwikkeling precies beïnvloed wordt door CIN. Dit komt mede doordat de manieren waarop CIN bestudeerd kan worden tot nu toe vrij beperkt waren. CIN is een proces dat bij voorkeur live gevolgd moet worden en tot nu toe zijn vaak aneuploïdien



gemeten als indicatie voor CIN. Ook is het niet altijd mogelijk om CIN te volgen in het weefsel van interesse omdat niet alle weefsels geschikt zijn voor celkweek. Tenslotte zijn er verschillende muismodellen ontwikkeld waarin mutaties in SAC en errorcorrectie genen zorgen voor celdelingsfouten. Echter, deze modellen zijn over het algemeen niet weefselspecifiek en in het geval van complete knock-outs van genen, niet levensvatbaar zodat hoge levels van delingsfouten niet bestudeerd kunnen worden. De effecten van de verschillende hoeveelheden delingsfouten zijn juist interessant om te onderzoeken omdat dit erg belangrijk kan zijn voor het uiteindelijke effect van CIN. Het is eerder geopperd dat lage levels CIN kunnen bijdragen aan aanpassing van het genoom om voordeel te krijgen over andere cellen en te kunnen overleven in een veranderende omgeving. Hoge CIN levels daarentegen zouden veel stress voor de cellen kunnen opleveren waardoor ze gevoeliger worden voor chemotherapie. Op deze manier zouden dan dus specifiek CIN cellen gedood kunnen worden door passende chemo. Het verhogen van CIN in combinatie met chemotherapie wordt momenteel klinisch getest.

Om specifiek te kunnen onderzoeken hoe de verschillende hoeveelheden CIN effect hebben op tumorontwikkeling, progressie en eventueel behandeling, hebben we een nieuw muismodel ontwikkeld waarin verschillende CIN levels geïnduceerd kunnen worden op een tijdstip en in weefsel naar keuze. In dit Cre-inducible Mps1 Knock-in (CiMKi) model kunnen door Cre-Lox recombinatie gemuteerde Mps1 allelen geactiveerd worden. Twee puntmutaties leiden tot verminderde of geen activiteit van het kinase en door deze mutant allelen met wildtype of elkaar te combineren, ontstaan er vijf verschillende levels van activiteit. Omdat de mutaties tijd en weefselspecifiek geïnduceerd kunnen worden, ontstaan er minder problemen tijdens de embryonale ontwikkeling en kunnen de effecten specifiek bestudeerd worden in relevante weefsels.



Onderzoek beschreven in dit proefschrift

Chromosomale instabiliteit vormt het middelpunt van destabilisering van het genoom, maar er zijn nog veel onbeantwoorde vragen over de precieze rol die CIN speelt in tumorontwikkeling. Dit proefschrift is gericht op het meer inzicht te krijgen in het belang van de hoeveelheid delingsfouten, en of het uitmaakt wanneer tijdens de tumorontwikkeling en in welk weefsel ze voorkomen.

In **hoofdstuk 2** wordt het CiMKi model gepresenteerd en leg ik uit hoe dit model tot stand is gekomen. Kort gezegd, CiMKi is een genetisch gemodificeerd muis model waar puntmutaties in het Mps1 kinase zorgen voor verminderde activiteit van het kinase. Een van de mutaties laat nog wat activiteit intact, de andere leidt tot een kinase-dood eiwit. Door de gemuteerde allelen met wildtype of elkaar te combineren, ontstaat er een range van activiteit en dit hoofdstuk laat zien dat de hoeveelheid delingsfouten correleert aan de ernst van de mutaties. We laten dit zien in MEFs (muis embryonale fibroblast cellen), darmweefsel en darm organoïden. Deze organoïden groeien in kweek uit darmstamcellen en nemen een driedimensionale structuur aan met gedifferentieerde celtypes waardoor ze een betere afspiegeling zijn van het weefsel dan tweedimensionale cellijnen. Deze organoïden zijn behandeld met een virus wat fluorescerende eiwitten produceert die aan het DNA binden, waardoor het mogelijk het DNA onder de microscoop te volgen tijdens de celdeling. Zo kan de hoeveelheid fouten die een bepaalde organoïd lijn maakt, geanalyseerd worden.

Als de CiMKi mutaties in de darm geïnduceerd worden, veroorzaakt een specifiek CIN level al op 12 weken darmtumoren, wat erg vroeg is in vergelijking met andere CIN modellen. Als we de verschillende CIN levels induceren in een muismodel dat een mutatie heeft in een gen dat ook in humane darmkanker vaak gemuteerd is ($Apc^{Min/+}$ muis), zien we dat het aantal tumoren bij matige CIN enorm toeneemt. Interessant is dat de $Apc^{Min/+}$ muis normaal gesproken vooral tumoren in de dunne darm ontwikkelt, maar mensen met de APC-mutatie dikke darm kanker krijgen. Door de toevoeging van matige tot hoge CIN in deze muis, ontstaan nu ook veel dikke darm tumoren, waardoor de muis nu meer op de humane ziekte lijkt. De CIN tumoren uit de muis zijn ook meer aneuploid dan de



niet-CIN tumoren. Alles bij elkaar toont dit dus aan dat de hoeveelheid en locatie van de CIN bepalend is voor het effect op tumorontwikkeling en hoe deze tumoren er genetisch uitzien. In dit experiment zijn de mutaties al erg vroeg geïnduceerd, op 12.5 dagen na bevruchting. Om te onderzoeken of het moment van inductie bepalend is en of hoge CIN levels kunnen zorgen voor tumor regressie, hebben we in de **appendix van hoofdstuk 2** een model gebruikt waar Cre-Lox recombinitie plaatsvindt op een gekozen moment door de injectie van tamoxifen. Deze vorm van Cre heet CreERT² en kan pas recombinitie veroorzaken na toevoeging van tamoxifen omdat het daarvoor geen toegang tot het DNA heeft. Door de muizen te injecteren wanneer ze vier of 12 weken oud zijn, wordt CIN geïnduceerd op het moment dat de eerste tumoren beginnen te ontstaan (vier weken) of wanneer ze al ontwikkeld zijn (12 weken). Het blijkt echter dat CIN bijna geen effect heeft op tumorontwikkeling wanneer het op deze momenten geïnduceerd wordt, wat dus leidt tot de conclusie dat het effect van CIN op darmtumorontwikkeling sterk afhankelijk is van level, locatie en dus ook het moment van inductie.

De CiMKi allelen kunnen in elk weefsel geïnduceerd worden, waardoor het een erg nuttig model is om verschillende tumorsoorten te bestuderen. In **hoofdstuk 3** wordt de invloed van CIN op tumorontwikkeling in de huid onderzocht. In een model waarbij met de chemicaliën DMBA en TPA tumorinitiatie en promotie veroorzaakt wordt, induceren we op verschillende momenten CIN. De belangrijkste vindingen in dit experiment zijn dat het moment van inductie en hoeveelheid CIN bepalend zijn voor het moment dat de tumoren ontstaan en het aantal tumoren dat de muizen krijgen. Wanneer bestaande tumoren behandeld worden met tamoxifen om matige tot zeer hoge CIN levels te induceren, verdwijnen deze tumoren bijna volledig; hier zou de inductie van CIN een behandelmethode kunnen zijn. Helaas groeien de tumoren ook snel weer terug en lijkt het erop dat de cellen die deze terugval veroorzaken onvolledige recombinitie hebben ondergaan. Om hoge CIN levels als behandeling toe te passen is het daarom erg belangrijk om deze hoge levels in alle cellen te hebben. Het is mogelijk dat de celdood veroorzaakt door hoge CIN de omgeving van de cellen zo beïnvloedt dat deze signalen afgeeft voor extra celdeling waardoor cellen met lagere CIN levels kunnen uitgroeien.



Kortom, het lijkt een samenspel van cel intrinsieke en extrinsieke factoren te zijn waardoor de tumoren snel terug groeien.

Om verder te onderzoeken of CIN invloed kan hebben om chemotherapeutische behandeling en of CIN als marker gezien kan worden voor therapie succes, is in **hoofdstuk 4** een set drug gescreend op hoe effectief ze organoids met oplopende CIN levels kunnen doden. We weten uit de literatuur dat hoge CIN levels dodelijk zijn voor cellen en ook in hoofdstuk 3 laten zien dat tumoren inderdaad slinken als we CIN induceren. Daarom hebben we nu onderzocht of we synergie kunnen vinden tussen een bepaalde hoeveelheid CIN en drugs die gebruikt worden voor de behandeling van kanker of daarvoor getest worden. Door darm organoids van muizen te gebruiken, hebben we een model dat dichterbij de mens staat dan cellijnen die veranderingen hebben moeten ondergaan om te kunnen groeien in kweek. Ook weten we de CIN levels van deze organoïd lijnen en hebben daarmee een schoon systeem om te relatie tussen CIN levels en therapie response te meten. De enige drugs die een lichte synergie met CIN laten zien, zijn drugs die de microtubulen beïnvloeden en daarmee dus extra CIN zouden kunnen veroorzaken. Dit effect was echter zeer klein en niet reproduceerbaar in humane tumor organoïden. Het is dus nog een uitdaging om CIN te linken aan therapie response.

De inzichten die zijn opgedaan tijdens het onderzoek dat is beschreven in dit proefschrift zijn samengevat in **hoofdstuk 5**, waarin ook een discussie van deze resultaten in het licht van de huidige literatuur te vinden is.



Conclusie

Het onderzoek beschreven in dit proefschrift geeft nieuwe inzichten in het effect van CIN op gezonde cellen en tijdens verschillende stadia van tumorontwikkeling. De opzet van dit onderzoek heeft gezorgd voor gedetailleerdere kennis over hoe belangrijk de hoeveelheid, locatie en moment van CIN inductie zijn voor tumor ontwikkeling en regressie. Het CiMKi model is ontwikkeld om preciezere studies naar de effecten van CIN op te zetten en gecombineerd met verbeterde celkweek en analysetechnieken is het nu mogelijk om dit aspect van kanker beter te onderzoeken. Dit proefschrift beschrijft de eerste experimenten met het CiMKi model, maar de mogelijkheden zijn eindeloos. Met CiMKi kunnen andere open vragen in het veld met betrekking tot de rol van CIN in bijvoorbeeld immuun regulatie en metastase onderzocht worden, als mede de verschillende reacties van diverse weefsels op CIN.



Curriculum Vitae

Wilma Hoevenaar werd geboren op 12 januari 1989 in Hooge en Lage Zwaluwe. In juli 2007 haalde ze haar VWO diploma aan het Dongemond College in Raamsdonksveer met het profiel Natuur en Gezondheid. In september van dat jaar begon ze met de bacheloropleiding Psychobiologie aan de Universiteit van Amsterdam die ze in 2010 afrondde. Ze vervolgde haar studie met de master Biomedische Wetenschappen richting "Pathophysiology and Psychopharmacology" - ook aan de UvA- en deze master werd in 2012 afgerond. Tijdens deze opleiding heeft Wilma onderzoeksstages gedaan in de groep van Prof. Dr. Miranda Olff in het Academisch Medisch Centrum Amsterdam naar de behandeling van posttraumatisch stressyndroom en in de groep van Dr. Mechiel Korte aan de Universiteit Utrecht, waar het onderzoek zich richtte op de rol van serotonine transporters in Lipopolysaccharide geïnduceerde anhedonie. In juni 2013 is Wilma begonnen met haar promotieonderzoek in de groep van Prof. Dr. Geert Kops en Dr. Nannette Jelluma in op de afdeling Molecular Cancer Research van het Universitair Medisch Centrum Utrecht. In september 2015 werd dit onderzoek voorgezet in het Hubrecht Institute in Utrecht. De resultaten van haar onderzoek zijn in dit proefschrift beschreven.



Dankwoord

Het laatste stukje! Niet het makkelijkste om te schrijven, want hoe druk je nou het beste uit hoe belangrijk anderen zijn geweest voor het voltooien van dit werk en voor alle hulp en steun de afgelopen jaren? Een PhD is zeker niet iets wat je alleen doet en ik ben dankbaar voor alle wetenschappelijke en zeker ook niet wetenschappelijke support die ik heb gekregen. Het is een heel intensief traject geweest, maar ik heb ook ongelooflijk veel plezier gehad en hele lieve mensen leren kennen, kortom een onvergetelijke periode!

Allereerst mijn promotor en co-promotor **Geert** en **Nannette**. Wat heb ik veel van jullie geleerd! Nannette, we hebben zeker de eerste jaren heel nauw samengewerkt in ons muizengroepje en het is een eer om jou eerste AiO geweest te zijn. Het was voor ons allebei soms even zoeken naar de beste aanpak, maar volgens mij zijn we er goed uitgekomen. Ik heb in ieder geval het idee dat ik geleerd heb om goed onderzoek te doen en ik zal nooit meer controles vergeten ;). Het is goed om te zien hoe je je eigen pad kiest en steeds zekerder bent geworden over het CiMKi project. Jouw stijl is heel anders dan die van Geert, maar op een paar kleine frustraties na was dat juist heel leuk. Geert, je bent altijd positief en enthousiast (en soms een beetje ongeduldig) geweest over het muizenwerk. Ik heb met veel plezier in je lab gewerkt en het is leuk om te zien hoe je zo'n gevarieerde groep mensen hebt verzameld met ieder een eigen niche in het lab.

De leden van mijn PhD commissie, **Susanne Lens** en **Patrick Derksen**. Heel erg bedankt voor jullie feedback op mijn projecten. Onze jaarlijkse meetings hebben me echt geholpen de progressie te zien wanneer ik soms dacht dat het allemaal niet zo veel was. Ik heb onze gesprekken altijd als erg positief ervaren! Ook de leden van de leescommissie, **Madelon Maurice**, **Onno Kranenburg** en **Jos Jonkers**, bedankt voor jullie tijd en interesse.

Dan mijn paranimfen **Antoinette** en **Banafsheh** die ervoor zorgen dat ik niet alleen sta bij mijn verdediging en me ook nooit alleen gevoeld heb in het lab! Jullie hebben me wegwijs gemaakt in het lab toen ik begon en daarom wil ik jullie naast me hebben. **Antoinette**, wat had ik toch zonder jou ontmoeten? Zonder celkweekervaring



werd ik aan jou overgeleverd en wat heb ik daar veel geluk mee gehad. Niet alleen wat werk betreft, maar ook omdat het altijd leuk was om met jou te werken. We hebben samen nog een groot project gedaan, dat had ik met niemand anders willen doen! Bedankt voor al je hulp, leuke gesprekken en dat je er altijd was. Ik hoop dat je heel veel plezier blijft hebben bij je nieuwe werk, ik heb je wel gemist de laatste maanden! En dan **Banafsheh**, je bent veel te lief voor deze wereld, ik ben blij dat ik je heb leren kennen! Je laat mensen nadenken over wat ze nou echt vinden en denken, zelfs als ze (ik) daar liever niet over willen praten. Voor jou is het belangrijk dat iedereen zich goed voelt en ik denk dat dat heel erg bijdraagt aan het feit dat iedereen in het lab erbij hoort. Heel fijn dat je een tijd naast me hebt gezeten op kantoor en dat je bij de mouse squad bent gekomen. Ik ga jou en onze gesprekken missen!

Then, the **Kops lab**! So many people over the years, but I enjoyed working alongside you all! First, my coffee buddy **Richard**, I don't know how much coffee we drank, but it was always a very welcome break to get some air and some good talks/rants. Our time in the lab started and finished around the same time and it was great having you around, the last months were not the same without you! I wish you all the best for the future (and since you already have the lovely **Camilla**, I think you're good). Then the next person I missed a lot during the last, intense months of my PhD, **Ajit**. We worked as a great team and I cannot thank you enough for all the help with the mouse work and being such a great support when I needed it. You are a great person and your bouncy energy is enough to brighten anyone's day. I'm sure you will do well in the future! The men of the **mouse squad**, **Pim** and **Bastiaan**, also many thanks to you for all the help and good times. You are both very talkative, sincere and nice to have around. It's a shame it has been for such a short time, Bastiaan, you didn't catch me at my finest hour (I'm actually a nice person, I promise), but thanks for sharing your cookies with me to cheer me up. **Carlos**, we have always been in the same office, which I liked because it is so nice to talk to you in the early morning. I hope you find your way towards your own lab, you really deserve it! **Spiros**, somehow we did not get together half as much as I would have liked. Good luck with the last bits, you will do great! **Bas**, **Timo** and **Sjoerd**, hiding away in the man cave, I wish you guys the best with finishing your PhD as well. **Ana**, I hope you have a bit more luck



with your projects and housing in the future, don't give up! **Kim, Emine, Joana** and **Nico**, sort of newbies in the office, thanks for the nice chats and help. I think there is a good vibe around, keep it up! Finally, **Jingchao**, don't stop making weird jokes, and **Anko**, thanks for all the microscope help! To all the people that left the lab before I did, **Claudia**, always fun to talk with you, **Eelco, Jolien** and **Joris**, I did not always understand your projects, but I know you did well! **Xiaorong**, sorry for scaring you with the mice, you are a funny guy. **Mathijs, Wilco, Tale**, pretty far done when I started, but you left your mark. **Richarda**, what a pleasure to have you in the lab for a year, all the best with your own lab now! **Debora**, I was really sad when you left, but so happy for you that you are doing so well now. **Vincent**, never sure where you were, even now, good luck with all your plans! And **Livio**, thanks for the microscope help and bringing good vibes to the lab. Finally, all the students that made life in the lab a bit more colourful, all the best with everything you wish to accomplish!

I should also mention the members of the **Lens, Galli, Tanenbaum** and **van Rooij** labs here. **Rutger, Amanda, Ingrid, Sanne, Michael** and **Martijn**, thanks for the Tuesday discussions when we were still in the Stratenum and the fun at the retreats! ML2 buddies, **Gaby, Suzan, Lenno, Sanne, Tim, Stijn, Deepak** and **Bram**, thanks for making the repetitive culturing more fun. **Charlotte** and **Bas M**, I got to know you through the PhD committee and then we became neighbours in the Hubrecht. Thanks for the good times and crazy remarks (Bas).

Also a big thank you to the people that collaborated on the projects with me. From the pathology department, **Johan, Folkert** and **Huiying**, that you for your help and insightful discussions. And **Emmy** and **Anke** from the PMC, without your help and input, the drugscreen would never have been possible on this scale. Thanks a lot!

Litha, jij bent een rots in de branding voor alle PhDs die opeens allerlei dingen moeten regelen voor hun promotie. Ik hoop dat het myphd systeem snel op orde is, maar ik twijfel er niet aan dat jij alle problemen hiermee weet te tackelen. In ieder geval heel erg bedankt voor je hulp.

Natuurlijk (gelukkig) zijn het niet alleen collega's die ik moet bedanken voor de afgelopen jaren. Juist ook degenen die weinig tot niks met wetenschap te maken hebben, zijn heel belangrijk geweest om even ergens anders aan te denken en over



te praten, gek te doen en wijntjes te drinken. **Lisette, Wendy en Elsemiek**, samen afgestudeerd en allemaal iets totaal anders gaan doen. Ik ben heel blij dat we elkaar toch blijven zien, het is iedere keer weer als vanouds en ik hoop dat we dit blijven volhouden! **Cynthia**, we kennen elkaar al zo lang en ik ben er trots op dat we al die tijd vriendinnen zijn. Ik mis de legendarische stapavondjes wel een beetje, misschien moeten we dat weer eens in plannen. Met jou ook lieve **Dayenne**! Sinds ons bijbaantje in de klimop kas is het alleen maar beter geworden denk ik. Je staat altijd voor iedereen klaar en ik weet dat ik altijd bij je aan kan kloppen. Ik kijk uit naar nog vele gezellige momenten met jou. Op sommige momenten wil je niets liever dan in de zon aan het zwembad liggen, **Amber, Rowdy, Else-Mieke en Rob**, gelukkig dachten jullie daar ook zo over! Hopelijk kunnen we dat nog eens doen, maar elkaar gewoon wat vaker zien zou ook al fijn zijn. Bedankt voor jullie vriendschap! Ook **Ingeborg en Peter, Moniek en Ivo**, hopelijk zien we elkaar snel weer!

En dan natuurlijk mijn (schoon) familie! **Guus en Astrid**, ik heb me altijd welkom en thuis gevoeld bij jullie. Hoe meer zielen hoe meer vreugd is echt van toepassing bij jullie en het is altijd leuk geweest om te zien hoeveel mensen er kunnen gourmetten in jullie woonkamer. **Jimi en Lindsay**, zo fijn om te zien hoe gelukkig jullie samen met **Nora** zijn. We zijn nu oom en tante op afstand, maar heel trots op jullie! **Agnes en Merijntje**, volgens mij matchen we goed bij elkaar! Bedankt voor de gezellige avondjes en als jullie tuin klaar is, komen we snel langs! Ook alle ooms, tantes, neven en nichten bedankt voor jullie interesse in wat ik nou eigenlijk aan het doen ben en voor de familiedagen en feestjes!

En als ik ergens trots op ben, is dat wel het warme nest waarin ik opgegroeid ben. Veel mensen vonden het bijzonder dat ik twee zussen en twee broers heb, maar ik kan het me niet anders voorstellen en zou niet anders willen. Ook al zijn we allemaal verschillend, ik weet zeker dat we altijd voor elkaar klaar staan. **Diny**, als oudste heb je het niet altijd makkelijk, bedankt dat je af toe de weg vrij hebt gemaakt voor mij en ik ben blij om te zien hoe goed je het voor elkaar heb met **Sam**. Je bent superzelfstandig maar je staat ook altijd klaar als iemand je nodig heeft. **Mathieu**, de stoere grote kerel, maar ook wel mijn jongere broertje. Je maakt overal een grapje van, maar ik weet wel dat je om ons geeft. Ik wens jou en **Sanne** het allerbeste met



jullie beestenboel! **Janet**, jij bent echt het lieve kleine zusje wat ineens niet meer klein is. Je bent een van de liefste mensen die ik ken en tegelijkertijd zo bijdehand dat ik er bijna jaloers van wordt. Ik ben super trots op hoe je gegroeid bent en ik weet zeker dat je met **Mirko** een mooie toekomst tegemoet gaat. En dan **Izaak**, de jongste maar de grootste van ons allemaal. Je bent altijd lekker bezig met vanalles. Heel knap dat je voor jezelf begonnen bent, het past ook helemaal bij je om lekker je gang te kunnen gaan. Ik hoop dat je met **Janneke** nog lekker gaat genieten van tochtjes in de Biesbosch en hopelijk nemen jullie ons een keertje mee!

Dat we allemaal zo goed terecht zijn gekomen is aan jullie te danken, lieve **papa** en **mama**. Ik kan me geen betere jeugd voorstellen dan die jullie ons gegeven hebben. Bedankt dat jullie er altijd zijn, altijd klaarstaan en willen luisteren. Jullie zijn zorgzaam en aanpakkers en hebben dat goed doorgegeven aan ons. Ook al zijn we geen pratere, een half woord is vaak genoeg en ik hoop dat jullie net zo trots op mij zijn als ik op jullie. Ondanks ik steeds verder weg ben gaan wonen, zal mijn eerste thuis altijd bij jullie zijn en ik vind het nog steeds heel fijn om bij jullie voor de kachel te komen zitten. Ik weet dat jullie soms geen idee hebben wat ik nou aan het doen ben, maar ik had het nooit zonder jullie steun gekund. Dankzij jullie opvoeding ben ik de persoon geworden die ik nu ben. Het was een lange weg van de Groenendijk naar Schotland, maar een met veel mooie herinneringen. Dank jullie wel voor alles, ge wit dagge bedankt zijt ;).

Mijn laatste woorden zijn voor jou, mijn lieve **Huub**. Volgens mij heb jij nog het meest geleden onder dit hele avontuur, maar je hebt er nooit over geklaagd. Jouw geduld met mij is net zo eindeloos als mijn liefde voor jou. Ik had dit nooit kunnen doen als ik jou niet naast me had. Je hebt me zo geholpen om de positieve dingen te blijven zien, ik sta er soms nog steeds van te kijken hoe je zo relaxed kan zijn. Bedankt dat je er altijd voor me was en bent. Iedere dag is leuker met jou en onze vier maanden apart heeft wel bevestigd dat we echt bij elkaar horen. Ik kijk uit naar onze toekomst samen, met z'n tweeën kunnen we alles aan, waar we ook zijn. Ik hou heel veel van je.

